2010-10-13

Functionalization of Diamond and Its Application in High Performance Liquid Chromatography and Solid Phase Extraction

Gaurav Saini
Brigham Young University - Provo

Functionalization of Diamond and its Application in High Performance Liquid Chromatography and Solid Phase Extraction

Gaurav Saini

A dissertation submitted to the faculty of
Brigham Young University
In partial fulfillment of the requirements for the degree of

Doctor of Philosophy

Matthew R. Linford
Milton L. Lee
Matthew C. Asplund
David V. Dearden
Robert C. Davis

Department of Chemistry and Biochemistry

Brigham Young University

December 2010

ABSTRACT

Functionalization of Diamond and its Application in High Performance

Liquid Chromatography and Solid Phase Extraction

Gaurav Saini

Department of Chemistry and Biochemistry

Doctor of Philosophy

The primary focus of my work was to chemically functionalize diamond as normal and reversed phases for solid phase extraction (SPE) and high performance liquid chromatography (HPLC). Diamond was functionalized with $-NH_2$ groups via self-limiting adsorption of an amine-containing polymer, polyallylamine (PAAm), onto oxidized diamond particles. The chemical stability of these particles was improved by thermal curing or chemical crosslinking with 1,2,5,6-diepoxycyclooctane. The reversed phase material for SPE was synthesized by reacting amine-functionalized diamond particles with long chain alkyl and a perfluorinated isocyanate. Unlike commercially available silica, functionalized diamond particles were stable under extreme pH conditions (pH 0-14). Functionalized diamond particles were used for SPE, although their lack of porosity resulted in poor analyte capacity. To create materials with greater surface area, core-shell diamond particles were synthesized via layer-by-layer deposition of PAAm and nanodiamond onto solid microdiamond. These particles had higher surface areas than solid diamond particles, and their application in SPE and HPLC was demonstrated.

As a related project, I demonstrated microlens array patterning (MAP) for selective adsorption of PAAm during microarray fabrication. Initially, alkyl monolayer terminated silicon surfaces were photopatterned with thousands of wells using a microlens array. PAAm was then deposited in the presence of a cationic surfactant to limit nonspecific adsorption of PAAm. Finally, reactions of selectively adsorbed PAAm were shown with glutaric anhydride, phenylenediisothiocyanate, biotin NHS-ester and an oligonucleotide (DNA).

My third project concerned the synthesis of an abrasion resistant hydrophobic coating on the surface of nylon and silicon oxide substrates using chemical vapor deposition (CVD) of two silanes. The synthesis consists of four steps: 1) plasma oxidation of the substrate, 2) treatment with 3-isocyanatopropyltrimethoxysilane, 3) exposure of the treated surfaces to water vapors, and 4) treatment with a perfluorinated silane to make the surfaces hydrophobic. The coating is not visible to the eye and does not change the feel of the surface. Time-of-flight secondary ion mass spectrometry (ToF-SIMS), X-ray photoelectron spectroscopy (XPS), spectroscopic ellipsometry, contact angle goniometry, scanning electron microscopy (SEM), environmental scanning electron microscopy (ESEM), Rutherford backscattering spectroscopy (RBS) and nuclear reaction analysis (NRA) were used to characterize the resulting materials.

Keywords: Diamond, polyallylamine, core-shell, microlens array patterning, silane, hydrophobic

ACKNOWLEDGEMENTS

I would like to extend my deep sense of gratitude to Dr. Matthew R. Linford for his mentorship, cooperation, compassion and encouragement. His constant guidance throughout my research has paved my way to the successful completion of the doctoral work.

I would like to acknowledge my committee members, Dr. Milton L. Lee, Dr. Matthew C. Asplund, Dr. David V. Dearden and Dr. Robert C. Davis, for their valuable suggestion at my progress reviews, and during various points of my research.

I extend my appreciation to my colleagues, Dr. Michael V. Lee, Dr. Li Yang, Dr. Guilin Jiang, Feng Zhang, Lei Pei, Landon Wiest, Dave Jensen, Nitesh Madan, Supriya Singh Kanyaal and David Hung, for making my graduate journey a memorable experience.

I thank US Synthetic, Laser Array Technologies, Sonic innovation and Xeromax Sciences for supporting major part of my research.

Finally I would like to acknowledge Brigham Young University and the Department of Chemistry and Biochemistry for providing me an opportunity to work as a graduate student.

TABLE OF CONTENTS

LIST OF TABLES

LIST OF FIGURES

PART I. INTRODUCTION

Chapter 1. Background Information*

Solid phase extraction (SPE) and high performance liquid chromatography (HPLC) are two of the most widely used techniques in separation science.[1-8] Solid phase extraction is used to preconcentrate analytes of interest and remove undesired components in solutions, and is often followed by HPLC. HPLC, on the other hand, is used to identify and quantify the components present in a sample mixture. In both techniques, the sample solution is passed through a column packed with functionalized particles. The analytes are retained differently on the functionalized particles depending on their relative physical/chemical interactions with them. In SPE, the retained components are eluted from the column using a solution which has stronger interaction with the analytes than the stationary phase.

The quest for more robust HPLC and SPE substrates dates back to the invention of HPLC and SPE. As described herein, various types of packing materials, *e.g.*, silica, zirconia, alumina, polymer, graphite and diamond, have been investigated, and each material has been found to have various advantages and disadvantages.

1.1. Silica

Silica is the most widely used material in separation science.[9-11] It has many advantages that make it the most sought for material in HPLC and SPE. Its surface chemistry is well

*Some of the sections of this chapter were taken, sometimes verbatim, from the introductory paragraphs of Chapters 2-6 of this thesis. Permission was obtained from the publishers of the documents to reproduce the papers herein.

understood, which makes its functionalization relatively straightforward.[12] It can also be synthesized as highly porous monodisperse particles with controlled porosity.[13] Nevertheless, silica has certain limitations. It is not stable under extreme pH conditions. The labile nature of the Si-O-Si bond between the substrate and the silane adsorbate under acidic conditions, and disintegration of silica at high pH values limit its use to a relatively narrow pH range. This creates a problem in the separation of charged analytes when one needs to use a high or low pH buffer to adjust the protonation or deprotonation state of the analyte and/or the stationary phase. However, at high pH values, the presence of residual silanol groups leads to secondary interactions with the analytes. This can result in peak broadening or tailing, and hence, a reduction in column efficiency. Endcapping of the silanol groups has been used to prevent secondary reactions with the analytes.[14,15] However these secondary interactions still exist to some extent due to incomplete reaction of the silanol groups during endcapping.

1.1.1. Improvement in pH Stability

A number of approaches have been taken to improve the pH stability of silica based stationary phases. In one approach, alkyl groups were doped into SiO_2 during its fabrication to improve its hydrolytic stability, *e.g.*, the XTerra® columns by Waters. In another approach, Kirkland and coworkers synthesized acid stable, sterically hindered octadecylsilane functionalized silica phases by replacing the methyl groups of a monofunctional silane adsorbate with bulky isopropyl groups or isobutyl groups.[16,17] These phases were able to withstand very harsh mobile phase conditions (1% TFA, pH 1.0, 1.0 ml./min., 25,000 column volumes). Carr and coworkers synthesized hypercrosslinked reversed phase silica phases[18-20] which were much more acid stable than the sterically hindered silica phases developed by Kirkland and

coworkers.[16,17] In the first step of their synthesis, chloromethyl-phenylethyl-trichlorosilane or chloromethyl-phenylethyl-dimethylchlorosilane was tethered to the silica surface. In the second step, a Friedel-Crafts reaction was used to condense the adjacent phenyl rings of the bonded silanes. A non-polymerizable styrene heptamer was used to condense adjacent chloromethylphenyl groups by the Friedel-Crafts reaction. This produced a highly crosslinked structure on the surface. In the final step, an additional Friedel-Crafts reaction was used to tether octyl functionalities to the phenyl groups. The resulting phases were very stable under highly aggressive mobile phase conditions (47.5/47.5/5.0 ACN/H_2O/TFA, pH 0.5; T = 150°C; flow rate = 2.0 ml/min.).

1.2. Polymeric materials

The potential of polymeric particles as packing materials has also been investigated. These materials are mostly used in ion exchange chromatography, ion pair chromatography, and size exclusion chromatography, where styrene/divinylbenzene copolymer particles are often used for these purposes.[21-23] The main advantage of these particles is their high stability over a wide pH range. However these particles suffer from slow mass transfer, which in turn negatively affects the efficiency of the separation. Their mechanical stability is not very good and, unless properly crosslinked, they have a tendency to swell in organic solvents.

1.3. Metal Oxides

1.3.1. Zirconia

Ziroconia has been investigated as another packing material in HPLC.[24,25] It is thermally and chemically very stable.[26] Much work has been done in Carr's group on the use of Zirconia as

a packing material in HPLC; they used zirconia as a stationary phase in reversed phase, normal phase and ion-exchange chromatography.[27-31] The presence of lewis acid sites on its surface leads to irreversible adsorption of certain species,[32-34] such as peptides and proteins, which prevents its use as a stationary phase in the separation of proteins and peptides.[35,36]

1.3.2. Alumina

Not much work has been done on the use of alumina as a stationary phase in HPLC. Tanaka *et al*. used a combination of an alumina column and an octadecylsilane functionalized silica column in series for the separation of small peptides.[37] Moreau *et al*. separated a mixture of wax esters, sterol esters and methyl esters using an alumina column at elevated temperature.[38]

1.4. Graphite

The potential of porous graphitic carbon as a substitute for silica has also been explored.[39-41] Hypercarb® columns from Thermo-Fischer have been used in separations.[42,43] Graphite is very stable at high pressures and temperatures. Unlike silica, it is very stable under extreme pH conditions. The resonance stabilization of sp^2 carbon atoms in its structure makes its functionalization very challenging. Porous graphitic carbon has been used in the separation of various polar compounds such as oligosaccharides,[39,44-46] guanidino compounds,[47,48] and free amino acids and small peptides.[49-51] The main disadvantage of graphite is its affinity for non-polar compounds, which makes desorption of such compounds from the surface very difficult.[40]

1.5. Diamond

Diamond is another substrate that has been explored as a potential stationary phase for HPLC and SPE.[52,53] It is very stable under extreme pH conditions, and has high thermal conductivity and mechanical strength. It is also optically transparent. These properties make it an ideal material for HPLC and SPE.

1.5.1. Functionalization of Diamond

For applications in separation science, the surface of diamond must be functionalized in order to exploit its remarkable properties. For example diamond's surface has been terminated with hydrogen and deuterium by thermal[54,55] and plasma treatments.[56-59] H-terminated diamond has been functionalized with terminal alkenes using UV light.[60-64] For example, Hamers and coworkers photochemically functionalized H-terminated diamond thin films with terminal alkenes using 254 nm UV light.[60] In their work, thin diamond films were grown on Si (111) wafers. The resulting diamond surfaces were functionalized with terminal alkenes by covering the surface with a thin liquid film of the alkene, and then exposing it to 254 nm UV light. Terminal alkenes such as perfluorodecene, 1-dodecene and trifluoroacetamide-protected 10-aminodec-1-ene (TFAAD) were used. Russell and coworkers have functionalized H-terminated diamond with perfluorobutyl chains.[65] In their work, perfluoroiodide was dispensed onto the surface as a liquid at 90 K. This resulted in the formation of condensed layers of perfluorobutyliodide. This surface was then exposed to UV wavelengths (<305 nm), which resulted in covalent attachment of perfluorobutyl moieties to the surface. Diamond's surface has also been modified with 1,3-butadiene through the Diels-Alder reaction,[66] in which H-terminated diamond was heated to 1310 K. This resulted in the desorption of hydrogen and reconstruction of

the surface. The reconstructed surface behaves like a source of C=C double bonds, which undergo Diels-Alder reaction with 1,3-butadiene.

A decent amount of work has also been done to functionalize diamond's surface with halogens. Accordingly, Freedman and coworkers have functionalized the diamond surface via fluorine using atomic and molecular fluorine.[67-69] The surface was exposed to these reagents under ultra-high vacuum conditions. X-ray photoelectron spectroscopy, low energy electron diffraction, and thermal desorption were used to monitor the adsorption of fluorine atoms. The reaction propagated through the formation of carbon-monofluoride species at the surface. It was observed that surface coverage with fluorine was greater when fluorine atoms were used instead of fluorine molecules. Smentkwoski *et al*. functionalized diamond (100) with fluorinated species by exposing C_4F_9I and CF_3I layers on diamond's surface to X-rays. This resulted in the decomposition of these molecules into reactive species, which in turn reacted with the surface. Interestingly X-ray photoelectron spectroscopy was used both for photodecomposition of the molecules and also as a characterization tool.[70,71] Gu *et al*. functionalized nanodiamond with fluorine by heating it in a mixture of fluorine and hydrogen.[72] This resulted in the introduction of almost 8.6 at. % fluorine. This fluorine functionalized nanodiamond was then reacted with alkyllithium reagents, diamines, and amino acids to obtain alkyl, amino, and amino acid functionalized diamond powder. Chlorine has also been used as another halogen to functionalize diamond's surface. Ando *et al*. attempted chlorination of hydrogen terminated diamond in the presence of Cl_2 gas.[73] [54,74-76] Ikeda *et al*. tried chlorination of hydrogen-terminated diamond by treatment with sulfuryl chloride.[77] Tsubota *et al*. attempted to chlorinate hydrogen terminated diamond powder in the presence of benzophenone (used as a photosensitizer), and AIBN (α,α′-azobisisobutyronitrile) and benzoyl peroxide as radical intitiators.[78,79] By FTIR, they observed

that hydrogen atoms could only be abstracted from the surface when benzoyl peroxide was the radical initiator. Although hydrogen atoms could be abstracted from the surface, the formation of C-Cl bonds on the surface could not be confirmed. Chlorination of the diamond surface with Cl_2 gas under UV light has also been successfully shown.[80,81]

Various groups have also tried to deposit metals on the surface of diamond. Nemanich *et al*. deposited titanium by resistively heating, which led to its deposition on the surface of a diamond crystal.[82] Jackman *et al*. deposited Cs on diamond.[83] Ion implantation has been used to deposit chromium ions into a diamond crystal.[84] Silane coupling agents have been used to modify the surface of oxidized diamond.[85-88] In one approach, Tsubota *et al*. oxidized hydrogen terminated diamond powder with H_2SO_4 or a mixture of H_2SO_4 and HNO_3 to increase the density of OH groups on the surface. The -OH terminated surface was then functionalized by exposing it to different kinds of silanes (*n*-octyltrimethoxysilane, 3-aminopropyltrimethoxysilane, or 3-mercaptopropyltrimethoxysilane).[89] Kuo *et al*. have performed electrochemical reduction of a phenyl diazonium salt on boron-doped diamond to modify the surface with nitrophenyl, trifluoromethylphenyl, and nitroazobenzene groups.[90]

Chlorinated diamond has also been used to introduce other functional groups onto diamond. Kusakabe *et al*. used chlorinated diamond to introduce amine groups.[91] In their approach, chlorinated diamond powder was treated with ammonia gas for 6 h at different temperatures. The reaction was characterized by XPS and DRIFT. Miller and Brown[80,81] and Miller[92] also attempted amination of chlorinated diamond powder by irradiating chlorinated diamond powder with UV light in an atmosphere of ammonia. Amine groups have also been introduced onto hydrogen-terminated diamond powder. Zhang *et al*. functionalized diamond with

amine groups by treating hydrogen terminated diamond either with an NH_3 plasma or with ammonia gas under UV light.[93,94]

Polymerization on diamond has also been attempted. Gu electropolymerized a thin film of a polyaniline/polyacrylate (PANI/PAA) copolymer onto a boron-doped diamond electrode to increase the density of carboxyl groups.[95] Jordan *et al*. grafted polystyrene onto an oxidized diamond surface by polymerization of styrene under UV light.[96] They also investigated the formation of self-assembled monolayers of 4-nitro-1,1-biphenyl-4-diazonium tetrafluoroborate (NBD) onto thin films of ultrananocrystalline nanodiamond.[96] The hydrogen-terminated surface was immersed in a saturated solution of 4-nitro-1,1-biphenyl-4-diazonium tetrafluoroborate in acetonitrile. The thickness of the resulting self-assembled monolayers was 1.2 nm. Cheng *et al*. functionalized nanodiamond particles with polymer brushes of polystyrene and poly(*t*-butyl methacrylate) (P*t*BMA).[97] Direct adsorption of amine-containing polymers to the oxidized surfaces of diamond particles has also been demonstrated. Saini *et al*. demonstrated the deposition of polyallylamine and its subsequent crosslinking with 1,2,5,6-diepoxycyclooctane.[98] Kong *et al*. showed noncovalent deposition of polylysine onto oxidized diamond powder.[99]

Atom transfer radical polymerization (ATRP) has been attempted to functionalize diamond. Matrab *et al*. used electrochemical reduction to grow polymethylmethacrylate and polystyrene brushes on thin diamond films.[100] Li *et al*. demonstrated the synthesis of methacrylate polymers on nanodiamond by atom transfer radical polymerization.[101]

Oxidation of diamond has been used to introduce different kinds of oxygen-containing functional groups such as hydroxyl, ether, carboxyl and carbonyl groups, *etc*. Many different oxidation techniques have been used for this purpose. As a wet chemical process, the surface can be treated with a solution of concentrated H_2SO_4 and HNO_3 at elevated temperatures.[102,103]

Other methods include oxygen plasma or exposure to beams of atoms,[104,105] thermal oxidation in an oxygen atmosphere,[106,107] ozone exposure,[108] photochemical oxidation,[87] electrochemical oxidation,[106,109] and hot-filament techniques.[110]

Use of diamond as a substrate for the attachment of biological molecules has also been investigated. DNA has been immobilized on diamond's surface using various approaches.[111,112] For example, Yang *et al*. functionalized diamond with thin films of oligonucleotides.[111] In their approach, they first aminated the surface of hydrogen terminated diamond. The resulting amine groups were then reacted with a crosslinker, sulphosuccinimidyl-4-(*n*-maleimidimethyl) cyclohexane-1-carboxylate (SSMCC). A thiolated DNA was then attached to the surface through the reaction between the –SH group of thiolated DNA and the carbon-carbon double bond of the cross-linker. X-ray photoelectron spectroscopy and optical fluorescence were used to characterize the resulting films.

1.5.2. Use of Diamond as a Sorbent in Separations

Many attempts have been made to use diamond as an adsorbent in separation science. The first attempt dates back to 1973 when Telepchak *et al*. tried to separate a mixture of benzene and anthracene using 10 µm diamond particles as a stationary phase in HPLC.[113] However, they could achieve only a partial separation of the two components. The number of theoretical plates was only 1500 per meter. Later Patel et al. used 3.8 µm particles of ultradisperse diamonds for both normal phase and reversed phase HPLC.[114] However, they could achieve only a partial separation of phenol and benzoic acid due to a very low column efficiency.

Nesterenko *et al*. continued research on the applicability of using diamond as a potential sorbent.[115-118] In one of their studies, they used irregularly shaped microdispersed, sintered

detonation nanodiamonds (MSDNs) as the packing material. Diamond particles (3-6 μm) were fractionated and washed with different organic solvents to narrow the size distribution of the particles. This helped improve the column efficiency. Particles were packed into a 150 × 4.0 mm i.d. stainless steel column. They separated a mixture of *n*-alkyl benzenes, and compared these results to those obtained using silica and alumina as packing materials.[115] A value of 15,400 theoretical plates per meter was obtained for *o*-xylene. Analytes had a much higher retention factor on diamond than on silica and alumina under similar conditions. Diamond's surface typically has a number of negatively charged oxygen-containing functional groups. Therefore, retention of polar aromatic compounds was also studied. The mobile phase was a mixture of *n*-hexane/2-propanol (97.5:2.5, v/v). The following retention order was observed for a series of benzene derivatives: bromobenzene < benzyl chloride < anisole < ethyl benzoate < nitrobenzene < benzaldehyde < benzyl alcohol < benzonitrile < acetophenone < benzophenone, which corroborates the presence of negatively charged functional groups on the surface.

In another study, Nesterenko and coworkers explored the possibility of using microdispersed sintered nanodiamond particles as an adsorbent for cation-exchange chromatography.[117] Two columns (100 mm × 4.0 mm and 50 mm × 4.0 mm) were connected in series. The mobile phase was 1.5 mM HNO_3 + 0.1 M KNO_3. Accordingly, a mixture of Mg^{2+}, Mn^{2+}, Co^{2+} and Cd^{2+} cations was separated, but peaks were broad and tailing. The authors attributed this effect to the presence of very small pores in the particles, which resulted in slow diffusion of metal ions. The height equivalent of a theoretical plate was 0.4 mm. In another experiment, a mixture of three metal cations, Mg^{2+}, Ca^{2+} and Ba^{2+}, was separated on a 100 mm × 4.0 mm column, where the eluent was 5 mM HNO_3.

In recent work, Nesterenko *et al*. demonstrated the use of microdispersed sintered nanodiamond as a stationary phase in normal phase chromatography.[118] They studied the retention characteristics of monoalkylbenzenes, polymethylbenzenes, di-*n*-alkylphthalates and polyaromatic hydrocarbons on diamond, and compared the retention characteristics of these analytes on diamond to silica gel, alumina and porous graphitic carbon. A mixture of eight alkyl benzenes was separated under normal phase conditions using *n*-pentane as the eluent. The authors were able to achieve nearly baseline separation of these analytes. A plate number of 45,300 plates per meter was observed for 1,3-diisopropylbenzene. The authors also demonstrated that if microdispersed, sintered nanodiamond particles were used, better selectivity could be achieved to separate a mixture of positional isomers of xylene, *i.e*., *o*-xylene, *m*-xylene and *p*-xylene.

Use of boron-doped diamond particles as a stationary phase in electrochemically modulated liquid chromatography (EMLC) has been demonstrated by Muna *et al*.[119] They were able to separate sodium 4-toluenesulfonate (TS), disodium 1,3-benzenedisulfonate (BDS), sodium benzenesulfonate (BS) and disodium 1,5-naphthalenedisulfonate (NDS).

Bondar *et al*. also investigated the possibility of using detonation nanodiamonds as an adsorbent in protein isolation.[120-123] In their recent work, they developed a new type of sorbent made from nanodiamonds and a polysaccharide matrix, which could be used for the separation of proteins in normal phase chromatography.[120] Chiganova[124] and Gordeev *et al*.[125] investigated the cation-exchange characteristics of synthetic ultradisperse diamonds. Chiganova used potentiometric titration to determine the types of carboxylic groups on the surface. He discovered that diamond's surface contains both strong and weak carboxylic groups, and found the following order of elution for alkali metal cations: $Li^+ > Na^+ > K^+$, which is in accordance with

the cation-exchange characteristics of a common carboxylic ion-exchange adsorbent. Bogatyreva *et al*.[126] studied cation-exchange properties of transition metal ions on diamond and found the following order of elution: $Fe^{2+} > Ni^{2+} > Cr^{4+}$.

Chang *et al*. used polyarginine-coated diamond nanoparticles for selective extraction of multiphosphorylated peptides.[127] In other work, they used carboxylated/oxidized diamond nanoparticles as a support for the removal of proteins and peptides from solution.[128,129] They have also used polylysine-coated diamond nanoparticles for the selective extraction of DNA oligonucleotides and their separation from proteins.[99] Sabu *et al*. also used carboxylated/oxidized diamond nanoparticles as a support for the extraction of proteins from biological samples.[130,131] Yang *et al*. modified diamond with polystyrene and sulfonated-polystyrene, and demonstrated the applicability of these materials as phenyl and cation-exchange phases, respectively.[132] 1-Naphthylamine was used as analyte to determine percent recovery, which for the phenyl- and cation-exchange phases were 65.8% and 101%, respectively. Both phases were chemically stable under extreme pH conditions.

1.6. Overview of My Dissertation

In this dissertation, I demonstrate the application of functionalized diamond in solid phase extraction and high performance liquid chromatography. In chapter 2, I demonstrated the applicability of amine-functionalized diamond powder in the solid phase extraction of cholesterol (a neutral lipid), hexadecanedioic acid (a fatty diacid) and palmitoyloleoylphosphatidylcholine (a polar lipid).[98] Diamond powder (38-65 μm) was functionalized with primary amine groups by first cleaning it in piranha solution and then treating it with an aqueous solution of polyallylamine (PAAm). Amine-functionalized diamond

powder was then either chemically crosslinked with 1,2,5,6-diepoxycyclooctane or thermally cured to improve its chemical stability. Stability studies were done on both functionalized diamond powder and a commercially available amino silica. It was found that diamond (both cross-linked and cured) was extremely stable from pH 0 to pH 14, while the amino-silica adsorbent disintegrated in basic solutions, and lost *ca.* 15% of its nitrogen under acidic conditions. However, the capacity of the amine-functionalized diamond sorbent was very low, which was attributed to the non-porous nature and, hence, low surface area of the diamond particles.

In chapter 3, I report the synthesis of C_{18}, C_8 and perfluoro phases on diamond powder by reaction of PAAm functionalized diamond powder with octadecylisocyanate, octylisocyanate and 3,3,4,4,5,5,6,6,7,7,8,8,9,9,10,10,10 heptadecafluorodecyl isocyanate, respectively.[133] Stability studies were performed on C_{18} functionalized diamond particles under extreme pH conditions (0-14). This phase was found to be reasonably stable under these conditions. Solid phase extraction was performed on C_{18} functionalized diamond powder using cyanazine and diazinon (two pesticides) as analytes. The percent recoveries of the C_{18} phase for diazinon and cyanazine were 98.7% and 101%, respectively. The column capacities of the C_{18} phase synthesized at room temperature and at 80°C were 12.980 ± 0.002 μg and 14.486 ± 0.007 μg of diazinon per gram of the coated support, respectively.

In chapter 4, I describe the synthesis of highly porous core-shell diamond particles and their use as a support for solid phase extraction and high performance liquid chromatography.[134] The particles were synthesized by layer-by-layer deposition of polyallylamine (PAAm) and nanodiamond particles (*ca.* 100-250 nm for SPE and *ca.* 10-50 nm for HPLC) around an oxidized microdiamond core (*ca.* 50 μm for SPE and *ca.* 3 μm for HPLC). These particles have

much higher surface area than particles employed in previous studies.[98,133] A *ca.* 80-fold increase in capacity was observed for the core shell particles compared to the non-porous particles employed in the earlier SPE studies.[98,133] Core-shell particles for normal phase and reversed phase HPLC were also prepared. I baseline separated a mixture of benzophenone and dinitrobenzene in the normal phase mode. I also achieved baseline separation of a mixture of benzene, toluene, xylene and mesitylene, and a mixture of two common pesticides, diazinon and cyanazine, on the reversed phase material. A plate number as high as 54,800 plates/meter was achieved for diazinon, which is the highest number ever achieved for a diamond-based LC column.

A unifying feature of the three chapters just described is the use of PAAm, where PAAm was used both for the functionalization of the surface and as an adhesive in the synthesis of diamond core-shell particles. The potential of PAAm in the functionalization of silicon surface was also investigated in another study (Chapter 5). In this work, microlens array patterning (MAP) and selective adsorption of PAAm was used in the fabrication of bioarrays on a silicon surface. A hexadecyl monolayer terminated silicon substrate was photopatterned using MAP in a few nanoseconds. A cationic surfactant was used to selectively deposit PAAm in the spots of a photopatterned silicon substrate. In the final step, reactions of adsorbed PAAm with various molecules of interest in bioconjugate chemistry were demonstrated.

I also completed a somewhat unrelated project that did not involve the use PAAm in surface functionalization. This work demonstrated the use of plasma/chemical vapor deposition to synthesize a durable hydrophobic coating on silicon and nylon substrates (Chapter 6). The substrate was air/oxygen plasma treated to remove adventitious contamination from the surface,

and introduce –OH groups onto it. A sequential chemical vapor deposition of two silanes was then performed to deposit a durable hydrophobic coating on the surface.

1.7. References

(1) Bennett, B.; Larter, S. R. *Anal. Chem.* **2000**, *72*, 1039-1044.

(2) Kaye, B.; Herron, W. J.; Macrae, P. V.; Robinson, S.; Stopher, D. A.; Venn, R. F.; Wild, W. *Anal. Chem.* **1996**, *68*, 1658-1660.

(3) Wang, J.; Ashley, K.; Marlow, D.; England, E. C.; Carlton, O. *Anal. Chem.* **1999**, *71*, 1027-1032.

(4) Hellstrom, J. K.; Mattila, P. H. *J. Agric. Food Chem.* **2008**, *56*, 7617-7624.

(5) Caboni, P.; Sarais, G.; Cabras, M.; Angioni, A. *J. Agric. Food Chem.* **2007**, *55*, 7288-7293.

(6) Volpi, N. *Anal. Chem.* **2007**, *79*, 6390-6397.

(7) Simpson, N. J. K. *Solid-Phase Extraction Principles, Techniques, and Applications*; Marcel Dekker: New York, 2000.

(8) Thurman, E. M.; Mills, M. S. *Solid-Phase Extraction Principles and Practice*; Wiley: New York, 1998.

(9) Nagy, K.; Jakab, A.; Fekete, J.; Vekey, K. *Anal. Chem.* **2004**, *76*, 1935-1941.

(10) Barrett, D. A.; Brown, V. A.; Davies, M. C.; Shaw, P. N. *Anal. Chem.* **1996**, *68*, 2170-2178.

(11) Berthod, A. *J. Chromatogr. A* **1991**, *549*, 1-28.

(12) Miller, J. M. *Chromatography: Concepts and Contrasts*; 2 ed.; John Wiley & Sons, Inc.: Hoboken, 2005.

(13) Nawrocki, J.; Dunlap, C.; McCormick, A.; Carr, P. W. *J. Chromatogr. A* **2004**, *1028*, 1 - 30.

(14) Layne, J. *J. Chromatogr. A* **2002**, *957*, 149-164.

(15) Cox, G. B. *J. Chromatogr. A* **1993**, *656*, 353-367.

(16) Kirkland, J. J.; Glajch, J. L.; Farlee, R. D. *Anal. Chem.* **1989**, *61*, 2-11.

(17) Glajch;, J. L.; Kirkland, J. J. **1989**.

(18) Trammell, B. C.; Ma, L. J.; Luo, H.; Jin, D. H.; Hillmyer, M. A.; Carr, P. W. *Anal. Chem.* **2002**, *74*, 4634-4639.

(19) Trammell, B. C.; Ma, L. J.; Luo, H.; Hillmyer, M. A.; Carr, P. W. *J. Am. Chem. Soc.* **2003**, *125*, 10504-10505.

(20) Trammell, B. C.; Ma, L. J.; Luo, H.; Hillmyer, M. A.; Carr, P. W. *J. Chromatogr. A* **2004**, *1060*, 61-76.

(21) Mistry, K.; Cortes, H.; Meunier, D.; Schmidt, C.; Feibush, B.; Grinberg, N.; Krull, I. *Anal. Chem.* **2002**, *74*, 617-625.

(22) McCormack, P.; Worsfold, P. J.; Gledhill, M. *Anal. Chem.* **2003**, *75*, 2647-2652.

(23) Lazaro, M. J.; Islas, C. A.; Herod, A. A.; Kandiyoti, R. *Energy Fuels* **1999**, *13*, 1212-1222.

(24) Nawrocki, J.; Rigney, M. P.; Mccormick, A.; Carr, P. W. *J. Chromatogr. A* **1993**, *657*, 229-282.

(25) Nawrocki, J.; Dunlap, C.; Li, J.; Zhao, J.; McNeff, C. V.; McCormick, A.; Carr, P. W. *J. Chromatogr. A* **2004**, *1028*, 31-62.

(26) Li, J. W.; Hu, Y.; Carr, P. W. *Anal. Chem.* **1997**, *69*, 3884-3888.

(27) Weber, T. P.; Carr, P. W.; Funkenbusch, E. F. *J. Chromatogr. A* **1990**, *519*, 31-52.

(28) Weber, T. P.; Carr, P. W. *Anal. Chem.* **1990**, *62*, 2620-2625.

(29) Blackwell, J. A.; Carr, P. W. *J. Chromatogr. A* **1992**, *596*, 27-41.

(30) Blackwell, J. A.; Carr, P. W. *Anal. Chem.* **1992**, *64*, 853-862.

(31) Mcneff, C.; Zhao, Q. H.; Carr, P. W. *J. Chromatogr. A* **1994**, *684*, 201-211.

(32) Blackwell, J. *Chromatogr.* **1993**, *35*, 133-138.

(33) Blackwell, J. A.; Carr, P. W. *J. Chromatogr. A* **1991**, *549*, 59-75.

(34) Blackwell, J. A.; Carr, P. W. *J. Liq. Chromatogr. Relat. Technol.* **1991**, *14*, 2875 - 2889.

(35) Sun, L.; Carr, P. W. *Anal. Chem.* **1995**, *67*, 3717-3721.

(36) Sun, L.; McCormick, A. V.; Carr, P. W. *J. Chromatogr, A* **1994**, *658*, 465-473.

(37) Tanaka;, H.; Koike;, M.; Nakajima, T. *Analyt. Sci.* **1986**, *2*, 385-388.

(38) Moreau, R. A.; Kohout, K.; Singh, V. *Lipids* **2002**, *37*, 1201-1204.

(39) Koizumi, K. *J. Chromatogr. A* **1996**, *720*, 119-126.

(40) Hanai, T. *J. Chromatogr. A* **2003**, *989*, 183-196.

(41) Ross, P.; Knox, J. H. *Adv. Chrom., Vol 37* **1997**, *37*, 121-162.

(42) West, C.; Elfakir, C.; Lafosse, M. *J. Chromatogr. A, In Press, Corrected Proof.*

(43) Pereira, L. *J. Liq. Chromatogr. Relat. Technol.* **2008**, *31*, 1687 - 1731.

(44) Kitahata, S.; Hara, K.; Fujita, K.; Nakano, H.; Kuwahara, N.; Koizumi, K. *Biosci. Biotethnol. Biochem.* **1992**, *56*, 1386-1391.

(45) Watanabe, Y.; Nakamoto, C.; Ozaki, S.; Sato, M.; Koizumi, K. *J. Carbohydr. Chem.* **1993**, *12*, 685-692.

(46) Koizumi, K.; Tanimoto, T.; Fujita, K.; Hara, K.; Kuwahara, N.; Kitahata, S. *Carbohydr. Res.* **1993**, *238*, 75-91.

(47) Hiraga, Y.; Kinoshita, T. *J. Chromatogr. A* **1985**, *342*, 269-275.

(48) Hung, Y. L.; Kai, M.; Nohta, H.; Ohkura, Y. *J. Chromatogr. A* **1984**, *305*, 281-294.

(49) Petritis, K.; Chaimbault, P.; Elfakir, C.; Dreux, M. *J. Chromatogr. A* **2000**, *896*, 253-263.

(50) Chaimbault, P.; Petritis, K.; Elfakir, C.; Dreux, M. *J. Chromatogr. A* **2000**, *870*, 245-254.

(51) Desportes, C.; Charpentier, N.; Duteurtre, B.; Maujean, A.; Duchiron, F. *J. Chromatogr. A* **2000**, *893*, 281-291.

(52) Haddad, P. R.; Nesterenko, P. N.; Buchberger, W. *J. Chromatogr. A* **2008**, *1184*, 456-473.

(53) Nesterenko, P. N.; Haddad, P. R. *Analyt. Bioanalyt. Chem.* **2010**, *396*, 205-211.

(54) Ando, T.; Ishii, M.; Kamo, M.; Sato, Y. *Journal of the Chemical Society-Faraday Transactions* **1993**, *89*, 1783-1789.

(55) Jiang, T. L.; Xu, K.; Ji, S. F. *J. Chem. Soc., Faraday Trans.* **1996**, *92*, 3401-3406.

(56) Yang, W. S.; Butler, J. E.; Russell, J. N.; Hamers, R. J. *Langmuir* **2004**, *20*, 6778-6787.

(57) Tse, K. Y.; Nichols, B. M.; Yang, W. S.; Butler, J. E.; Russell, J. N.; Hamers, R. J. *J. Phys. Chem. B* **2005**, *109*, 8523-8532.

(58) Wang, S. H.; Swain, G. M. *J. Phys. Chem. C* **2007**, *111*, 3986-3995.

(59) Kondo, T.; Aoshima, S.; Honda, K.; Einaga, Y.; Fujishima, A.; Kawai, T. *J. Phys. Chem. C* **2007**, *111*, 12650-12657.

(60) Strother, T.; Knickerbocker, T.; Russell, J. N.; Butler, J. E.; Smith, L. M.; Hamers, R. J. *Langmuir* **2002**, *18*, 968-971.

(61) Nichols, B. M.; Butler, J. E.; Russell, J. N.; Hamers, R. J. *J. Phys. Chem. B* **2005**, *109*, 20938-20947.

(62) Yang, W. S.; Auciello, O.; Butler, J. E.; Cai, W.; Carlisle, J. A.; Gerbi, J.; Gruen, D. M.; Knickerbocker, T.; Lasseter, T. L.; Russell, J. N.; Smith, L. M.; Hamers, R. J. *Nat. Mater.* **2003**, *2*, 63-63.

(63) Lu, M. C.; Knickerbocker, T.; Cai, W.; Yang, W. S.; Hamers, R. J.; Smith, L. M. *Biopolymers* **2004**, *73*, 606-613.

(64) Hartl, A.; Schmich, E.; Garrido, J. A.; Hernando, J.; Catharino, S. C. R.; Walter, S.; Feulner, P.; Kromka, A.; Steinmuller, D.; Stutzmann, M. *Nat. Mater.* **2004**, *3*, 736-742.

(65) Kim, C. S.; Mowrey, R. C.; Butler, J. E.; Russell, J. N. *J. Phys. Chem. B* **1998**, *102*, 9290-9296.

(66) Wang, G. T.; Bent, S. F.; Russell, J. N.; Butler, J. E.; D'Evelyn, M. P. *J. Am. Chem. Soc.* **2000**, *122*, 744-745.

(67) Freedman, A.; Stinespring, C. D. *Appl. Phys. Lett.* **1990**, *57*, 1194-1196.

(68) Freedman, A.; Stinespring, C. D. *Carbon* **1990**, *28*, 806-806.

(69) Freedman, A. *J. Appl. Phys.* **1994**, *75*, 3112-3120.

(70) Smentkowski, V. S.; Yates, J. T. *Science* **1996**, *271*, 193-195.

(71) Smentkowski, V. S.; Yates, J. T.; Chen, X. J.; Goddard, W. A. *Surf. Sci.* **1997**, *370*, 209-231.

(72) Liu, Y.; Gu, Z. N.; Margrave, J. L.; Khabashesku, V. N. *Chem. Mater.* **2004**, *16*, 3924-3930.

(73) Ando, T.; Yamamoto, K.; Matsuzawa, M.; Takamatsu, Y.; Kawasaki, S.; Okino, F.; Touhara, H.; Kamo, M.; Sato, Y. *Diamond Relat. Mater.* **1996**, *5*, 1021-1025.

(74) Ando, T.; NishitaniGamo, M.; Rawles, R. E.; Yamamoto, K.; Kamo, M.; Sato, Y. *Diamond Relat. Mater.* **1996**, *5*, 1136-1142.

(75) Ando, T.; Yamamoto, K.; Kamo, M.; Sato, Y.; Takamatsu, Y.; Kawasaki, S.; Okino, F.; Touhara, H. *J. Chem. Soc., Faraday Trans.* **1995**, *91*, 3209-3212.

(76) Ando, T.; Yamamoto, K.; Suehara, S.; Kamo, M.; Sato, Y.; Shimosaki, S.; Gamo, M. N. *J. Chin. Chem. Soc.* **1995**, *42*.

(77) Ikeda, Y.; Saito, T.; Kusakabe, K.; Morooka, S.; Maeda, H.; Taniguchi, Y.; Fujiwara, Y. *Diamond Relat. Mater.* **1998**, *7*, 830-834.

(78) Tsubota, T.; Hirabayashi, O.; Ida, S.; Nagaoka, S.; Nagata, M.; Matsumoto, Y. *Diamond Relat. Mater.* **2002**, *11*, 1360-1365.

(79) Tsubota, T.; Urabe, K.; Egawa, S.; Takagi, H.; Kusakabe, K.; Morooka, S.; Maeda, H. *Diamond Relat. Mater.* **2000**, *9*, 219-223.

(80) Miller, J. B.; Brown, D. W. *Diamond Relat. Mater.* **1995**, *4*, 435-440.

(81) Miller, J. B.; Brown, D. W. *Langmuir* **1996**, *12*, 5809-5817.

(82) Vanderweide, J.; Nemanich, R. J. *J. Vac. Sci. Technol. B* **1992**, *10*, 1940-1943.

(83) Loh, K. P.; Foord, J. S.; Egdell, R. G.; Jackman, R. B. *Diamond Relat. Mater.* **1997**, *6*, 874-878.

(84) Stock, H. R.; Kohscheen, J.; Mayr, P. *Analyt. Bioanalyt. Chem.* **2002**, *374*, 1335-1337.

(85) Notsu, H.; Fukazawa, T.; Tatsuma, T.; Tryk, D. A.; Fujishima, A. *Electrochem. Solid-State Lett.* **2001**, *4*, H1-H3.

(86) Hernando, J.; Pourrostami, T.; Garrido, J. A.; Williams, O. A.; Gruen, D. M.; Kromka, A.; Steinmuller, D.; Stutzmann, M. *Diamond Relat. Mater.* **2007**, *16*, 138-143.

(87) Boukherroub, R.; Wallart, X.; Szunerits, S.; Marcus, B.; Bouvier, P.; Mermoux, M. *Electrochem. Commun.* **2005**, *7*, 937-940.

88) Actis, P.; Manesse, M.; Nunes-Kirchner, C.; Wittstock, G.; Coffinier, Y.; Boukherroub, R.; Szunerits, S. *Phys. Chem. Chem. Phys.* **2006**, *8*, 4924-4931.

(89) Tsubota, T.; Ida, S.; Hirabayashi, O.; Nagaoka, S.; Nagayama, S.; Nagata, M.; Matsumoto, Y. *J. Ceram. Soc. Jpn.* **2002**, *110*, 904-910.

(90) Kuo, T. C.; McCreery, R. L.; Swain, G. M. *Electrochem. Solid-State Lett.* **1999**, *2*, 288-290.

(91) Sotowa, K. I.; Amamoto, T.; Sobana, A.; Kusakabe, K.; Imato, T. *Diamond Relat. Mater.* **2004**, *13*, 145-150.

(92) Miller, J. B. *Surf. Sci.* **1999**, *439*, 21-33.

(93) Szunerits, S.; Jarna, C.; Coffinier, Y.; Marcus, B.; Delabouglise, D.; Boukherroub, R. *Electrochem. Commun.* **2006**, *8*, 1185-1190.

(94) Zhang, G. J.; Song, K. S.; Nakamura, Y.; Ueno, T.; Funatsu, T.; Ohdomari, I.; Kawarada, H. *Langmuir* **2006**, *22*, 3728-3734.

(95) Gu, H. R.; di Su, X.; Loh, K. P. *J. Phys. Chem. B* **2005**, *109*, 13611-13618.

(96) Lud, S. Q.; Steenackers, M.; Jordan, R.; Bruno, P.; Gruen, D. M.; Feulner, P.; Garrido, J. A.; Stutzmann, M. *J. Am. Chem. Soc.* **2006**, *128*, 16884-16891.

(97) Cheng, J. L.; He, J. P.; Li, C. X.; Yang, Y. L. *Chem. Mater.* **2008**, *20*, 4224-4230.

(98) Saini, G.; Yang, L.; Lee, M. L.; Dadson, A.; Vail, M. A.; Linford, M. R. *Anal. Chem.* **2008**, *80*, 6253-6259.

(99) Kong, X. L.; Huang, L. C. L.; Liau, S. C. V.; Han, C. C.; Chang, H. C. *Anal. Chem.* **2005**, *77*, 4273-4277.

(100) Matrab, T.; Chehimi, M. M.; Boudou, J. P.; Benedic, F.; Wang, J.; Naguib, N. N.; Carlisle, J. A. *Diamond Relat. Mater.* **2006**, *15*, 639-644.

(101) Li, L.; Davidson, J. L.; Lukehart, C. M. *Carbon* **2006**, *44*, 2308-2315.

(102) Maier, F.; Ristein, J.; Ley, L. *Phys. Rev. B* **2001**, *64*, art. no.-165411.

(103) Ando, T.; Inoue, S.; Ishii, M.; Kamo, M.; Sato, Y.; Yamada, O.; Nakano, T. *J. Chem. Soc., Faraday Trans.* **1993**, *89*, 749-751.

(104) Wilson, J. I. B.; Walton, J. S.; Beamson, G. *J. Electron. Spectrosc. Relat. Phenom.* **2001**, *121*, 183-201.

(105) Loh, K. P.; Xie, X. N.; Yang, S. W.; Zheng, J. C. *J. Phys. Chem. B* **2002**, *106*, 5230-5240.

(106) Ferro, S.; Dal Colle, M.; De Battisti, A. *Carbon* **2005**, *43*, 1191-1203.

(107) Nakamura, J.; Ito, T. *Appl. Surf. Sci.* **2005**, *244*, 301-304.

(108) Riedel, M.; Ristein, J.; Ley, L. *Diamond Relat. Mater.* **2004**, *13*, 746-750.

(109) Goeting, C. H.; Marken, F.; Gutierrez-Sosa, A.; Compton, R. G.; Foord, J. S. *Diamond Relat. Mater.* **2000**, *9*, 390-396.

(110) Pehrsson, P. E.; Mercer, T. W. *Surf. Sci.* **2000**, *460*, 74-90.

(111) Yang, W. S.; Auciello, O.; Butler, J. E.; Cai, W.; Carlisle, J. A.; Gerbi, J.; Gruen, D. M.; Knickerbocker, T.; Lasseter, T. L.; Russell, J. N.; Smith, L. M.; Hamers, R. J. *Nat. Mater.* **2002**, *1*, 253-257.

(112) Ushizawa, K.; Sato, Y.; Mitsumori, T.; Machinami, T.; Ueda, T.; Ando, T. *Chem. Phys. Lett.* **2002**, *351*, 105-108.

(113) Telepchak, J. *Chromatographia* **1973**, *6*, 234.

(114) Patel, B. A.; Rutt, K. J.; Padalko, V. I.; Mikhalovsky, S. V. *J. Superhard Mater.* **2002**, *6*, 51.

(115) Nesterenko, P. N.; Fedyanina, O. N.; Volgin, Y. V. *Analyst* **2007**, *132*, 403-405.

(116) Fedyanina, O. N.; Nesterenko, P. N. *Russ. J. Phys. Chem. A* **2010**, *84*, 476-480.

(117) Nesterenko, P. N.; Fedyanina, O. N.; Volgin, Y. V.; Jones, P. *J. Chromatogr. A* **2007**, *1155*, 2-7.

(118) Nesterenko, P. N.; Fedyanina, O. N. *J. Chromatogr. A* **2010**, *1217*, 498-505.

(119) Muna, G. W.; Swope, V. M.; Swain, G. M.; Porter, M. D. *J. Chromatogr. A* **2008**, *1210*, 154-159.

(120) Purtov, K. V.; Puzyr, A. P.; Bondar, V. S. *Dokl. Biochem. Biophys.* **2008**, *419*, 72-74.

(121) Puzyr, A. P.; Purtov, K. V.; Shenderova, O. A.; Luo, M.; Brenner, D. W.; Bondar, V. S. *Dokl. Biochem. Biophys.* **2007**, *417*, 299-301.

(122) Bondar, V. S.; Pozdnyakova, I. O.; Puzyr, A. P. *Fiz. Tverd. Tela* **2004**, *46*, 737-739.

(123) Bondar, V. S.; Puzyr, A. P. *Konstr. Kompoz. Mater.* **2005**, 80-94.

(124) Chiganova, G. A. *Kolloidnyj Zhurnal* **1994**, *56*, 266-268.

(125) Gordeev, S. K.; Taushkanova, O. G.; Smirnov, E. P.; Martynova, L. M. *Zhurnal Obshchei Khimii* **1983**, *53*, 2426-2428.

(126) Bogatyreva, G. P.; Marinich, M. A.; Voloshin, M. N.; Malogolovets, V. G.; Gvyazdovskaya, V. S.; Gavrilova, V. S. *J. Superhard Mater.* **1999**, *6*, 41-44.

(127) Chang, C. K.; Wu, C. C.; Wang, Y. S.; Chang, H. C. *Anal. Chem.* **2008**, *80*, 3791-3797.

(128) Tzeng, Y. K.; Chang, C. C.; Huang, C. N.; Wu, C. C.; Han, C. C.; Chang, H. C. *Anal. Chem.* **2008**, *80*, 6809-6814.

(129) Kong, X. L.; Huang, L. C. L.; Hsu, C. M.; Chen, W. H.; Han, C. C.; Chang, H. C. *Anal. Chem.* **2005**, *77*, 259-265.

(130) Sabu, S.; Yang, F. C.; Wang, Y. S.; Chen, W. H.; Chou, M. I.; Chang, H. C.; Han, C. C. *Anal. Biochem.* **2007**, *367*, 190-200.

(131) Chen, W. H.; Lee, S. C.; Sabu, S.; Fang, H. C.; Chung, S. C.; Han, C. C.; Chang, H. C. *Anal. Chem.* **2006**, *78*, 4228-4234.

(132) Yang, Li. PhD dissertation, Brigham Young University, Provo, Utah

(133) Saini, G. W., L.A.; Herbert, D.; Biggs, K.N.; Dadson, A.; Vail, M.A.; Linford, M.R. *J. Chromatogr. A* **2008**.

(134) Saini, G.; Jensen, D. S.; Wiest, L. A.; M.A., V.; Dasdon, A.; M.L., L.; Shutthanandan, V.; Linford, M. R. *Anal. Chem.* **2010**, 4448-4456.

PART II. FUNCTIONALIZATION OF DIAMOND AND ITS APPLICATION IN SPE AND HPLC

Chapter 2. Amino-Modified Diamond as a Durable Stationary Phase for Solid-Phase Extraction*

2.1. Abstract

A highly stable amino stationary phase has been synthesized on diamond, and its application demonstrated in solid-phase extraction (SPE). The synthesis consists of spontaneous and self-limiting adsorption of polyallylamine (PAAm) from aqueous solution onto oxidized diamond. Thermal curing under reduced pressure or chemical cross-linking with a diepoxide fixed the polymer to the particles. The resulting adsorbents are stable under even extreme pH conditions (from at least pH 0-14) and significantly more stable than a commercially-available amino SPE adsorbent. Coated diamond particles were characterized by X-ray photoelectron spectroscopy (XPS) and diffuse reflectance Fourier transform-infrared spectroscopy (DRIFT). Model silicon surfaces were characterized by spectroscopic ellipsometry and wetting. Solid-phase extraction was demonstrated using cholesterol, hexadecanedioic acid, and palmitoyloleoylphosphatidylcholine as analytes, and these results were compared to those obtained with commercially-available materials. Breakthrough curves indicate that, as expected, porous diamond particles have higher analyte capacity than nonporous solid particles.

---

*This chapter is reproduced with permission from (Gaurav Saini, Li Yang, Milton L. Lee, Andrew Dadson, Michael A. Vail and Matthew R. Linford) *Anal Chem*. **2008**, *80(16)*, 6253-6259.

2.2. Introduction

Solid-phase extraction (SPE) is a much-used technique for sample preparation, purification, concentration, and cleanup.[1,2] It has, in many cases, replaced liquid-liquid extraction, and it often precedes high-performance liquid chromatography (HPLC) in analytical analyses. SPE has been referred to as on/off chromatography because ideally it is designed to either perfectly retain or completely release (not retain) analytes of interest.

Diamond is an extraordinary material because of its chemical inertness, hardness, high thermal conductivity, and optical transparency. Diamond's chemical inertness and hardness make it an ideal material in a number of applications. Indeed, there is increasing recognition (*vide infra*) that synthetic diamond, which has become relatively inexpensive, might function well as a stationary phase for HPLC and SPE.

I demonstrate the spontaneous and self-limiting adsorption of a water-soluble polymer to diamond and its application as an SPE stationary phase. This polyelectrolyte (polyallylamine, PAAm,[3,4] see Figure 2.1) contains pendant primary amines along its backbone, and is commercially available in a variety of molecular weights. Primary amines are one of the most useful reactive functional groups in organic and bioconjugate chemistry.[5,6] These amine groups should allow PAAm-coated diamond particles to function in a manner analogous to commercially available amino phases for SPE and HPLC. PAAm adsorption and its subsequent reactivity are confirmed on diamond particles by X-ray photoelectron spectroscopy (XPS) and diffuse reflectance Fourier transform-infrared spectroscopy (DRIFT) and on model silicon surfaces by spectroscopic ellipsometry and wetting. Stability tests show that under strongly basic and acidic conditions, the adsorbed PAAm coating on diamond is moderately stable. These results are compared to the stability of a commercially available SPE amino phase. Through

chemical cross-linking or by thermal curing, I show that the PAAm coated diamond can be given complete stability at both very high and very low pH. I then successfully demonstrate the use of PAAm-coated diamond as a sorbent for SPE, and compare my results to those obtained with materials from two different vendors.

There are now a few recent examples of the use of diamond in SPE and HPLC. For example, Chang and co-workers have used uncoated diamond nanoparticles terminated with carboxyl groups for the extraction of proteins.[7] They also reported protein capture using uncoated diamond nanoparticles,[8] and in another study, they demonstrated the use of polylysine coated diamond nanocrystals for capturing oligonucleotides from solution.[9] No SPE was performed in this study, and the polylysine was not cross-linked or cured. Nesterenko and co-workers have also demonstrated HPLC with uncoated diamond as a stationary phase.[10,11]

2.3. Experimental Section

2.3.1. Reagents

(See Figure 1.1) Poly(allylamine) (M_w approximately 65 000, 20 wt % solution in water, Aldrich, Milwaukee, WI), 1,2,5,6- diepoxycyclooctane (96%, Aldrich), 1,16-hexadecanedioic acid (≥98%, Aldrich), cholesterol (95%, Aldrich), 2-propanol (99.5%, Mallinckrodt Chemicals, Phillipsburg, NJ), and palmitoyloleoylphosphatidylcholine (Avanti Polar Lipids, Alabaster, AL) were used as received. Diamond powder (70 μm and sintered) was provided by U.S. Synthetic (Orem, UT).

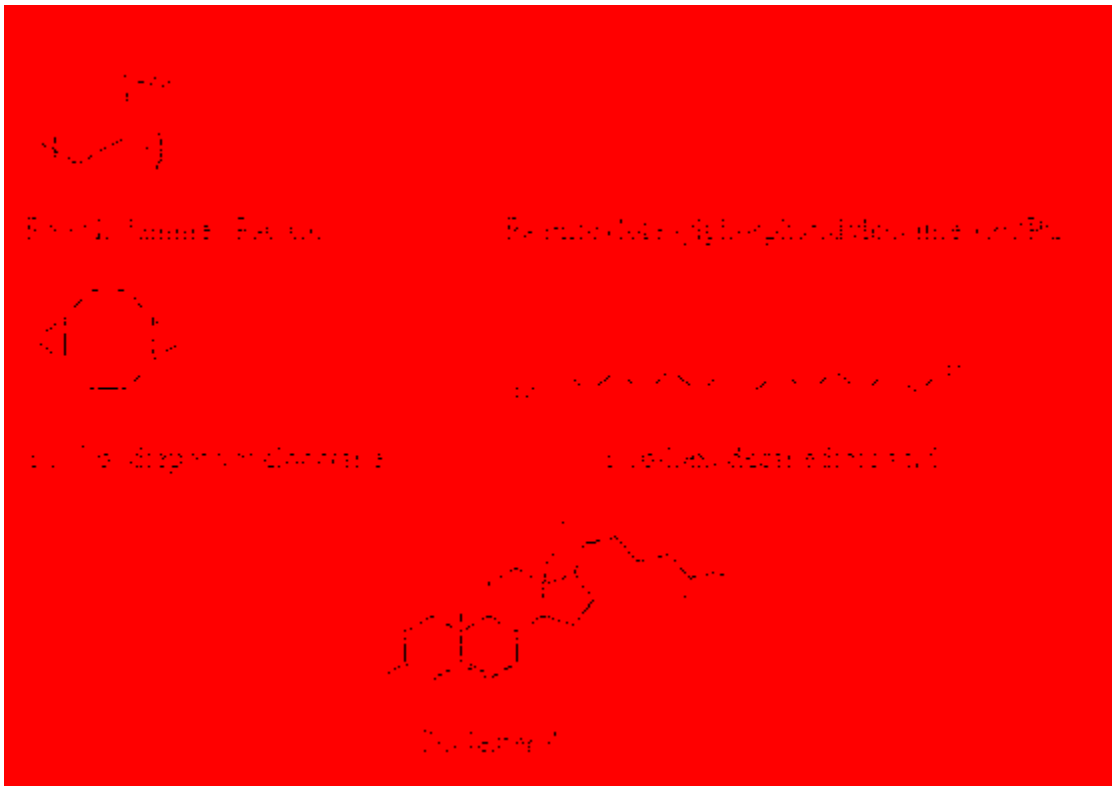

Figure 2.1. Structure of chemicals used in the study.

2.3.2. Substrates

Silicon wafers (test grade, n-type, <1-0-0> orientation, 2−6 Ω cm) were purchased from UniSil (Santa Clara, CA) and cleaved into approximately 1.5 cm × 1.5 cm pieces. Porous diamond particles were prepared by pressing 2 μm diamond grit and then by crushing and sizing it. The 38−65 μm fraction was employed as an adsorbent for SPE in this study.

2.3.3. Surface Cleaning

Prior to any surface treatment, diamond powder was cleaned in 100 mL of piranha solution (70% H_2SO_4/30% concentrated H_2O_2) at 100°C for 1 h and then thoroughly washed with deionized water. Silicon wafers were lightly brushed with a camel hair brush using 2 wt % sodium dodecylsulfate solution in water, then rinsed thoroughly with ultrapure water obtained from a Milli-Q (OM-154) water system from Millipore, and finally plasma cleaned at high power (16 W applied to the RF coil) for 1 min using a plasma cleaner (model PDC-32G) from Harrick Plasma (Ithaca, NY).

2.3.4. Hydrogen Termination of Diamond Powder

Diamond powder was hydrogen terminated by heating it in a furnace in an atmosphere of 5% H_2 in Ar at 900°C for 28 h (this is a noncombustible gas mixture). Hydrogen termination of diamond can also be performed using pure H_2 gas.[12] The powder was shaken twice during this process to facilitate hydrogen termination over all surfaces of the particles.

2.3.5. Poly(allylamine) (PAAm) Deposition

A 0.375 wt % solution of poly(allylamine) was made by dissolving 0.75 g of PAAm (20 wt % solution in water) in 40 mL of ultrapure water. Piranha-cleaned diamond powder (5 g) was poured into this solution, and polymer adsorption was allowed to take place for 1 h at room temperature. The solution was shaken every 5 min for approximately 10 s to completely expose the diamond particles to the PAAm solution. After adsorption, PAAm-functionalized diamond powder was sonicated in ultrapure water for approximately 10 min. The water was exchanged 4−5 times during this sonication procedure. Finally, the PAAm functionalized diamond powder was captured on a filter funnel and washed with copious amounts of ultrapure water for approximately 30 min. This coating and cleaning procedure was employed for both the 70 μm and porous 38-65 μm diamond material employed in this study, with the exc eption that the 38−65 μm material was not filtered. The porous particles were repeatedly sonicated in approximately 200 mL of ultrapure water, where the water was decanted and replaced with fresh water 5−6 times during the cleaning procedure. The particles were then dried in a vacuum oven. For deposition of PAAm onto native silicon oxide on silicon, silicon wafers were immersed in 10 mL of a 0.1 wt % solution of PAAm for 35 min. The wafers were then washed with ultrapure water and dried with a jet of nitrogen.

2.3.6. Curing of PAAm Functionalized Diamond Powder

Curing of PAAm functionalized diamond powder took place in a vacuum oven at reduced pressure and at elevated temperature (approximately 115°C, for 2.5 h). The vacuum for this oven was provided by a rotary vane pump. The system contained a dry ice/acetone cooled trap that prevented back streaming of oil from the pump.

2.3.7. Chemical Cross-Linking of PAAm-Functionalized Diamond Powder

Adsorbed PAAm on diamond powder was cross-linked with 1,2,5,6-diepoxycyclooctane. This molecule has two strained epoxide rings that make it reactive with the primary amine groups of PAAm. Since cross-linking of adsorbed PAAm with 1,2,5,6-diepoxycyclooctane results in the immobilization of hydrophobic cyclooctyl rings and hydrophilic -OH groups on the surface, this reaction will lead to the formation of a stationary phase with some mixed mode character. A 3.65 wt % solution of 1,2,5,6-diepoxycyclooctane was made in isopropanol, and 5 g of PAAm-functionalized diamond powder was immersed in 40 mL of this solution. Alcohols are effective solvents for catalyzing amine-epoxide reactions. The reaction was performed in a sealed, thick-walled glass reaction vessel at 80°C for 12 h. After this reaction, the powder was sonicated first in approximately 70 mL of isopropanol for 5 min and then in approximately 70 mL of dichloromethane for 5 min. The solvents were exchanged with clean solvent three times during sonication with each solvent. Finally, the powder was captured on the glass frit of a filter funnel (ChemGlass, 15 mL, fine pore size frit), and washed with copious amounts of dichloromethane for 15 min. To cross-link PAAm on planar silicon, the PAAm-functionalized surface was immersed in 10 mL of 0.6 wt % 1,2,5,6-diepoxycyclooctane in isopropanol. This reaction was also performed in a sealed, thick-walled glass tube at 80°C for 12 h. After the reaction, the surfaces were rinsed first with isopropanol and then with dichloromethane.

2.3.8. Stability Studies

Approximately 2.5 M NaOH and 2.5 M HCl solutions were prepared for pH stability studies. An amount of 0.2 g of each adsorbent was immersed separately in either the NaOH or

HCl solution for 38 h. Finally, the particles were captured on a filter funnel as before (*vide supra*) and rinsed with copious quantities of ultrapure water.

2.3.9. Surface Analysis

X-ray photoelectron spectroscopy (XPS) was performed with an SSX-100 instrument from Surface Sciences (Bend, OR) using an Al Kα source and a hemispherical analyzer. An electron flood gun was employed for charge compensation, and this charge compensation was further enhanced with a fine Ni mesh approximately 0.5-1.0 mm above the surface. FT-IR was performed with a Magna-IR 560 spectrometer from Nicolet (Madison, WI). Spectroscopic ellipsometry was performed with an M-2000 instrument from the J.A. Woollam Company (Lincoln, NE). The optical constants of silicon dioxide were used to model adsorbed PAAm films, which is appropriate because of the similarity between the optical constants of SiO_2 and most organic materials, especially over much of the visible region of the spectrum and also because of the thinness of the PAAm films. Advancing water contact angles were measured with a contact angle goniometer, model 100-00 from Ramé-Hart (Netcong, NJ).

2.3.10. Electrospray Ionization-Mass Spectrometry (ESI-MS)

ESI-MS was performed on an Agilent Technologies LC/MSD TOF system by direct infusion of several microliters of sample along with the mobile phase: 75% MeOH and 25% water with 5 mM ammonium formate. In positive ion mode, the charging voltage and the capillary voltage were set at 900 and 3500 V, respectively, and the skimmer was operated at 60 V. The nebulizer was at 35 psi, and the gas temperature was 350°C. The flow rate of the nitrogen drying gas was set at 12 L/min. All of the instrument parameters in negative ion mode were

identical to those in positive ion mode except the capillary voltage and drying gas flow rate, which were set at 4000 V and 8 L/min, respectively.

The ESI-MS is a communal instrument that gets heavy use in the department; it is not uncommon to see spurious peaks in the spectra from the instrument. The peak at *m*/*z* 199.01 (*vide infra*) showed up only in the mass spectra of three fractions in the SPE of 1,16-hexadecanedioic acid, *i.e.*, in panels b-d of Figure 2.2, which were taken on the same day. This peak did not show up in the breakthrough volume determination study, which used 1,16-hexadecanedioic acid as the analyte, or in the 2% acetic acid/diethyl ether fraction during SPE of the three component mixture, *i.e.*, cholesterol, 1,16-hexadecanedioic acid, and POPC, which were taken on other days. Thus it was inferred that this peak was due to contamination and was therefore removed.

2.4. Solid-Phase Extraction

SPE of different analytes was performed with commercially-available amino columns (Phenomenex Strata NH_2, 55 μM, 70 Å, 1.2 cm^3 of packing material, Torrance, CA, and Varian Bond Elut NH_2, 47–60 μM, 58−87 Å, 0.95 cm^3, Lake Forest, CA) and amine-functionalized diamond particles. For SPE experiments, the material in a commercially available cartridge (from Phenomenex) was replaced by the amine-functionalized diamond stationary phase. A control experiment was performed that showed that neither the plastic cartridge nor the frits retained analytes. The same volume (approximately 1.40 cm^3) of packing material was used in all experiments. To improve packing, the cartridges were washed with water under negative pressure from the house vacuum during loading. Finally, the columns were dried using house vacuum.

Prior to SPE, cartridges containing the amino-diamond phase were first conditioned with six column volumes of 0.5 M NH_4OH to deprotonate any protonated amine groups and then with three column volumes each of isopropanol, 50% isopropanol/50% hexane, and hexane. Analyses of individual analytes were then performed by loading 0.1 mL of cholesterol in chloroform (0.05 mg/mL), 0.1 mL of palmitoyloleoylphosphatidylcholine in chloroform (0.05 mg/mL), or 0.1 mL of 1,16-hexadecanedioic acid dissolved in a 4:1 mixture (v/v) of chloroform and isopropanol (0.5 mg/mL).

A lipid separation protocol was used to test PAAm-coated diamond. In this procedure, neutral lipids are eluted with chloroform, fatty acids are eluted with 2% acetic acid in diethyl ether, and phospholipids are eluted with methanol. This method was originally developed by Kaluzny and co-workers for performing solid-phase extraction of lipid mixtures on amino SPE phases.[13] This procedure, or a modified version of it, has been used a number of times to this end.[14-16] (I used a slightly modified version of the Kaluzny protocol, employing chloroform instead of 2:1 chloroform/2-propanol in the first elution).

In practice, amino-modified diamond SPE adsorbents could be repeatedly used without noticeable degradation. Before each reuse, the column was washed with methanol several times to remove any traces of palmitoyloleoylphosphatidylcholine (POPC) from the previous run. ESI-MS was performed on the final methanol wash to verify the absence of POPC in the column.

2.4.1. Solid-Phase Extraction of the Three Component Mixture

Solid-phase extraction was also performed on a mixture of cholesterol, hexadecanedioic acid, and POPC. A solution of these three components was made by dissolving 0.4 mg of POPC, 4.0 mg of hexadecanedioic acid, and 5.0 mg of cholesterol in a mixture of chloroform (9 mL)

and isopropanol (1 mL). The diamond amino column was conditioned using the same procedure as mentioned before. The Phenomenex and Varian materials were similarly conditioned but not with the NH_4OH solution. A volume of 0.1 mL of the three component solution was loaded onto the column after conditioning, and cholesterol, hexadecanedioic acid, and palmitoyloleoylphosphatidylcholine were eluted with three column volumes of chloroform, 2% acetic acid in diethyl ether, and methanol, respectively.

2.4.2. Breakthrough Curves

The analyte used for determination of breakthrough volumes was 1,16-hexadecanedioic acid. The column was first conditioned using the procedures mentioned above. After conditioning, the analyte solution was loaded onto the cartridge. The column was kept wet, and the flow rate was kept constant during the process. Equal volumes of the fractions eluting from the column were collected in separate vials. Finally, these fractions were analyzed by ESI-MS. Breakthrough curves had sigmoidal shapes. The breakthrough volume was calculated from the point on the curve corresponding to 5% of the average value at the maximum (plateau region).

2.5. Results and Discussion

2.5.1. PAAm Adsorption, Thermal Curing, and Chemical Cross-Linking

Prior to polyelectrolyte adsorption, diamond particles were cleaned in piranha solution, which is an extremely reactive solution that is widely used for removing organic contamination from silicon and glass surfaces. Caution: Piranha solution reacts explosively with a number of organic solvents and materials, *e.g.*, acetone, and should be handled with great care. The fact that this 1 h cleaning does not appear to affect the diamond particles is consistent with diamond's

tremendous chemical stability. This work is to be compared to an earlier study that showed polylysine deposition onto diamond. In this study, effective deposition of an amine-containing polymer (PAAm) was demonstrated on cleaned, but otherwise unfunctionalized, diamond. In these earlier studies, diamond surfaces were oxidized by heating in 9:1 sulfuric acid/ nitric acid for 1 day to form surface carboxyl groups that facilitated polylysine adsorption.[9,17] Fewer surface attachment points, as would be expected with this method, is preferable because a large number of surface carboxyl groups should decrease the capacity for SPE of an adsorbed amine-containing polymer.

After adsorption of polyallylamine (PAAm), coated diamond particles were characterized by XPS, Fourier transform-infrared spectroscopy (FT-IR), and chemical stability tests. The nitrogen-to-carbon ratio on this material, measured by the ratio of the N1s to the C1s XPS signals, was 0.036 ± 0.002, where all such ratios quoted in the text were obtained from XP narrow scans. No nitrogen signal was discernible by XPS prior to PAAm adsorption (see Figure 2.3). Diffuse reflectance FT-IR showed no C-H stretches after piranha cleaning and before PAAm adsorption but showed clearly defined signals in the C-H stretching region after PAAm adsorption (see Figure 2.4).

Chemical stability tests were performed by immersing PAAm-coated diamond particles into 2.5 M HCl or 2.5 M NaOH for 38 h. Following this treatment, approximately one-third of the nitrogen was removed from the surface; after exposures to acid and base, the N1s/C1s ratios decreased to 0.024 ± 0.003 and 0.026 ± 0.003, respectively. These results were compared to the stability of a commercially available SPE stationary phase (Phenomenex Strata NH_2, 55 μM, 70 Å), which is primarily composed of silica, where the Si 2p peak (a substrate peak) is a better reference peak for XPS than the C1s signal. Prior to stability tests, the N1s to Si2p ratio by XPS

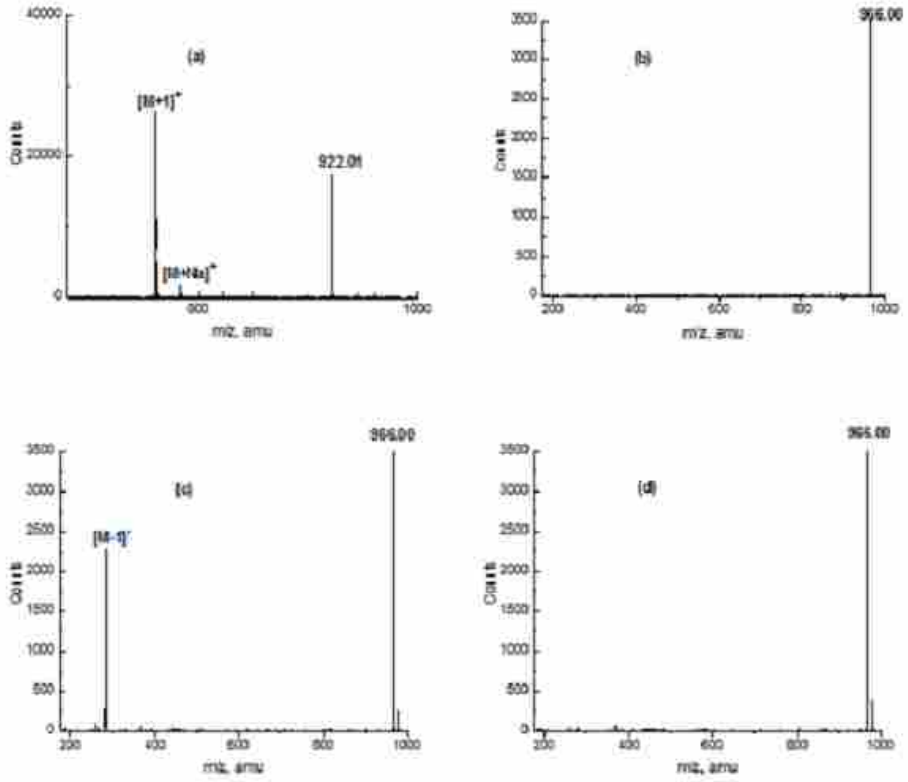

Figure 2.2. ESI-MS spectra of SPE fractions of individual analytes (not from a mixture of these analytes) from sequential elution of amino-coated diamond with chloroform, 2% acetic acid in diethyl ether, and methanol. (a) Positive ion spectrum of POPC eluted in methanol showing the $[M + H]^+$ and $[M + Na]^+$ peaks of POPC, and negative ion spectra of 1,16-hexadecanedioic acid eluted in (b) chloroform (no analyte present), (c) 2% acetic acid in diethyl ether, and (d) methanol (no analyte present). An unidentified peak at m/z 199.01 is not shown in panels b-d. The reference peak at m/z 966.00 is much higher in intensity than shown in panels b-d.

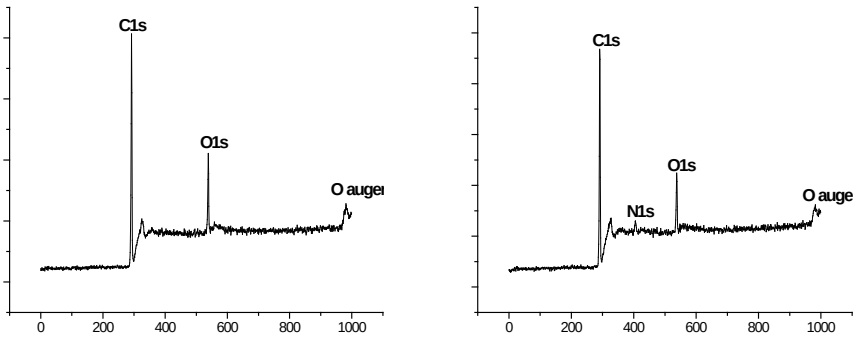

Figure 2.3. XPS survey scans of piranha-cleaned diamond powder (left) and PAAm-functionalized diamond powder (right).

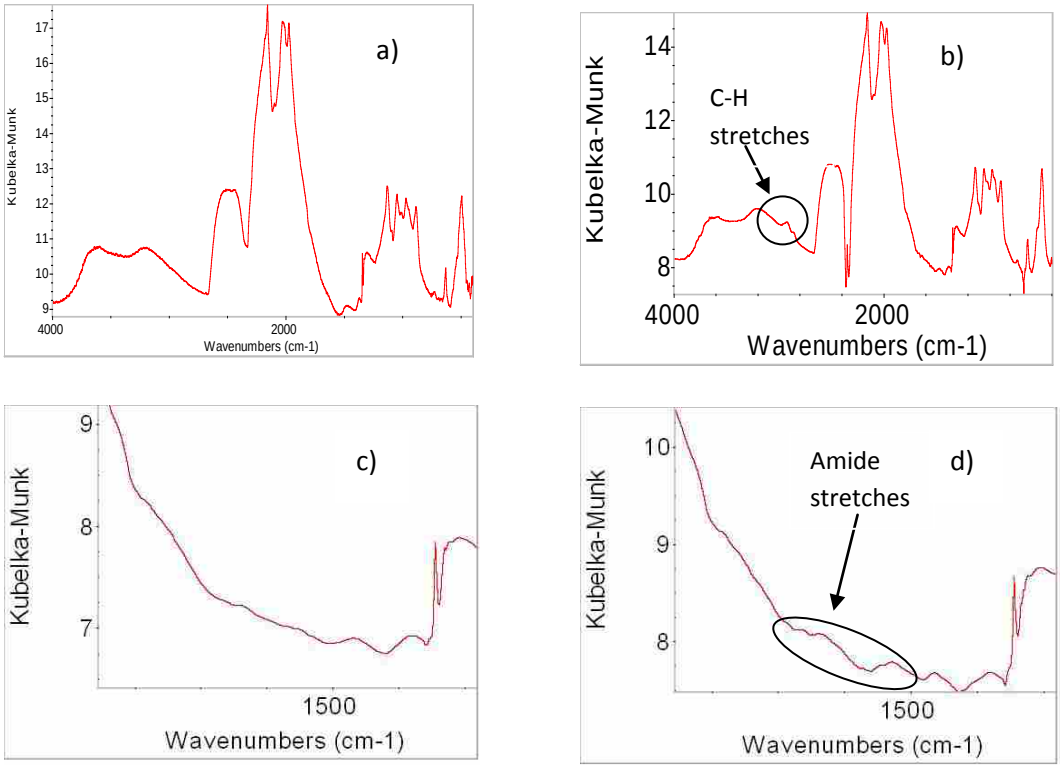

Figure 2.4. FTIR spectra of the piranha-cleaned (a), and PAAm-functionalized (b) diamond particles. Amide stretching region of uncured PAAm-functionalized (c), and cured PAAm-functionalized (d) diamond particles. The large peaks in around 2000 cm^{-1}, and again at lower energy, are artifacts attributable to the large size of the diamond powder used in the DRIFT experiment, and are not chemically significant in this study.

was 0.135 ± 0.002. After immersion of these particles in 2.5 M NaOH for 6 h, the particles dissolved completely. To further verify the dissolution of these particles, the resulting clear solution was filtered. It easily passed through the filter, leaving no material behind. The Phenomenex particles were also immersed in 2.5 M HCl for 36 h. A small decrease in the N1s/Si2p ratio was observed (down to 0.117 ± 0.012), which suggests that a little less than 15% of the nitrogen-containing coating on the particles had been lost. Thus, the deposited PAAm coatings on diamond are somewhat less stable in acid than the comparable amino coating on a commercially available SPE packing material, while being much more stable to base.

While these results might suggest that direct adsorption of PAAm onto clean diamond may create a stationary phase that is useful in a variety of situations, the primary objective of this work was to create an extremely stable stationary phase for solid phase extraction. Two approaches were taken to accomplish this: thermal curing and chemical cross-linking. For thermal curing, the PAAm coated diamond particles were heated under vacuum to 115°C for 2.5 h. Such conditions have been shown to create amide linkages in polyelectrolyte multilayers that contain carboxyl and amine groups.[18] While the number of carboxyl groups on our diamond surfaces appeared to be small by XPS, after curing, a series of small peaks appeared in the FT-IR spectrum at the positions expected for the amide stretches (see figure 2.4),[19] *i.e.*, (1690−1620 cm^{-1}) due to C=O stretching (the amide I band), and (1570-1520 cm^{-1}) due to coupled C-H stretching and N-H bending (the amide II band). Stability tests were then performed on this cured material. Prior to curing, the N1s/C1s ratio of the PAAm-coated diamond powder was 0.036 ± 0.002 (*vide supra*). After curing, this ratio remained essentially constant (i.e., 0.036 ± 0.001). After immersion of this cured material into 2.5 M HCl and 2.5 M NaOH for 38 h, the N1s/C1s ratios were essentially unchanged (i.e., 0.034 ± 0.002 and 0.036 ± 0.003, respectively). These

results indicate that a thermal cure can significantly improve the high and low pH stability of PAAm coated diamond particles.

Chemical cross-linking was also investigated as a possible method for increasing the stability of PAAm on diamond. The effect of this change would be to increase the molecular weight of the adsorbed PAAm, which would increase its stability. Accordingly, PAAm-coated diamond was treated with 1,2,5,6-diepoxycyclooctane. The O1s/C1s ratio, after cross-linking, measured by XPS increased to 0.15 ± 0.01 from a value of 0.12 ± 0.01 prior to cross-linking. This increase in the oxygen content of the surface is consistent with the chemisorption of an oxygen-containing species (the diepoxide). The N1s/C1s ratio, by XPS, after this cross-linking reaction was 0.025 ± 0.001. The decrease in the N1s/C1s ratio, compared to the ratio found before cross-linking (vide supra), is presumably due to the increased amounts of carbon and oxygen added to the surface through chemisorption of the diepoxide. After the cross-linking reaction, the pH stability of the material was measured. After immersion of the cross-linked material into 2.5 M HCl and 2.5 M NaOH for 38 h, the N1s/C1s ratios were essentially unchanged at 0.023 and 0.026, respectively[20]. These results indicate that chemical cross-linking can also significantly improve the high- and low-pH stability of PAAm-coated diamond particles.

Further information about this cross-linking reaction was obtained using a planar silicon surface. Because of the expected self-limiting nature of PAAm adsorption onto materials, adsorption of PAAm onto silicon oxide is expected to be similar to adsorption of this polymer onto diamond. An additional advantage of a planar substrate is that optical ellipsometry can be performed on it. Accordingly, a clean silicon surface with its thin native oxide layer was immersed in a dilute solution of PAAm, where the PAAm was found to adsorb spontaneously

onto the surface. The resulting PAAm film was 8.7 ± 1.5 Å thick. After reaction with 1,2,5,6-diepoxycyclooctane, the film thickness increased by 9.6 ± 0.6 Å. These changes in surface chemistry were also followed by wetting (contact angle goniometry). Initially, the clean silicon oxide surface is easily wetted by water. After adsorption of PAAm, the advancing water contact angle of the surface was 32 ± 6°, and after reaction with the diepoxide, the advancing water contact angle was 65 ± 8°. These increases in film thickness and the corresponding advancing water contact angles are again consistent with the expected surface chemistry.

2.5.2. Solid-Phase Extraction with PAAm-Coated Diamond Particles

PAAm-coated diamond particles were loaded into columns and used for solid-phase extraction. A demonstration of the retention and release of analytes was performed with cholesterol, 1,16-hexadecanedioic acid, and palmitoyloleoylphosphatidylcholine (POPC) (see Figure 2.1).

A modified literature SPE procedure for amino-coated packing material that fractionates biological tissue extracts into neutral lipids, fatty acids, and phosphatidylcholines was used to demonstrate the effectiveness of this new stationary phase.[13] The columns were first conditioned with 0.50 M NH_4OH to deprotonate them, a high pH solution that would only be appropriate for a very stable stationary phase, followed by isopropanol, 50% isopropanol/50% hexane, and hexane. Individual analytes, and later a three component mixture, were then loaded onto the columns, after which they were eluted sequentially with chloroform (to elute neutral lipids), 2% acetic acid in diethyl ether (to elute fatty acids), and methanol (to elute phosphatidylcholines). In some cases, comparison SPE columns made of piranha cleaned, untreated diamond powder or hydrogen-terminated diamond powder were also employed. ESI-MS confirmed the presence or

absence of the analytes in the fractions that were taken. During SPE, these analytes eluted only in their respective eluents and not in other eluents, *i.e.*, cholesterol eluted only in chloroform, 1,16-hexadecandioic acid eluted only in 2% acetic acid in diethyl ether, and POPC eluted only in methanol. Solid-phase extraction was done in this manner many times using the same diamond material; the same column could be reused multiple times without showing any significant signs of deterioration.

On hydrogen-terminated diamond packing material, POPC eluted in the first fraction (chloroform). In contrast, POPC eluted in the last fraction (methanol) but not in the first two fractions (chloroform and 2% acetic acid in diethyl ether) for uncoated (oxidized) diamond and for PAAm-coated diamond (the as-deposited, not cured or cross-linked coating). Figure 2.2 shows an ESI-MS spectrum of the corresponding methanol fraction from PAAm coated diamond that is dominated by three peaks: the $[M + H]^+$ and $[M + Na]^+$ peaks for POPC and a reference peak at 922 amu. SPE was then performed with 1,16-hexadecanedioic acid using the as-deposited PAAm-coated diamond. This analyte elutes only in the second fraction (2% acetic acid in ether) as the $[M - H]^-$ ion, as it should, where Figure 2.2 shows ESI-MS negative ion spectra for the chloroform, 2% acetic acid, and methanol fractions. Finally, with the use of this procedure, cholesterol was shown to elute only in the first fraction (chloroform).

With the employment of the above procedure, cholesterol, 1,16-hexadecanedioic acid, and POPC were separated on uncured PAAm-modified diamond as a three-component mixture. As expected, upon elution with chloroform, cholesterol appears exclusively in the first fraction, as shown by *m*/*z* 369 and 409 peaks, due to the $[M - OH]^+$ and $[M + Na]^+$ peaks of cholesterol, respectively. In the second fraction, 1,16-hexadecanedioic acid appears exclusively upon elution

with 2% acetic acid in diethyl ether. Finally, POPC appears exclusively in the final fraction with methanol elution.

A comparison of the extraction performance of the diamond amino column was also made by doing SPE of the three-component mixture on amino phase from Phenomenex and Varian. The diamond amino column was conditioned as before. However the 0.5 M ammonia solution was not used during the conditioning of the Phenomenex and Varian amino columns. Otherwise the rest of the procedure for the commercial materials was identical to that used for the diamond amino column. It was observed that the three-component mixture could be separated using the diamond amino column, but it could *not* be separated effectively using the method employed in this study (essentially the Kaluzny[13] procedure) with the Varian and Phenomenex amino columns. On these columns, 1,16-hexadecanedioic acid did not elute in the 2% acetic acid in diethyl ether fraction, as would have been expected. Rather, it eluted with POPC in the final methanol fraction.

To further characterize the as-deposited, thermally-cured, and chemically cross-linked diamond SPE materials, breakthrough curves were obtained for 1,16-hexadecanedioic acid. From these breakthrough curves, the column capacities were calculated to be 0.16 mg, 0.11 mg, and 0.11 mg for the as-deposited, thermally-cured, and chemically cross-linked columns, respectively. It is clear from these results that the column capacity decreases somewhat for this analyte upon thermal curing and chemical cross-linking. Thermal curing should convert some ammonium ions that are adjacent to carboxylates into amides, which will reduce the possible number of active amine groups in the coating. Tighter attachment of the polymer coating to the diamond substrate may also reduce the accessibility of some of its amines; chemical cross-

linking of adsorbed PAAm should decrease diffusion of analytes into the coating, decreasing the column capacity.

The pressure-flow behavior of amino-coated diamond (70 μm particles) was compared to that of a commercially available amino-coated silica-based SPE material (Phenomenex Strata NH_2). Different solvents have different viscosities; therefore, pressure-flow behavior of the column varies with the solvent type. The pressure-flow behavior of the column was studied using water (a fairly viscous solvent for chromatography) as the fluid. Equal volumes of the diamond and commercially available sorbent (1.02 cm^3) were placed in an SPE column. The column was connected to an HPLC. The flow, F (in mL/min), was determined as a function of back pressure, P (in psi), between 165 and 550 psi. The resulting curves were fit to straight lines. The two materials had nearly equal pressure-flow properties. The linear fit to the pressure-flow curves were $F = 0.0128P + 0.996$ with an R^2 value of 0.997 for the diamond particles and $F = 0.0128P + 1.05$ with an R^2 value of 0.996 for the commercially available material. In a more practical (but less quantitative) sense, liquid could be easily forced through all the home-built and commercially available SPE columns studied in this work with a plastic syringe that was compressed manually.

2.5.3. Increase in Particle Surface Area to Increase Column Capacity

The breakthrough curve of 1,16-hexadecanedioic acid on amino-coated ~70 μm diamond powder was compared to the breakthrough curve on commercially-available amine-coated silica. This comparison indicates that the capacity of diamond columns is approximately 1/300th of the capacity of commercially available material. The logical explanation for this difference is the lack of porosity (surface area) of diamond particles, which are solid and quite large.

To increase the surface area of diamond packing materials, 2 μm diamond particles were sintered, and the resulting porous solid was crushed and sized. These porous particles were then coated with PAAm and packed into columns for SPE. The N1s/C1s ratio by XPS for these coated, porous diamond particles was 0.046. This ratio is larger than the value obtained with nonporous particles (*vide supra*) and is attributed to the greater surface area of this porous material. The capacity of the resulting columns (1.40 cm^3 of diamond material), as measured by the breakthrough curve of 1,16-hexadecanedioic acid, was 3.26 mg for the 38-65 μm fraction (2.3 mg/cm^3) (see Figure 2.5), which is a greater than a 20-fold increase in column capacity compared to the solid ~70 μm diamond particles (The Phenomenex Strata NH_2 sorbent has a capacity of 17.5 mg for 0.45 cm^3 of material or 39 mg/cm^3). Thus, porous diamond particles have about 1/17th the capacity of the commercially available sorbent.

2.6. Conclusions

I have reported the formation of a highly stable amino stationary phase on diamond and demonstrated its use in solid-phase extraction. The pH stability of this amino coating on diamond was compared to the pH stability of a commercially available SPE amino adsorbent. After chemical cross-linking or thermal curing, this amino coating on diamond was stable under extremely acidic and basic conditions, while a commercially available amino SPE adsorbent disintegrated and dissolved in a high pH medium, and approximately 15% of its amino coating was lost in a highly acidic medium. Solid-phase extraction was demonstrated on amino coated diamond using cholesterol, palmitoyloleoylphosphatidylcholine, and hexadecanedioic acid, and these results were compared to SPE on commercially available sorbents.

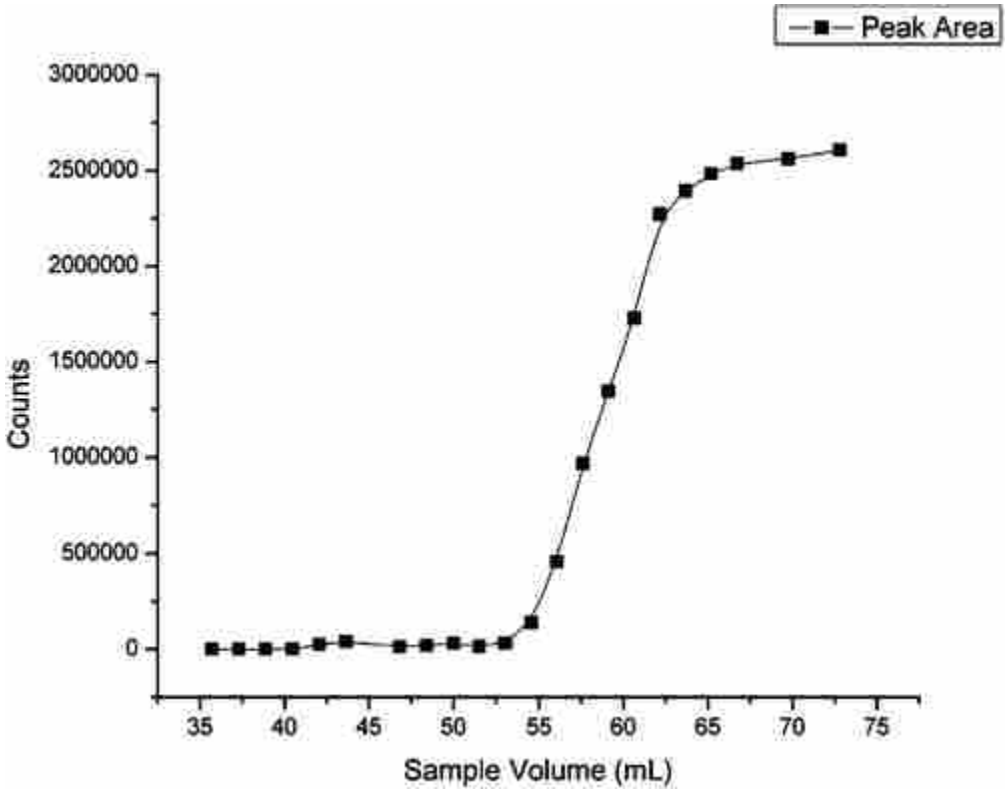

Figure 2.5. Breakthrough curve for 1,16-hexadecanedioic acid on PAAm-coated, sintered, and crushed 2 μm diamond particles (38−65 μm fraction of porous diamond powder). Each point represents the area of the analyte peak from a negative ion ESI-MS analysis of the fractions that were collected.

2.7. References

(1) Solid-Phase Extraction Principles, Techniques, and Applications; Simpson, N. J. K., Ed. Marcel Dekker, Inc.: New York, 2000.

(2) Thurman, E. M., and Mills, M. S. Solid Phase Extraction Principles and Practice; John Wiley & Sons Inc.: New York, 1998; Vol. 147.

(3) Here in PAAm is used as the abbreviation for poly(allylamine) and not PAA, which is the common abbreviation for polyacrylic acid. The use of "PAAm" is also to distinguish this (nearly) neutral polymer from polyallylamine hydrochloride, which has been widely used for building polyelectrolyte multilayers and has the abbreviation "PAH".

(4) Dyer, M. A.; Ainslie, K. M.; Pishko, M. V. *Langmuir* **2007**, *23*, 7018-7023.

(5) Hermanson, G. T. *Bioconjugate Techniques*; Academic Press: SanDiego, 1996.

(6) March, J. March's Advanced Organic Chemistry: Reactions, Mechanisms, and Structure, 6th ed.; John Wiley & Sons: New York, 2007.

(7) Sabu, S.; Yang, F. C.; Wang, Y. S.; Chen, W. H.; Chou, M. I.; Chang, H. C.; Han, C. C. *Anal. Bioche.* **2007**, *367*, 190-200.

(8) Chen, W. H.; Lee, S. C.; Sabu, S.; Fang, H. C.; Chung, S. C.; Han, C. C.; Chang, H. C. *Anal. Chem.* **2006**, *78*, 4228-4234.

(9) Kong, X. L.; Huang, L. C. L.; Liau, S. C. V.; Han, C. C.; Chang, H. C. *Anal. Chem.* **2005**, *77*, 4273-4277.

(10) Nesterenko, P. N.; Fedyanina, O. N.; Volgin, Y. V. *Analyst* **2007**, *132*, 403-405.

(11) Nesterenko, P. N.; Fedyanina, O. N.; Volgin, Y. V.; Jones, P. *J. Chromatogr. A* **2007**, *1155*, 2-7.

(12) Tsubota, T.; Hirabayashi, O.; Ida, S.; Nagaoka, S.; Nagata, M.; Matsumoto, Y. *Diamond Relat. Mater.* **2002**, *11*, 1374-1378.

(13) Kaluzny, M. A.; Duncan, L. A.; Merritt, M. V.; Epps, D. E. *J. Lipid Res.* **1985**, *26*, 135-140.

(14) Bateman, H. G.; Jenkins, T. C. *J. Agric. Food Chem* **1997**, *45*, 132-134.

(15) Bodennec, J.; Koul, O.; Aguado, I.; Brichon, G.; Zwingelstein, G.; Portoukalian, J. *J. Lipid Res.* **2000**, *41*, 1524-1531.

(16) Akesson-Nilsson, G. *J. Chromatogr. A* **2003**, *996*, 173-180.

(17) Ushizawa, K.; Sato, Y.; Mitsumori, T.; Machinami, T.; Ueda, T.; Ando, T. *Chem. Phys. Lett.* **2002**, *351*, 105-108.

(18) Harris, J. J.; DeRose, P. M.; Bruening, M. L. *J. Am. Chem. Soc.* **1999**, *121*, 1978-1979.

(19) Zhang, J.; Oettmeier, W.; Gennis, R. B.; Hellwig, P. *Biochemistry* **2002**, *41*, 4612-4617.

(20) In both of these experiments, two spots were analyzed on each surface and identical results were obtained.

Chapter 3. C_{18}, C_8, and Perfluoro Reversed Phases on Diamond for Solid-Phase Extraction*

3.1. Abstract

In spite of advances in solid-phase extraction (SPE) technology, there are certain disadvantages to current SPE silica-based, column packings. The pH range over which extraction can occur is limited and each column is generally only used once. New diamond-based reversed SPE phases (C_{18}, C_8, and perfluorinated) were developed in this work. Studies were done that show that these phases do not have the same limitations as traditional silica-based stationary phases. The synthesis and properties of these diamond-based phases are presented, and the stability, percent recovery, and column capacity are given for the C_{18} phase.

3.2. Introduction

Because of its high hardness and unusual inertness, diamond is a unique material with potential value in chromatography and solid-phase extraction (SPE). Thus far, relatively little diamond functionalization has been reported for chromatography. Research done by Chen and co-workers showed that the diamond surface could be functionalized by exposing it to oxidizing acids which left carboxyl, carbonyl and other oxygen containing functional groups on the diamond surface.[1] This phase could then be used for SPE of proteins. Other work performed by

---

This chapter is reproduced with permission from (Gaurav Saini, Landon A. Wiest, David Herbert, Katherine N. Biggs, Andrew Dadson, Michael A. Vail and Matthew R. Linford) *J. Chromatogr. A* 1216(16), 2009, 3587-3593, Copyrighy 2008 Elseveir

this group showed protein isolation using uncoated nanocrystalline diamond[2] and oligonucleotide isolation using polylysine-coated nanocrystalline diamond.[3] Nesterenko *et al*. used sintered diamond as an HPLC stationary phase for ion exchange chromatography[4] and normal phase chromatography,[5] but with less than ideal resolution and high back pressures in their columns. Nakamura *et al*. chemisorbed perfluorinated chains onto oxidized diamond powder,[6] and Korolkov *et al*. showed grafting of alkyl chains onto nanodiamond.[7] Neither work mentioned the use of these materials for SPE or HPLC.

Amine-functionalized diamond has recently been created by treating clean diamond with polyallylamine (PAAm).[8] This procedure results in an ultra-thin coating of PAAm on the diamond surface which can be stabilized by thermal curing or chemical crosslinking.[9]

Reversed-phase SPE[10,11] and columns are frequently used in environmental chemistry to extract/isolate organic compounds from aqueous solutions.[12] SPE is also ideal for isolating trace amounts of organic materials, such as pesticides from ground water for toxicology studies. The pesticides diazinon and cyanazine (see Figure 3.1) have low solubility in water and are good candidates for testing new reversed-phase SPE materials because of their non-polar nature.

Current SPE phases have certain limitations. Silica-based column packings, although the industry standard, function well only at moderate pH. Silica dissolves under basic conditions and can lose functionality under acidic conditions. Here I report the formation of C_{18}, C_8, and perfluoro phases on diamond particles and demonstrate the application of the C_{18} phase in SPE. Diamond functionalization was performed by reacting PAAm-functionalized diamond with octadecyl isocyanate, and other isocyanates, which creates a urea linkage from primary amine groups (see Figure 3.2). Synthesis and characterization of these novel diamond-based SPE phases, and stability, capacity, and percent recovery of the C_{18} diamond phase is reported.

3.3. Experimental

3.3.1. Reagents

Chemicals were obtained as follows: poly(allylamine) (avg. M_w *ca*. 65,000, 20% (w/w) solution in water, Aldrich, Milwaukee, WI, USA), ethyl acetate (Mallinckrodt Baker, Phillipsburg, NJ, USA), dichloromethane (ChromAR grade, Mallinckrodt Baker), methanol (HPLC grade, Sigma–Aldrich, St. Louis, MO, USA), 2-propanol (HPLC grade, Sigma–Aldrich), anhydrous tetrahydrofuran (THF, reagent grade material from Sigma–Aldrich, dried using an Apex filter system), sulfuric acid (ACS grade, EMD Chemicals, Darmstadt, Germany), ammonium hydroxide (ACS grade, EMD Chemicals), hydrogen peroxide (30% (w/w) solution in water, Fisher Scientific, Fair Lawn, NJ, USA), octyl isocyanate (97%, Aldrich), octadecyl isocyanate (98% Aldrich), 3,3,4,4,5,5,6,6,7,7,8,8,9,9,10,10,10-heptadecafluorodecyl isocyanate (≥97.0%, Aldrich), diazinon (98%, Sigma–Aldrich), and cyanazine (99.8% Sigma–Aldrich). Diamond powder (70 μm) was provided by US Synthetic, Orem, UT, USA. Deionized water was purified using a Millipore (Billerica, MA, USA) Milli-Q (OM-154) purification system to produce ultrapure water, which was the only water used in this work.

3.3.2. Surface cleaning and amine functionalization

Diamond powder was cleaned and functionalized with PAAm as described by Linford and coworkers.[9]

3.3.3. Formation of the C_{18} phase on diamond

Prior to reaction with octadecyl isocyanate [$CH_3(CH_2)_{17}NCO$], amine-functionalized diamond powder was washed with aqueous 0.5 M ammonium hydroxide to deprotonate any

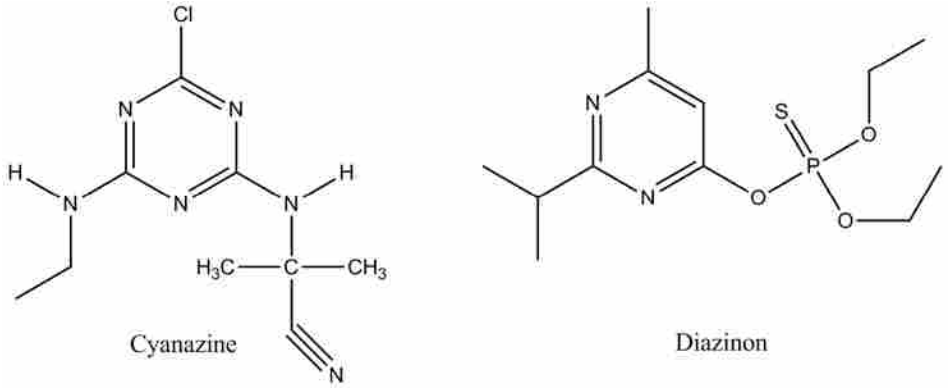

Figure 3.1. Chemical structures of cyanazine and diazinon.

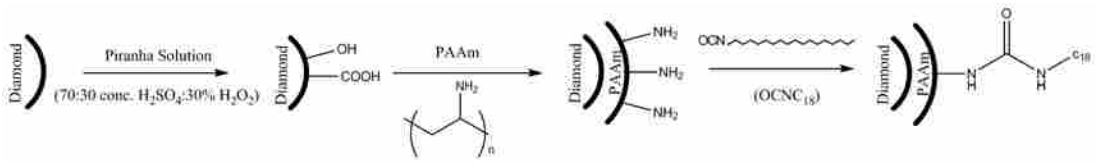

Figure 3.2. Scheme showing the diamond-based C_{18} phase synthesis.

protonated amines, and hence make the surface more reactive. PAAm-functionalized diamond powder (2.9 g) was then poured into a 4.9 % (w/v) solution of octadecyl isocyanate (1.07 g in 22 mL anhydrous tetrahydrofuran). This procedure was performed under N_2 atmosphere in a glove bag. The reaction was then allowed to take place at room temperature for 15 h. After the reaction, the diamond powder was sonicated first in THF and then in dichloromethane. Each solvent was exchanged four times during the sonication procedure. Finally the diamond powder was washed with *ca.* 400 mL of dichloromethane in a filter funnel. The mass of the stationary phase was 2.64 g.

After characterization and SPE on the material prepared above, 2.33 g of the same C_{18}-functionalized diamond particles were refunctionalized in a 5.4% (w/w) solution of octadecyl isocyanate heated to 80°C for *ca*. 15 h. These particles were washed and cleaned as described for the room temperature reaction above. A separate batch of C_{18}-functionalized diamond particles was also made in a single reaction at 75°C using the concentrations and cleaning procedure described in the paragraph above for use in stability and percent recovery studies.

3.3.4. Synthesis of the C_8 phase on diamond

Octyl isocyanate [$CH_3(CH_2)_7NCO$] was similarly employed to prepare a C_8 phase on PAAm-functionalized diamond particles. PAAm-functionalized diamond particles were deprotonated as in the formation of the C_{18} phase. 3 g of PAAm functionalized diamond was then immersed in 20 mL of a 15 vol.% solution of octyl isocyanate in anhydrous THF for 15 h. After the reaction, the powder was washed following the same procedure used for the C_{18} phase.

3.3.5. Synthesis of the perfluorinated phase on diamond

PAAm functionalized diamond powder was prepared and cleaned as in the C_{18} phase synthesis. 2.5 g of PAAm-functionalized diamond was immersed in *ca.* 30 mL of a 2.9% (w/w) solution of 3,3,4,4,5,5,6,6,7,7,8,8,9,9,10,10,10-heptadecafluorodecyl isocyanate (heptadecafluorodecyl isocyanate). This reaction was performed in a thick-walled glass tube at 75°C for 4 h.

3.3.6. Stability studies

To investigate whether the C_{18} stationary phase on diamond can withstand extreme pH conditions, chemical stability tests were performed. Approximately 2.5 M NaOH and 2.5 M HCl solutions were made in a 9:1 (v/v) mixture of water and methanol, respectively. Methanol was present in this solution to decrease the surface tension of the solution, and thus increase the wetting of hydrophobic diamond particles with the test solutions. C_{18}-functionalized diamond powder was immersed in these solutions for 38 h. Finally diamond particles were washed with copious amounts of water. 2.5 M HCl and 2.5 NaOH solutions were also prepared in 50:50 water:isopropanol to increase the fraction of the organic phase, and thus further improve substrate wetting by the test solution as well as the solubility of any desorbed species. PAAm–C_{18}-functionalized diamond powder prepared at room temperature was immersed in these solutions for 36 h. The particles were then washed with copious amounts of water.

3.3.7. Material characterization

X-ray photoelectron spectroscopy (XPS) was performed with an SSX-100 instrument from Surface Sciences (Bend, OR, USA) using an Al *Kα* source and a hemispherical analyzer.

The standard deviations reported herein are from two different spots analyzed on the same material. An electron flood gun was employed for charge compensation. FTIR was performed with a Magna-IR 560 spectrometer from Nicolet (Madison, WI, USA). BET isotherm measurements were performed by Micromeritics (Norcross, GA, USA).

3.3.8. Acid–base titration

Acid–base titration was performed to determine the surface concentration (mole percent) of $–NH_2$ groups on PAAm functionalized diamond powder, the degree of conversion of $–NH_2$ groups into the urea derivative, and the percent carbon loading of the PAAm–C_{18} stationary phase. PAAm and PAAm–C_{18} functionalized diamond powders were first deprotonated by immersion in 2.3 M ammonia solution (containing 6.25% isopropanol) for 6 h. Isopropanol was added to increase the wetting of the PAAm–C_{18} functionalized diamond powder by the ammonia solution. 4.33 g of PAAm-functionalized or 3.81 g of PAAm–C_{18}functionalized diamond powder was immersed in 40 mL of 0.088 M HCl for 24 h under an inert atmosphere. The solutions were kept in an oil bath at 300 K and shaken periodically. After the treatment of the solution with HCl, a 10 mL aliquot of the supernatant was taken from each flask and titrated with 0.093 M NaOH as monitored with a pH meter (CMS Labcraft). By utilizing the difference in the volume of 0.093 M NaOH needed for the neutralization of 40 mL of 0.088 M HCl solution, and the actual volume of 0.093 M NaOH used for neutralization of 40 mL of HCl solution (treated with PAAm and PAAm–C_{18} functionalized diamond powder), the mole percent of amine groups on PAAm-functionalized diamond, degree of conversion of amine groups into the urea derivative, and percent carbon loading of the PAAm–C_{18} phase was determined.

3.4. Solid-phase extraction

3.4.1. Solution preparation

Standard solutions of pesticides were made at near saturated concentrations in water.[13] 39.5 mg of cyanazine and 12.2 mg of diazinon were placed in 250 mL volumetric flasks and sonicated until the solutes had dissolved completely. Serial dilution of this solution was confirmed using electrospray ionization (ESI) MS on an Agilent Technologies (Santa Clara, CA, USA) Model No. G1969A LC/time-of-flight (TOF) MS instrument and the data obtained were plotted as a calibration curve (see Table 3.1). The dynamic range was determined from these calibration curves and new solutions were made (19.9 mg/L cyanazine and 5.6 mg/L diazinon) to ensure that all data from SPE runs would be within this linear range.

3.4.2. Breakthrough curves

The 5.6 mg/L diazinon solution was used to determine the capacity of the columns. The columns were conditioned by eluting 3 mL methanol and 3 mL water through the columns. The cartridge used in this study was 6.4 cm long, and had an internal diameter of 0.90 cm. It contained 1.34 cm^3 of the packing material. A 1 mL aliquot of the 5.6 mg/L diazinon solution was placed on top of the column and allowed to elute slowly (at *ca.* 2 mL/min). After 1 mL of liquid had been collected in a 1.8 mL vial, another 1 mL aliquot of the same diazinon solution was added and this procedure was repeated until a total of 26 mL of the solution had been eluted through the column. The diazinon content was determined by analyzing the collected samples

Table 3.1. Regression data for calibration curves.

	R^2	S_x	m	b
Diazinon	0.999	0.0555	3.15×10^6	-6.36×10^5
Cyanazine	0.998	0.366	3.53×10^6	3.66×10^5

with an Agilent ESI-MS instrument in positive ion mode. The results were graphed and the breakthrough concentrations (or column capacity) were determined for each column.

3.4.3. Recovery

199 μL of one of the standard solutions (128 mg/L cyanazine or 48.8 mg/L diazinon) was added to the column (prepared as previously described) with an automatic pipette. The column was then allowed to equilibrate for 3 min and then dried under a flow of air induced by negative pressure for another 3 min. The column was eluted with 3 mL ethyl acetate and the ethyl acetate eluent was collected in a 6-dram vial. The eluent was evaporated off using N_2 gas and the remaining analyte was redissolved with 5×199 μL methanol and 199 μL water. A reference solution was also created by adding 199 μL of the pesticide solution to 5×199 μL methanol. Since the solutions were of the same solvent composition, there was no need to worry about ion suppression or different responses of the ESI-MS to the analytes. Each solution was then analyzed with the ESI-MS and the $[M+H]^+$ peak for each respective analyte was integrated and compared to the reference peak area.

3.5. Results and Discussion

3.5.1. Diamond cleaning and PAAm deposition

Prior to PAAm deposition, diamond powder was cleaned in piranha solution. Piranha solution is an oxidizing solution, and is commonly used to remove organic contamination from glass and silicon/silicon oxide surfaces, especially in the semiconductor industry. *Warning: Piranha solution is a dangerous solution that must be handled with care*. The cleaned diamond powder was characterized by XPS and FTIR. The O1s and C1s signals were prominent in the XP

spectrum of the clean diamond powder (see Figure 3.3a). Essentially no C–H stretches could be discerned by diffuse reflection infrared Fourier transform (DRIFT) spectroscopy (see Figure 3.4a).

PAAm was deposited on diamond by immersing the clean diamond particles in an aqueous 20% (w/w) PAAm solution for 1 h. After polyelectrolyte deposition, the surfaces were again characterized by XPS and DRIFT. Figure 3.3b shows the XP spectrum of amine-functionalized diamond particles. A small N1s peak appears after PAAm deposition. The N1s/C1s ratio from XPS narrow scans for amine functionalized diamond powder was 0.039 ± 0.000, in good agreement with the previously reported value.[9] Figure 3.4a shows the DRIFT of PAAm functionalized diamond particles, which clearly shows C–H stretching from the polymer.

3.5.2. Functionalization with alkyl chains

3.5.2.1. Formation of the C_{18} phase

3.5.2.1.1. Formation of the C_{18} phase at room temperature

The C_{18} phase on diamond particles was synthesized by performing the reaction of PAAm-functionalized diamond powder with octadecyl isocyanate in anhydrous tetrahydrofuran at room temperature for *ca*. 15 h. After the formation of the C_{18} phase on diamond, the diamond powder was characterized by XPS and DRIFT. Figure 3.3c shows the XP spectra of C_{18}-functionalized diamond powder. A decrease in the N/C ratio was observed after the formation of the C_{18} phase, i.e., N1s/C1s ratio decreased from 0.039 ± 0.000 for PAAm functionalized diamond powder to 0.033 ± 0.002 for C_{18}-functionalized diamond powder. This decrease is attributed to an increase in carbon content of the surface after the functionalization of the surface

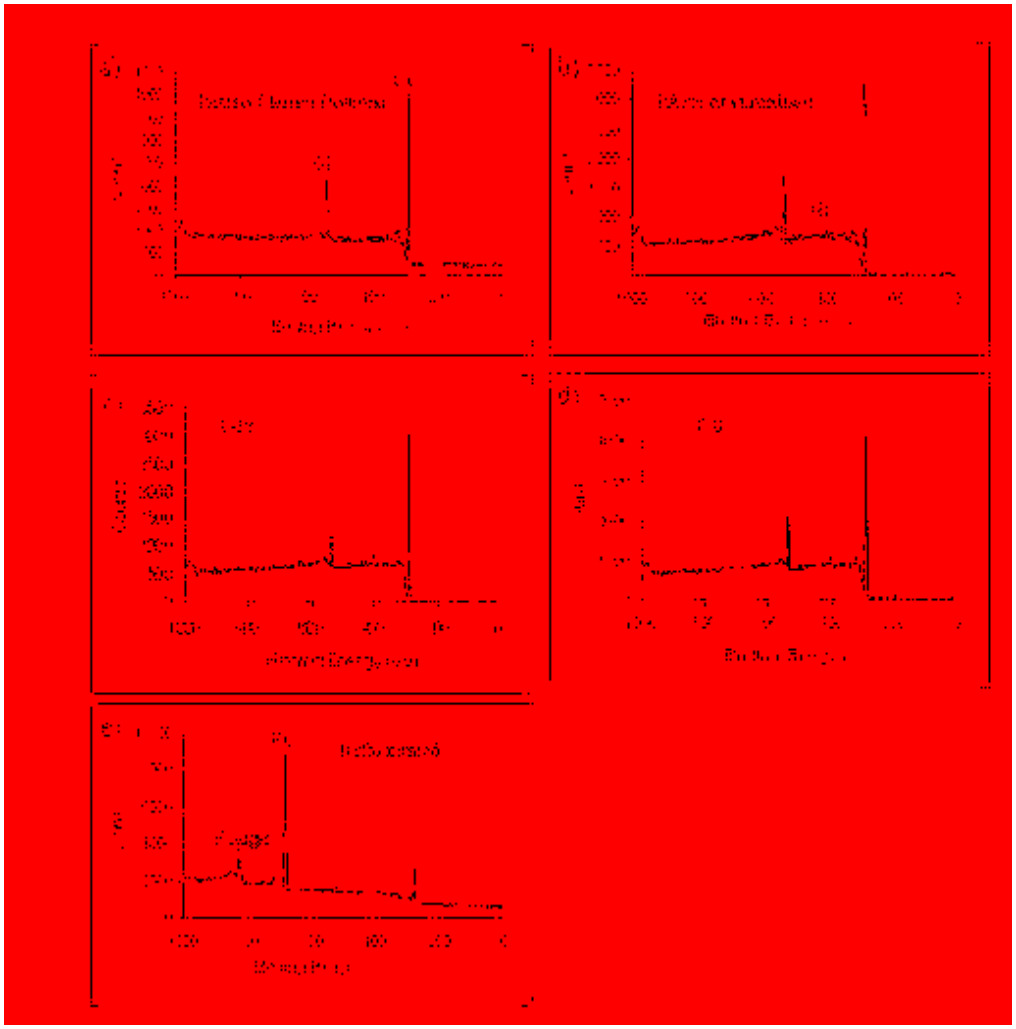

Figure 3.3. XPS data showing the predicted functionalizations. (a) Piranha-cleaned diamond; (b) PAAm-functionalized diamond; (c) C_{18}-functionalized diamond; (d) C_8-functionalized diamond; (e) perfluorinated diamond.

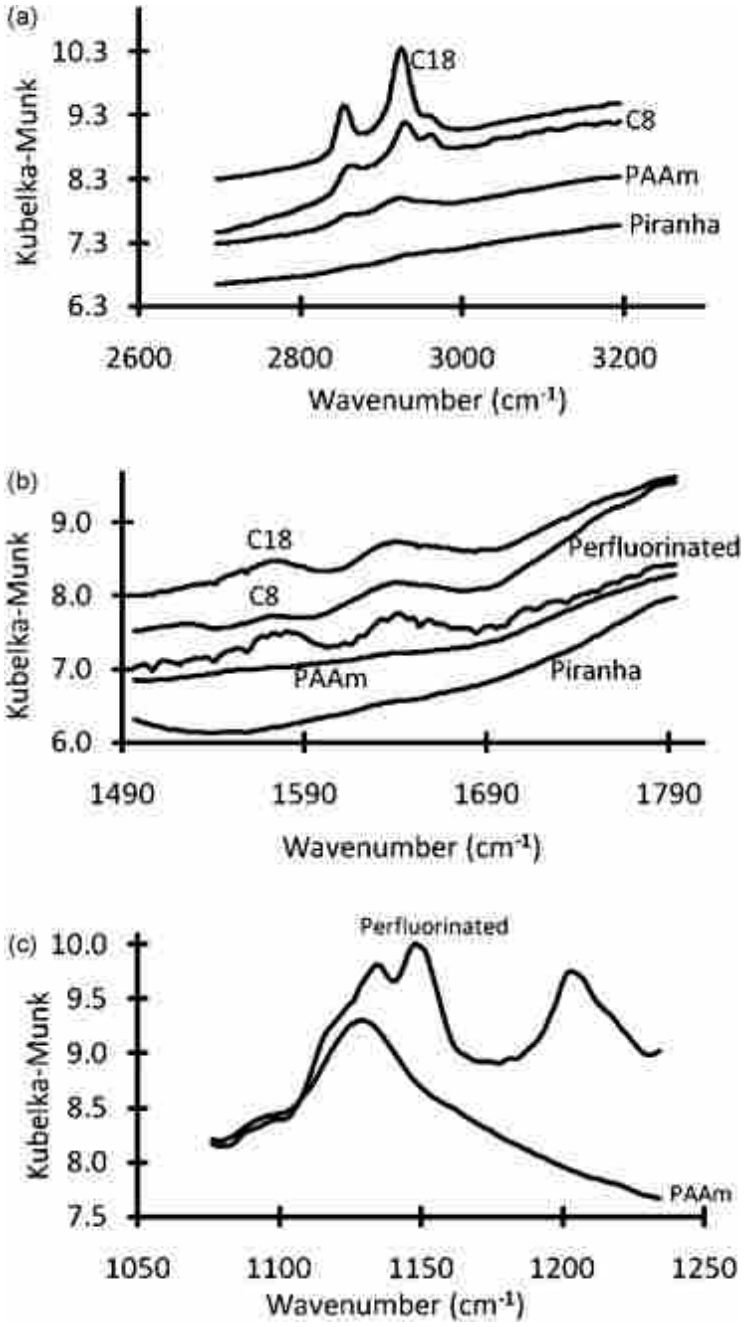

Figure 3.4. DRIFT data. (a) the C–H stretching region; (b) the amide stretching region; (c) the C–F stretching region.

with octadecyl chains, along with some attenuation of N1s photoelectrons by the C_{18} overlayer. A decrease in the O1s/C1s ratio was also observed, i.e., the O1s/C1s ratio decreased from 0.16 ± 0.00 for PAAm functionalized diamond powder to 0.11 ± 0.00 for C_{18}-functionalized diamond powder. The change in the O1s/C1s ratio is similarly attributed to an increase in carbon at the surface with concomitant attenuation of O1s photoelectrons. Figure 3.4a shows the DRIFT spectrum of the C_{18}-functionalized diamond powder. Intense symmetric and asymmetric CH_2 stretches are present in this material, which confirms the expected amine–isocyanate reaction. The asymmetric methylene stretch appears at 2923.6 cm^{-1}, and the symmetric methylene stretch at 2854.2 cm^{-1}, which indicates that the chemisorbed alkyl chains are in a liquid-like conformation. A series of peaks were also observed at 1642 cm^{-1} (amide I band) and 1576 cm^{-1} (amide II band) in the DRIFT spectrum (see Figure 3.4b), which are due to the urea linkage formed in the reaction between the NH_2 group of adsorbed PAAm and the NCO group of octadecyl isocyanate.[14-16]

3.5.2.1.2. Additional functionalization of the PAAm–C_{18} phase with octadecyl isocyanate at higher temperature

To promote the reaction of residual amine groups, PAAm–C_{18} diamond powder (functionalized at room temperature) was treated with an excess of octadecyl isocyanate at 80°C for *ca*. 15 h. After the reaction, the diamond powder was characterized with DRIFT. An increase of 37% in peak area of the asymmetric methylene stretch was observed for this material, and the peak positions of the asymmetric and symmetric methylene stretches decrease to 2921.7 and 2852.2 cm^{-1}, respectively (see above), consistent with a more solid-like packing on the alkyl chains. Apparently, the use of higher temperature helps reduce the steric effects from bulky

octadecyl chains, and therefore leads to an increase in the number density of octadecyl moieties on the surface.

3.5.2.2. Formation of the C_8 phase

The C_8 phase on diamond particles was synthesized via the reaction of PAAm-functionalized diamond powder with octyl isocyanate in anhydrous THF at room temperature for *ca.* 15 h. After the formation of the C_8 phase, the diamond powder was characterized by XPS and DRIFT. Figure 3.3d shows the XP spectrum of C_8 functionalized diamond powder. The N1s/C1s ratio for this surface by XPS was 0.043 ± 0.001, which is *ca.* 10% greater than that for PAAm-functionalized diamond powder. The increase in the N1s/C1s ratio for PAAm–C_8 functionalized diamond powder can be attributed to the thinness of C_8 layer, which is not able to attenuate N1s electrons very effectively. That is, since the nitrogen content of the surface must increase after reaction of PAAm-functionalized diamond powder with octyl isocyanate, but the attenuation of the N1s photoelectrons is not as great as should be found with the octadecyl isocyanate because of the thinner overlayer, the N1s/C1s ratio increases accordingly. A decrease in the O1s/C1s ratio was observed for C_8 functionalized diamond, i.e., the O1s/C1s ratio decreased from 0.16 ± 0.00 for PAAm-functionalized diamond powder to 0.14 ± 0.01 for C_8-functionalized diamond powder, which can be attributed to attenuation by the addition of carbon in spite of the increase in oxygen at the surface due to formation of the urea linkage. As expected, the C1s/O1s ratio for the C_8-functionalized diamond particles is smaller than that for the C_{18}-functionalized diamond. Figure 3.4a shows the DRIFT spectrum of C_8 functionalized diamond powder. In addition to increased C–H stretching compared to the PAAm-functionalized diamond, a pair of peaks appears in the amide stretching region for this phase due to the amide I and amide II

bands. The peak positions of the asymmetric and symmetric methylene stretches are 2925.5 and 2858.0 cm^{-1}, which suggests a liquid-like conformation for these chains.

3.5.2.3. Formation of a perfluorinated phase

A perfluorinated phase on diamond powder was synthesized by performing the reaction of PAAm-functionalized diamond powder with heptadecafluorodecyl isocyanate in anhydrous THF. XPS and DRIFT were again used to characterize this new phase. Figure 3.3e shows the XP spectrum of perfluorinated diamond powder. A large peak due to fluorine appears in the XP spectrum of the perfluorinated diamond powder, which is absent in the XP spectrum of PAAm-functionalized diamond powder. The F1s/C1s ratio by XPS for the perfluorinated diamond powder was 0.81 ± 0.03. Figure 3.4c shows the DRIFT spectrum of perfluorinated diamond powder. A pair of peaks at 1204 and 1149 cm^{-1}, due to the asymmetric and symmetric CF_2 stretches, respectively, appears in the DRIFT spectrum of perfluoro functionalized diamond. The amide I and amide II stretches (see Figure 3.4b) also appear in the amide stretching region for the perfluorinated diamond powder.

3.5.3. Percent surface coverage

Acid–base titration employing PAAm-functionalized and PAAm-C_{18} functionalized diamond powder was done to determine the surface concentration of amine groups, the degree of conversion of amine groups to the urea derivative, and the percent carbon loading of the PAAm-C_{18} phase. Based on these titrations, and assuming carbon to be the only constituent of diamond, the mole % of $–NH_2$ functional groups in PAAm functionalized diamond powder and PAAm-C_{18} functionalized diamond powder was 0.0139% and 0.00702%, respectively. The low

concentration of $–NH_2$ functional groups on the PAAm-functionalized diamond surface can be attributed to the low surface area of the non-porous microdiamond employed in this work. The degree of conversion of primary amines on PAAm functionalized diamond to urea linkages of PAAm-C_{18} functionalized diamond prepared at room temperature was 49.5%. The lack of complete conversion, although *ca*. 50% conversion is quite high for an adsorbed polymer, is no doubt due to steric repulsion among bulky C_{18} chains. Higher degrees of conversion should be possible at higher temperatures (see above), which might open up the polymer to a greater extent and expose more amine groups. The percent carbon loading was calculated using the titration data. Assuming that the weight of the PAAm layer is negligible in comparison to the weight of diamond powder, the percent carbon loading of the C_{18} phase was 0.17%. The BET surface area of piranha-cleaned diamond powder, as measured at an external lab, is 0.1990 m^2/g.

3.5.4. Stability studies

Stability studies on C_{18} diamond were performed by immersing C_{18} functionalized diamond powder in HCl or NaOH solution. Table 3.2 lists the data for the stability studies performed on C_{18}-functionalized diamond powders (prepared at different reaction temperatures) under different conditions. To improve the wetting of the particles by the test solution, 10% MeOH was added in the test solution, and as a final effort to insure the wetting of the hydrophobic diamond particles by the test solution and removal (dissolution) of desorbed material, 50% IPA was added to the test solution. As is evident from the data, the N1s/C1s ratio for PAAm-C_{18} functionalized diamond remained essentially constant to within the standard deviation of the measurement, or decreased by a small amount, perhaps *ca*. 10%, after stability studies. The high stability of this phase can be attributed to an increase in the molecular weight

Table 3.2. Results of stability studies: immersion in strongly acidic and basic solutions[a,b].

PAAm + C18-NCO (Reaction temperature)	Solvent	2.5M HCl	2.5M NaOH	N1s/C1s ration (after stability test/before stability test)
RT	H_2O	√		0.029±0.002/0.031
RT	H_2O		√	0.029±0.001/0.031
RT	90:10 H_20:MeOH	√		0.031/0.031
RT	90:10 H_20:MeOH		√	0.026±0.004/0.031
RT	90:10 H_20:IPA	√		0.029/0.031
RT	90:10 H_20:IPA		√	0.027/0.031
75°C	90:10 H_20:MeOH	√		0.025/0.027
75°C	90:10 H_20:MeOH		√	0.026/0.027

[a]C_{18}-NCO, RT, H_2O, MeOH and IPA stand for stearyl isocyanate, room temperature, water, methanol and isopropanol, respectively.
[b]All immersion times in the acidic or basic solutions were 38 h.
[c]Unless otherwise indicated, all standard deviations for the numbers in this column were 0.000.

of the polymer after its reaction with stearyl isocyanate, which decreases the solubility of the polymer, and the extremely high stability of the urea linkage.

3.5.5. Column capacity

The breakthrough concentration was determined by calculating a quantity of diazinon equal to 5% of the saturation level of the column, as determined by the counts from the mass spectra (see Figure 3.5). The room temperature-functionalized C_{18} material broke through after 6.1 mL of the diazinon solution had passed through the column. The capacity of the column was determined to be on average 12.980 ± 0.002 μg of diazinon per gram of coated support. The 80°C functionalized C_{18} diamond powder was employed in the same way to determine the breakthrough concentration. The breakthrough concentration for this column was on average 14.486 ± 0.007 μg of diazinon per gram of coated support.

3.5.6. Recovery and column reusability

Percent recovery studies were found to be consistent between various evaluators of the column. Two values for percent recovery were obtained for diazinon: 98.7% and 95.9%. The percent recovery found for cyanazine was 101%. These numbers show that most, if not all, of the analyte can be recovered from this column. For comparison, percent recovery studies were also performed on a Phenomenex C_{18} column, which also showed *ca*. 100% analyte recovery.

The reusability of the same column was assessed by measuring its percent recovery multiple times. Before each reuse, the C_{18} diamond phase SPE column was flushed with 100 mL ethyl acetate. Mass spectra of the final few milliliters of the washing were examined by ESI-MS,

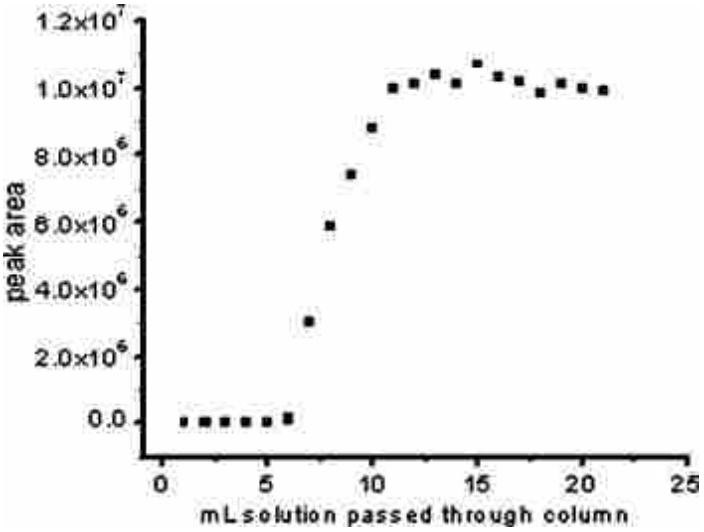

Figure 3.5. Breakthrough curve showing breakthrough occurring after 6.1 mL of the 5.6 mg/L aqueous diazinon solution has passed through the column.

and it was found that no traces of the any analyte were present. The data obtained from a reused column always reproduced the data previously obtained from the same column.

3.6. Conclusions

As evidenced by XPS and DRIFT, PAAm-coated diamond particles were modified as C_{18}, C_8, and perfluorinated phases. Particles functionalized at room temperature gave a lower C–H signal on DRIFT spectra than the re-reacted particles functionalized at 80°C. The room temperature particles also had a lower capacity as evidenced by breakthrough curve data. As expected, the C_8 phase gave smaller signals in the XPS and DRIFT spectra than either of the C_{18} phases. The perfluoronated phase showed a large F1s peak in the XP spectrum and CF_2 stretches in the DRIFT spectrum. Stability tests demonstrate the solid pH stability of these new materials.

The C_{18} column functionalized at room temperature had a capacity of 12.980 ± 0.002 μg diazinon per gram coated support, and the C_{18} column functionalized at 80°C had a capacity of 14.486 ± 0.007 μg of diazinon per gram of stationary phase. The breakthrough column capacity studies evidence the reusability of this diamond phase. The percent recovery of the column for cyanazine and diazinon were on average 97.3% and 101%, respectively.

3.7. References

(1) Sabu, S.; Yang, F. C.; Wang, Y. S.; Chen, W. H.; Chou, M. I.; Chang, H. C.; Han, C. C. *Anal. Biochem.* **2007**, *367*, 190-200.

(2) Chen, W. H.; Lee, S. C.; Sabu, S.; Fang, H. C.; Chung, S. C.; Han, C. C.; Chang, H. C. *Anal. Chem.* **2006**, *78*, 4228-4234.

(3) Kong, X. L.; Huang, L. C. L.; Liau, S. C. V.; Han, C. C.; Chang, H. C. *Anal.Chem.* **2005**, *77*, 4273-4277.

(4) Nesterenko, P. N.; Fedyanina, O. N.; Volgin, Y. V.; Jones, P. *J. Chromatogr. A* **2007**, *1155*, 2-7.

(5) Nesterenko, P. N.; Fedyanina, O. N.; Volgin, Y. V. *Analyst* **2007**, *132*, 403-405.

(6) Nakamura, T.; Ishihara, M.; Ohana, T.; Koga, Y. *Chem. Commun.* **2003**, 900-901.

(7) Korolkov, V. V.; Kulakova, I. I.; Tarasevich, B. N.; Lisichkin, G. V. *Diamond Relat. Mater.* **2007**, *16*, 2129-2132.

(8) Dyer, M. A.; Ainslie, K. M.; Pishko, M. V. *Langmuir* **2007**, *23*, 7018-7023.

(9) Saini, G.; Yang, L.; Lee, M. L.; Dadson, A.; Vail, M. A.; Linford, M. R. *Anal. Chem* **2008**, *80*, 6253-6259.

(10) Simpson, N. J. K. *Solid-Phase Extraction Principles, Techniques, and Applications*; Marcel Dekker: New York, 2000.

(11) Thurman, E. M.; Mills, M. S. *Solid-Phase Extraction Principles and Practice*; Wiley: New York, 1998.

(12) Mills, M. S.; Thurman, E. M. *Anal. Chem.* **1992**, *64*, 1985-1990.

(13) H. M. van Es, Pesticide Management for Water Quality, Cornell University, Ithaca, NY, USA (1990) http://pmep.cce.cornell.edu/facts-slides-self/facts/pestmgt-water-qual-90.html.

(14) Porter, M. D.; Bright, T. B.; Allara, D. L.; Chidsey, C. E. D. *J.Am.Chem.Soc.* **1987**, *109*, 3559-3568.

(15) Snyder, R. G.; Maroncelli, M.; Strauss, H. L.; Hallmark, V. M. *J.Phys.Chem.* **1986**, *90*, 5623-5630.

(16) Snyder, R. G.; Strauss, H. L.; Elliger, C. A. *J.Phys.Chem.* **1982**, *86*, 5145-5150.

Chapter 4. Core-Shell Diamond as a Support for Solid Phase Extraction and High Performance Liquid Chromatography*

4.1. Abstract

Here in I report the formation of core-shell diamond particles for solid phase extraction (SPE) and high performance liquid chromatography (HPLC) made by layer-by-layer (LbL) deposition. Their synthesis begins with the amine functionalization of microdiamond by its immersion in an aqueous solution of a primary amine-containing polymer, polyallylamine (PAAm). The amine-terminated microdiamond is then immersed in an aqueous suspension of nanodiamond, which leads to adsorption of the nanodiamond. Alternating (self-limiting) immersions in the solutions of the amine-containing polymer and the suspension of nanodiamond are continued until the desired number of nanodiamond layers is formed around the microdiamond. At least at the beginning of the process, each deposition appears to result in a partial layer of either PAAm or nanodiamond – when we refer to a bilayer herein we mean a deposition of PAAm followed by a deposition of nanodiamond, whatever the surface coverage of these materials may be. Finally, the core-shell particles are crosslinked with 1,2,5,6-diepoxycyclooctane or reacted with 1,2-epoxyoctadecane. Layer-by-layer deposition of PAAm and nanodiamond is also studied on planar Si/SiO_2 surfaces, which were characterized by SEM, Rutherford backscattering spectrometry (RBS) and nuclear reaction analysis (NRA). Core-shell particles are characterized by diffuse reflectance infrared Fourier transform spectroscopy

*This chapter was reproduced with permission from (Gaurav Saini, David S. Jensen, Landon A. Wiest, Michel A. Vail. Andrew Dadson, Milton L. Lee, V. Shutthanandan and Matthew R. Linford) *Anal. Chem.* **2010**, 82(11), 4448-4456. Copyright 2010 American Chemical Society

(DRIFT), environmental scanning electron microscopy (ESEM), and Brunauer Emmett Teller (BET) surface area and pore size measurements. Larger (*ca*. 50 μm) core-shell diamond particles have much higher surface areas, and analyte loading capacities in SPE than nonporous solid diamond particles. Smaller (*ca*. 3 μm), normal and reversed phase, core-shell diamond particles have been used for HPLC, with 36,300 plates per meter for mesitylene in a separation of benzene and alkyl benzenes on a C_{18} adsorbent, and 54,800 plates per meter for diazinon in a similar separation of two pesticides.

4.2. Introduction

Silica is the dominant support material employed in liquid chromatography (LC), and it is also heavily used in solid phase extraction (SPE).[1,2] It can be synthesized as highly uniform and spherical particles with controllable porosity, and its surface chemistry is well understood, allowing straightforward functionalization by silanization.[2] Its disadvantages include the labile nature of the Si-O-Si bond between silane adsorbates and the SiO_2 substrate under acidic conditions, the inherent instability of SiO_2 under basic conditions, and the often undesirable acidity of residual silanol groups.[2,3] Both silica and polymeric stationary phases are commonly employed in SPE, where polymeric SPE adsorbents are generally much more stable against acid or base hydrolysis than their silica counterparts.[4] However, polymeric materials appear to be less than optimal supports for LC – if not highly cross-linked they may swell in the presence of organic solvents, they tend to have low mechanical strengths, and they often suffer from poor efficiencies.

To avoid the problem of silica-based stationary phase/support instability one might limit oneself to mobile phases at moderate pH values.[3] This window of stability (perhaps pH 3 – 8)

allows successful separation of a large number of analytes. However, many analytes, *e.g.*, those with weakly acidic or basic moieties, benefit substantially from either very acidic or very basic mobile phases,[1] where these conditions set the protonation state of the analytes and stationary phase. A further need for stationary phase stability comes because chromatographic performance is often enhanced at higher temperatures, where mass transport of analytes is higher and solvent viscosity is lower. In summary, because of the limitations of silica, materials with improved pH stability have been and continue to be sought for in liquid chromatography.

A variety of approaches have been taken to increase the stability of silica-based stationary phases. For example, alkyl groups have been deliberately doped into SiO_2 during its fabrication to render it more resistant to hydrolysis, *e.g.*, the XTerra® columns by Waters (Milford, MA). Another approach has been to replace the methyl groups that were traditionally on monofunctional silane adsorbates with bulky side groups, *e.g.*, isopropyl groups.[5] While these approaches have extended the useful pH range of silica-based stationary phases, there is still room for improvement.

Another approach to this problem has been to replace silica with a more fundamentally stable material. For example, both porous graphitic carbon, *e.g.*, the Hypercarb™ columns from Thermo Scientific,[6,7] and zirconia-based stationary phases, *e.g.*, from ZirChrom®, as well as alumina and titania, have been explored as possible LC stationary phases,[3,8] Zirconia has high chemical and thermal stability and can be used over a wide pH range,[9-11] It can be coated with polybutadiene to prepare a reversed-phase material[12,13]; however, Lewis acid sites on its surface lead to strong adsorption of certain species,[14-16] such as proteins,[12,13] and, generally speaking, surface functionalization of zirconia has proved somewhat challenging.[3,17]

Diamond has also received some attention as a possible adsorbent for SPE and LC.[17] Diamond is remarkable; it is chemically inert, stable at both extremes of pH, and has high hardness, low compressibility, excellent optical transparency, and high thermal conductivity (ultimately, this may be important for eliminating thermal gradients in UPLC that effect separation efficiencies due to Joule heating).[18,19] Both Linford's and Nesterenko's group have recently prepared and/or modified diamond as a substrate for SPE and/or LC. Nesterenko and coworkers performed normal phase HPLC on microdispersed sintered detonation nanodiamonds (MSDNs).[20] They showed substantial improvements over previous attempts to use diamond in HPLC, *i.e.*, they reported baseline separation of various compounds with 15,400 theoretical plates per meter on *o*-xylene, although their peaks generally showed noticeable asymmetry (tailing), especially at longer retention times. In a related study, Purtov and coworkers developed a detonation nanodiamond-polysaccharide stationary phase for low-pressure (column) liquid chromatography.[21] Nesterenko and coworkers also used uncoated porous diamond materials derived from sintered detonation nanodiamonds for ion chromatography.[22] Work in the Linford group at BYU has focused on chemical modification of diamond. They first showed polyallylamine (PAAm)[23] adsorption from aqueous solution onto microdiamond, and SPE of lipids on this amine-terminated diamond.[24] They then demonstrated that various alkyl and a perfluoroalkyl isocyanate would react with PAAm-terminated diamond.[25] An SPE extraction of pesticides from water could be performed on the resulting C_{18} material. In a different direction, the Linford group modified deuterium-terminated diamond powder with di-*tert*-amyl peroxide,[26] and also demonstrated the functionalization of this substrate with polymers,[27] where the resulting modified diamond materials could again be used for SPE.

Two types of porous particles are commonly employed in LC today. The first, and more common, particle is completely porous. The second is pellicular and based on porous shells of material around solid cores (core-shell particles).[28] This latter approach benefits from faster mass transfer of analytes in and out of particles, which translates into an improvement in the "C term" of the Van Deemter equation, as evidenced by a flattening of the Van Deemter curve at higher mobile phase velocities.

Herein I explore the layer-by-layer (LbL) deposition of PAAm and nanodiamond on core particles to create high surface area particles for SPE and HPLC. In related work,[29,30] Ge and coworkers coated SiO_2 core particles with a surfactant (sodium dodecyl sulfate, SDS), which could then be coated with TiO_2 particles, followed by SDS in an alternating fashion to produce core-shell particles.[31] The final step in their process was a sintering at 525°C to burn out the SDS. Kirkland and Langlois reported the preparation of core-shell particles prepared on silica cores with silica/polyelectrolyte multilayers as shell layers. These particles were also heated to high temperature to remove the polyelectrolyte "glue".[32] In contrast, my substrate is diamond, not SiO_2, and I employ a mostly neutral polymer as the material that holds the particles together in the assembly – weak bases, such as amines, at the concentrations I employ, are mostly deprotonated (not charged) in water – a simple equilibrium calculation based on a 7.5 wt.
% aqueous solution of allyl amine (pK_b 4.31)[33] as a model compound for the PAAm polymer solution used to prepare the particles for HPLC indicates that *ca*. 0.6% of the amine groups on the PAAm polymer would be protonated (charged). This result justifies the use of a model compound for the polymer in this analysis because it indicates that the density of charged groups on the polymer will be low. The PAAm polymer is not removed by heating after formation of the particles. That this polymer remains is an advantage because it allows subsequent stationary

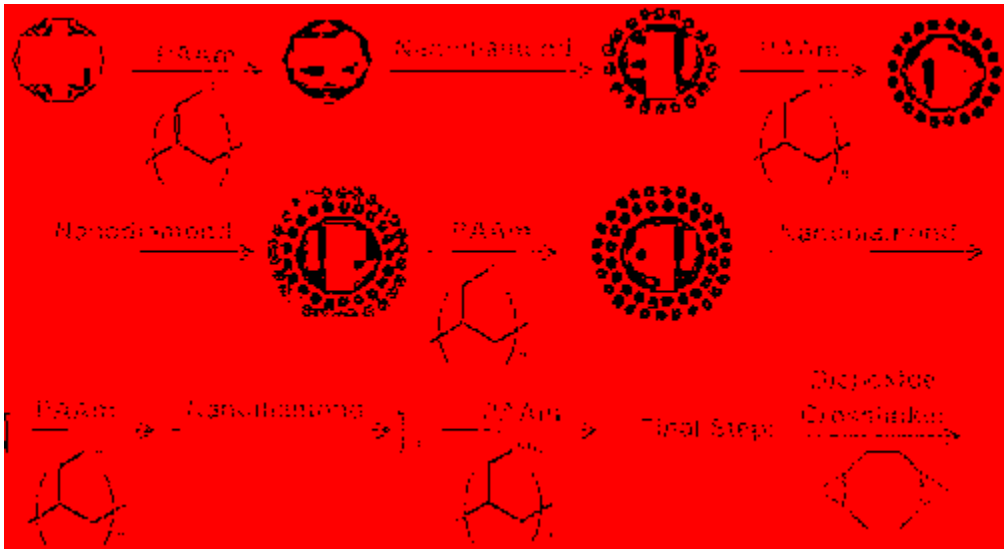

Figure 4.1. Synthesis of core-shell particles.

phase creation through reactive primary amine groups. This work also differs from earlier studies in which Linford group used low surface area, nonporous particles.[24,25,27,34] Particle preparation is shown in Figure 4.1. PAAm adsorbs from aqueous solution onto core diamond particles. These PAAm-terminated core particles are then immersed in a suspension of nanodiamond particles, which adsorb onto the PAAm-coated particles. This process is repeated in an alternating fashion. Finally, the particles are reacted with a cross-linker (1,2,5,6 diepoxycyclooctane) and/or a long-chain epoxide (1,2-epoxyoctadecane). The resulting core-shell particles have significantly more surface area than the original solid particles. Larger, *ca*. 50 μm particles, are used for SPE, and smaller, *ca*. 3 μm particles are used for HPLC. To the best of my knowledge, HPLC separations with these core-shell diamond particles now show the highest efficiencies yet reported for a diamond stationary phase.

4.3. Experimental

4.3.1. Reagents

Poly(allylamine) (PAAm) (Mw *ca.* 65,000 or 17,000, 20 wt.% solutions in water, Aldrich, Milwaukee, WI), 1,2,5,6-diepoxycyclooctane (96%, Aldrich), 1,2-epoxyoctadecane (90%, Alfa Aesar, Ward Hill, MA), and 1,16-hexadecanedioic acid (≥ 98%, Aldrich) were used as received. Monocrystalline diamond powders (1.7 μm, 5 μm, 50 – 70 μm, 10 – 50 nm and 100 – 250 nm), which had been crushed and sized, were obtained from Advanced Abrasives (Tennsauken, NJ). The 10 – 50 nm nanodiamond particles were obtained as a stable, aqueous suspension and used as received. The 100 – 250 nm diamond powder was obtained as a dry material and used as received – it did not appear opportune to clean it because of its small size.

Silicon wafers (test grade, n-type, <1-0-0> orientation, 2 – 6 Ω-cm) were purchased from UniSil Corporation, California.

4.3.2. Deposition of PAAm-Nanodiamond bilayers on Si/SiO_2

Native oxide-terminated silicon wafers were cleaved into *ca*. 1.5 x 1.5 cm pieces, cleaned with a 2 wt.% sodium dodecyl sulfate solution in water using a camel hair brush, and then rinsed thoroughly with deionized water. These clean substrates were plasma cleaned for 1 min in a plasma cleaner (model PDC-32G from Harrick Plasma (Ithaca, NY) on its high power setting – 16 W applied to the RF coil), immersed in an aqueous solution of PAAm (0.25 wt.%) for 5 minutes, and removed and rinsed thoroughly with deionized water. The resulting PAAm-coated surfaces were then immersed in an aqueous suspension of 250 nm nanodiamond (1.0 wt.%) for 5 minutes. The surface was rinsed thoroughly with deionized water to remove non-specifically adsorbed nanodiamond particles. This led to the formation of the first bilayer of PAAm-nanodiamond on the surface. Surfaces containing 2, 3, 4, 5, and 9 bilayers were similarly made by alternating immersions in the PAAm solution and nanodiamond suspension.

4.3.3. Synthesis of Core-Shell Particles of SPE

Core-shell particles for SPE were synthesized from 50-70 μm (core) and 100-250 nm (shell) diamond particles. Prior to PAAm deposition, the microdiamond was cleaned in piranha solution (70% H_2SO_4:30% H_2O_2 (conc.)) at 100°C for 1 h, sonicated in ultrapure water, and washed extensively with ultrapure water on a filter funnel. Core-shell particles containing 0 - 5 and 9 bilayers of PAAm-nanodiamond were prepared. A 0.25 wt.% solution of poly(allylamine) was made from 1.55 g of a solution of PAAm (Mw 65,000, 20 wt.% solution) in 125 mL of

ultrapure water, and 12 g of piranha-cleaned microdiamond powder was poured into this solution. The solution was shaken for *ca*. 10 s every 10 min for 1 h to fully expose the particles to PAAm. The diamond powder was then washed extensively with ultrapure water on a filter funnel. An aqueous suspension of 100 – 250 nm nanodiamond powder was prepared by sonicating 1 g of nanodiamond in 120 mL of ultrapure water, and 12 g of PAAm-functionalized microdiamond powder was poured into this suspension for 1 h. This suspension was again shaken gently for *ca*. 10 s every 10 min to expose all surfaces of the coated microdiamond particles to nanodiamond particles. The aqueous suspension was then filtered on a medium pore size (25-50 μm) filter funnel. As the size of the nanodiamond particles is much smaller than the pore size of the filter funnel, unbounded nanodiamond particles in the suspension easily passed through the pores of the filter funnel leaving microdiamonds coated with nanodiamond particles. These particles were washed extensively with ultrapure water on the filter funnel to remove any weakly adsorbed or unbound nanodiamonds. Approximately 2.8 g of these coated microdiamonds were then taken for characterization, and the remainder was poured into the next aqueous solution of PAAm for 1 h to amine functionalize the outer surface of the nanodiamonds particles in the first layer. The cleaning procedure was repeated as before. This powder was then poured into an aqueous suspension of nanodiamonds as in the first deposition of nanodiamond. Another 2.8 g of this functionalized diamond powder was taken, and the remainder was modified with more PAAm and nanodiamond. This general procedure was repeated until the desired number of PAAm-nanodiamond bilayers was deposited.

4.3.4. Chemical cross-linking of core-shell particles

The mechanical stability of core-shell particles is expected to be somewhat low because nanodiamond particles, microdiamond particles, and adsorbed PAAm are most likely held together through non-covalent interactions. The mechanical stability of these particles was improved by chemical cross-linking with 1,2,5,6- diepoxycyclooctane. To wit, *ca*. 2.6 g of each of the different core-shell particles was crosslinked with a 2.3 wt. % solution of 1,2,5,6-diepoxycyclooctane (0.175 g of the diepoxide dissolved in 7.5 mL isopropanol). The reaction was performed in a sealed, thick-walled glass reaction vessel at 80°C overnight. After the reaction, the core-shell diamond powder was washed extensively on a filter funnel with copious quantities of isopropanol, followed by dichloromethane.

4.3.5. Surface analysis

FTIR was performed with a Magna-IR 560 spectrometer from Nicolet (Madison, WI). ESEM images of the samples were acquired using an FEI (Philips) XL30 ESEM FEG instrument. Since diamond is an insulator, the diamond powder was adhered to a conductive, double-sticky carbon tape, and the ESEM FEG instrument was operated in low vacuum mode to prevent surface charging. Samples were sent to Micromeritics (Norcross, GA) for surface area (BET) and pore size analysis. Rutherford backscattering (RBS) and nuclear reaction analysis (NRA) were performed at EMSL, Environmental Molecular Sciences Laboratory, at the Pacific Northwest National Laboratory. RBS measurements were performed with 2.0 MeV He^+ ions and the backscattered He^+ ions from the sample were collected using a surface barrier detector positioned at a scattering angle of 165°. NRA measurements were performed using 0.94 MeV D^+ ions. The $^{12}C(d,p)\ ^{13}C$ nuclear reaction was used to measure the total amount of C in the samples

and was calibrated with a 500 Å carbon standard that contains 568 x 10^{15} carbon atoms/cm^2. A surface barrier detector at the scattering angle of 170° was used to collect the protons generated from the nuclear reaction. An aluminized Mylar® foil was positioned in front of the detector to block the backscattered D^+ ions from entering the detector.

4.3.6. Solid-Phase Extraction

The analyte used to determine breakthrough volumes was 1,16-hexadecanedioic acid in 3:1 $CHCl_3$:isopropanol (IPA). The column was first conditioned with six column volumes of 0.5M NH_4OH to deprotonate any protonated amines, and then washed with three column volumes each of IPA, 50% IPA/50% hexane, and hexane. After conditioning, the analyte was loaded onto the cartridge. The column was maintained wet and the flow rate was constant throughout the process. Equal volumes of the fractions eluting from the column were collected in individual vials. Lastly, each individual fraction was analyzed by ESI-MS (Agilent LC/MSD TOF Model No. G1969A).

4.3.7. Synthesis of core-shell particles for HPLC

Core-shell particles for HPLC were synthesized from 1.7 μm diamond core and 10-50 nm diamond particles. Particles were made in a 50 mL screw cap plastic tube. An aqueous suspension of 2.4 g of 1.7 μ diamond particles was made in the screw cap tube, and 250 μl of 7.5 wt.% aqueous solution of PAAm (17,000 Mw) was added to it. The tube was then shaken for 3 minutes to homogeneously expose the particles to PAAm.

After treatment with PAAm solution, the tube was centrifuged at 5000 rpm for 2 minutes. The supernatant was decanted, and the settled particles were washed twice with 45 ml of

deionized water. An aqueous suspension of these particles was then made, and 1 ml of an 8.32 wt.% aqueous suspension of 10-50 nm diamond was added to it. The tube was shaken for 3 minutes to expose the PAAm-functionalized diamond particles to the nanodiamond particles. After this treatment, the tube was again centrifuged for 2 minutes at 5000 rpm. The supernatant was decanted and the particles were washed twice with 45 ml of deionized water. This alternating treatment with PAAm and nanodiamond was continued until the desired number of PAAm nanodiamond bilayers was formed.

4.3.8. HPLC column packing

Core-shell particles were packed in a 30 mm × 4.6 mm column using a Chrom Tech (Apple Valley, MN) packing system. A slurry of these particles was prepared in 50:50 acetone:water. Column packing was done at constant flow (0.8 mL/min.) for 25 minutes.

4.3.9. Cross-linking of core-shell particles for HPLC

Core-shell particles were chemically crosslinked with a 0.38 wt.% solution of 1,2,5,6-diepoxycyclootane in xylenes and cyclohexanol (6.7:1) (v/v) mixture. The reaction was done overnight under nitrogen at 130°C. The particles were then washed extensively with xylenes and then isopropanol.

4.3.10. Functionalization of core-shell particles with C_{18} groups

A 1.7 wt.% solution of 1,2-epoxyoctadecane (made in a 6.7:1 xylene:cyclohexanol mixture) was used to attach C_{18} chains to core-shell particles that had not previously been cross-

linked. The reaction was done overnight in a nitrogen atmosphere at 130°C. After the reaction, the particles were washed extensively with xylene and then isopropanol.

4.3.11. HPLC on core-shell particles

A Waters 1525 HPLC system was employed with an absorbance detector set at 254 nm. The instrument software (Breeze Version 3.30 SPA) was used to calculate retention factors (k), numbers of theoretical plates per meter (N/m), and asymmetry factors. (The software calculated the number of theoretical plates at full width at half maximum for all the chromatographic peaks.) Core-shell particles cross-linked with 1,2,5,6-diepoxycyclooctane were employed as a normal phase to separate benzophenone and dinitrobenzene. The mobile phase was 70:30 hexanes:ethylacetate (each solvent contained 0.2% (v/v) triethylamine). The flow rate was 0.3 mL/min. C_{18} functionalized core-shell particles were used as a reversed phase to separate cyanazine and diazinon, and also a mixture of benzene, toluene, xylene and mesitylene. The mobile phase composition was 50% acetonitrile and 50% water (each solvent contained 0.1% (v/v) triethylamine). The flow rate was 0.2 mL/min.

4.4. Results and Discussion

4.4.1. Core-Shell Diamond Particles for Solid Phase Extraction

LbL deposition of PAAm and nanodiamond on planar Si/SiO_2 was studied by scanning electron microscopy (SEM), Rutherford backscattering spectrometry (RBS), and nuclear reaction analysis (NRA). RBS and NRA are well suited as analytical techniques for these surfaces because of the high energies (deep surface penetrations) of their incident and scattered/created particles. Figure 4.2 shows SEM images of the silicon surfaces containing 0, 1, 2, 3, 5 and 9

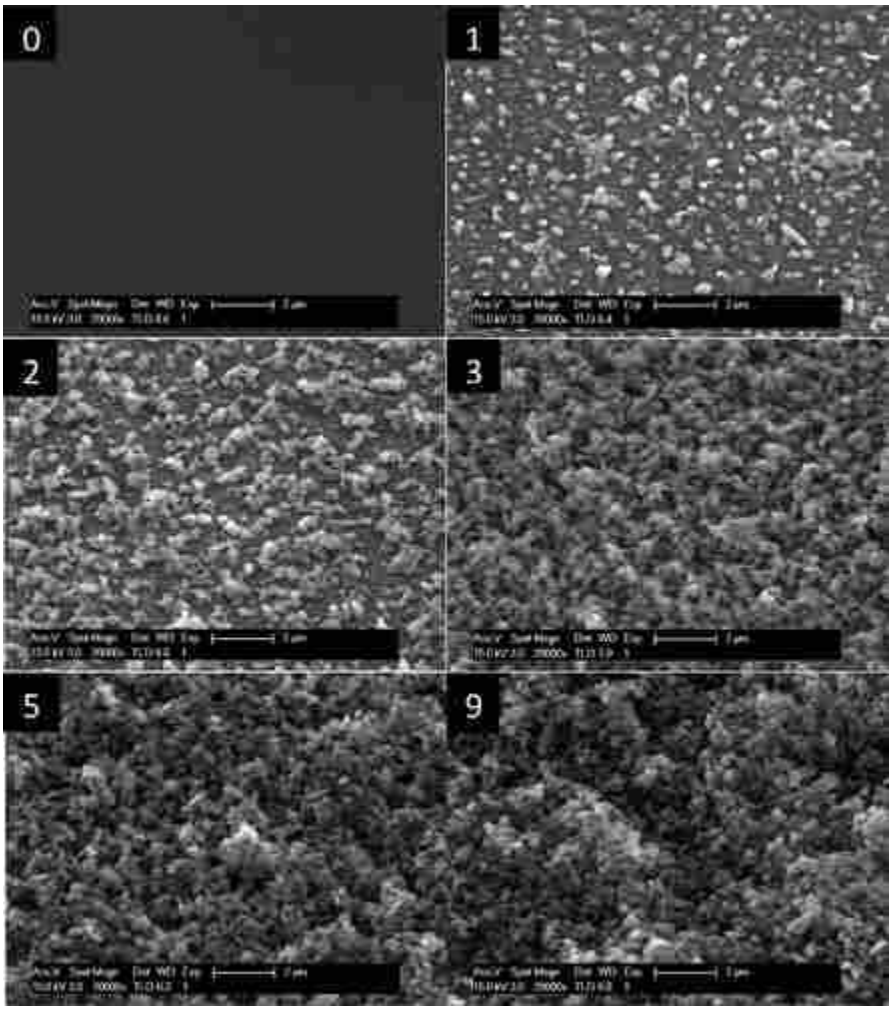

Figure 4.2. SEM images of silicon surfaces containing various numbers of PAAm-nanodiamond (100-250 nm) bilayers: zero, one, two, three, five and nine.

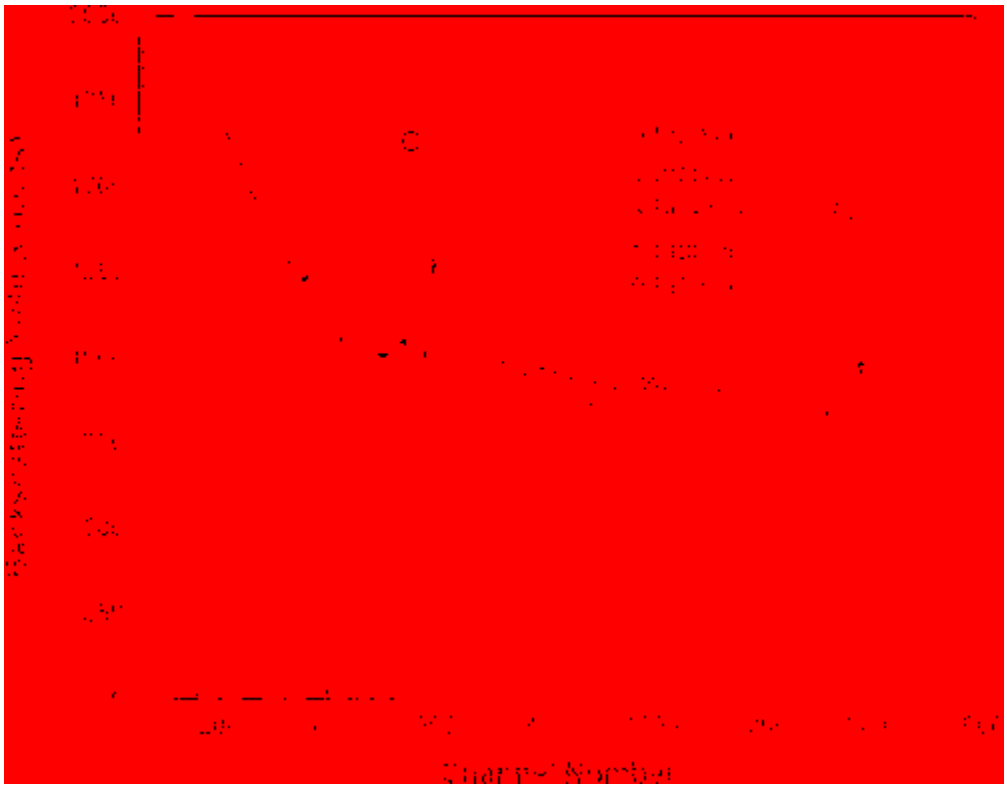

Figure 4.3. RBS spectra of silicon surfaces containing zero, one, two, three, five, and nine bilayers of PAAm-nanodiamond (100-250 nm).

bilayers of PAAm-nanodiamond. As is evident, the surface is not fully covered by nanodiamond after the deposition of one bilayer, as bare silicon is still visible in some regions. But with an increase in the number of PAAm-nanodiamond bilayers, the number density of nanodiamond particles at the surface increases with a concomitant disappearance of the underlying silicon surface. Figure 4.3 shows the RBS spectra of the surfaces containing 0, 1, 3, 5 and 9 bilayers of PAAm-nanodiamond.

The spectra show the silicon and/or carbon edges that originate from the silicon substrate and/or the carbon in the nanodiamond, and obviously to a lesser degree from PAAm. The RBS spectrum of the surface containing no bilayer is dominated by the silicon edge. In the spectrum of the surface containing one bilayer, a small peak due to C appears, which confirms the deposition of PAAm and nanodiamond on the surface. In addition, the peak due to Si decreases in intensity around its edge, although a significant fraction (*ca*. 50%) of the edge remains, which is consistent with the partial coverage of the silicon substrate by one bilayer shown by SEM in Figure 4.2. As the number of PAAm-nanodiamond bilayers increases, the step height of C at its edge increases due to an increase in the amount of carbon on the surface, and the signal due to unattenuated silicon at its edge decreases. For the surface containing nine bilayers of PAAm-nanodiamond, it is significant that the Si edge has disappeared (it is fully attenuated), leaving only the C edge at its maximum intensity.

Figure 4.4 shows the carbon signal, along with the number of carbon atoms per cm^2, from NRA of surfaces containing different numbers of PAAm-nanodiamond bilayers. In this NRA analysis, energetic deuterons fuse with ^{12}C nuclei and eject energetic protons: ($^{12}C(d,p)^{13}C$, *i.e.*, $^{12}C + {}^{2}H \rightarrow {}^{1}H + {}^{13}C$). The carbon signal increases steadily with an increase in the number of PAAm-nanodiamond bilayers, which further reinforces the observations derived from the SEM

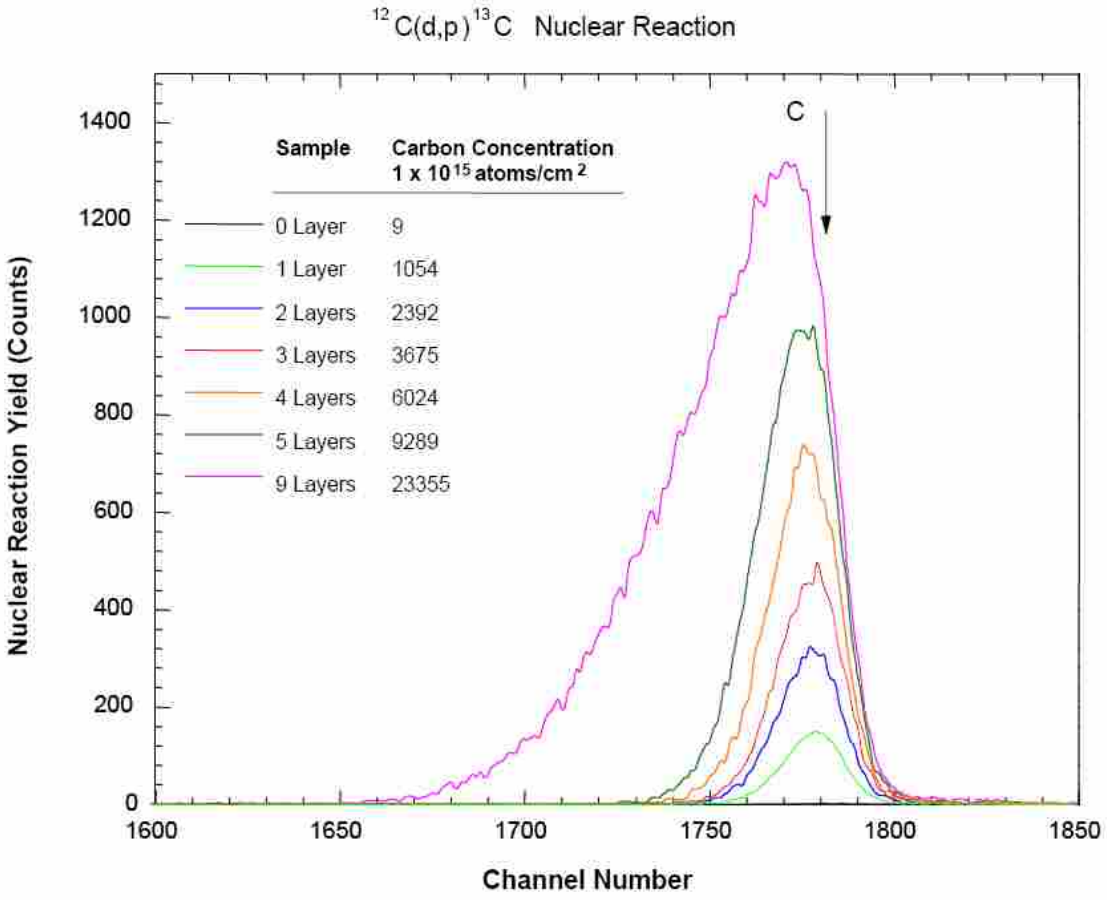

Figure 4.4. NRA spectra of silicon surfaces containing zero, one, two, three, five, and nine bilayers of PAAm-nanodiamond (100-250 nm).

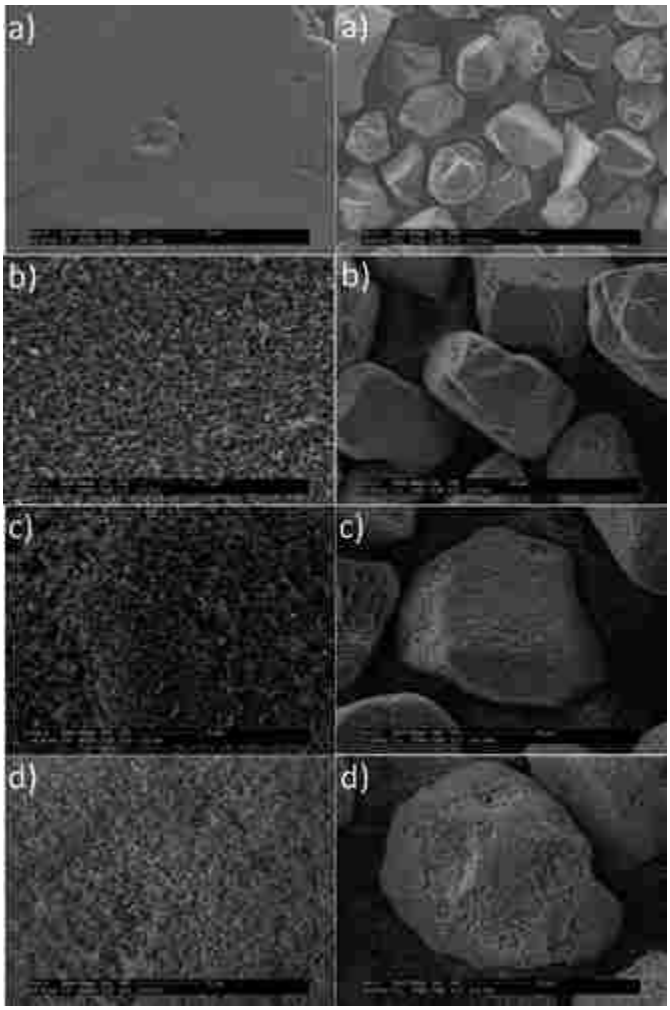

Figure 4.5. ESEM images of 50-70 μm diamond particles containing (a) zero, (b) three, (c) five, and (d) nine bilayers of PAAm-nanodiamond (110-250 nm).

and RBS data. The significant tailing of the nine-bilayer sample is a result of attenuation of the protons in the thicker multilayer film. It is significant that the NRA signal provides absolute quantization of the total carbon content (atoms/cm^2) at the silicon surface.

In the synthesis of core-shell particles, the LbL deposition of nanodiamond particles around a solid microdiamond core was monitored by four techniques: diffuse reflectance Fourier transform infrared spectroscopy (DRIFT), environmental scanning electron miscroscopy (ESEM), Brunauer Emmett and Teller (BET) surface area measurements, and sorbent (analyte) capacity measurements obtained during solid phase extraction. Figure 4.5 shows ESEM images of micron-sized core-shell diamond particles containing 0, 3, 5, and 9 bilayers of PAAm nanodiamond.

As was the case for the planar surfaces, it is clear that nanodiamond particles begin to adsorb onto the surface of PAAm-functionalized microdiamonds after their first immersion in an aqueous suspension of nanodiamonds. ESEM shows that with an increase in the number of nanodiamond layers, the surface becomes fuzzier in appearance, suggesting higher porosity. Core-shell particles were also characterized by DRIFT. Figure 4.6 shows a plot of the area of the C-H stretching region of the core-shell particles as a function of the number of PAAm nanodiamod bilayers. It is evident that the area of the C-H stretching region increases with an increase in the number of bilayers where this increase is attributed to C-H stretches in the PAAm polymer. The fact that the surface area, C-H stretching area, and analyte capacity do not increase linearly with number of PAAm-nanodiamond bilayers in Figure 4.6 may be attributable to the well known “induction period” in LbL deposition – often, a few layers must be deposited before the system begins to show linear increases.[35-36] Two other effects that may also contribute to this lack of linearity may be the increasing radii of the particles and the increase in surface

roughness, and therefore area of the outermost surface, suggested in the ESEM images shown herein.

The primary objective of this work was to synthesize porous diamond powder with high surface areas. Theoretically, deposition of multilayers of nanodiamond particles around a solid microdiamond core would make the structure porous, and increase its surface area. Figure 4.6 shows a plot of the BET surface area of the core-shell particles vs. the number of PAAm-nanodiamond bilayers. As expected, with an increase in the number of nanodiamond layers, the structure becomes more porous. The average pore size of the core-shell particles containing 9 layers of nanodiamond particles was 134 Å by the BET method.

As further characterization, the SPE capacity of the core-shell particles was determined. Figure 4.6 contains a plot of the capacity of the core-shell particles vs. the number of nanodiamond layers. As expected, the analyte capacity increases with an increase in the surface area. For core-shell particles containing 9 layers of nanodiamond particles a *ca.* 80-fold increase in capacity was observed compared to solid, non-porous diamond powder.

4.4.2. Core-Shell Diamond Particles for HPLC

The general LbL strategy outlined above for making diamond-based particles for SPE was also applied to create particles for HPLC, where the core and shell particles were *ca*. 1.7 or 5 μm and 10 – 50 nm, respectively. Figure 4.5 shows ESEM images of such particles with 14 and 28 bilayers of PAAm and nanodiamond. These particles showed much higher surface areas than those made for SPE (see Table 4.1). For example, 13 bilayers of PAAm-nanodiamond on 5 μm core diamond particles produced materials with *ca*. 7 m^2/g of surface area. (Note that diamond is

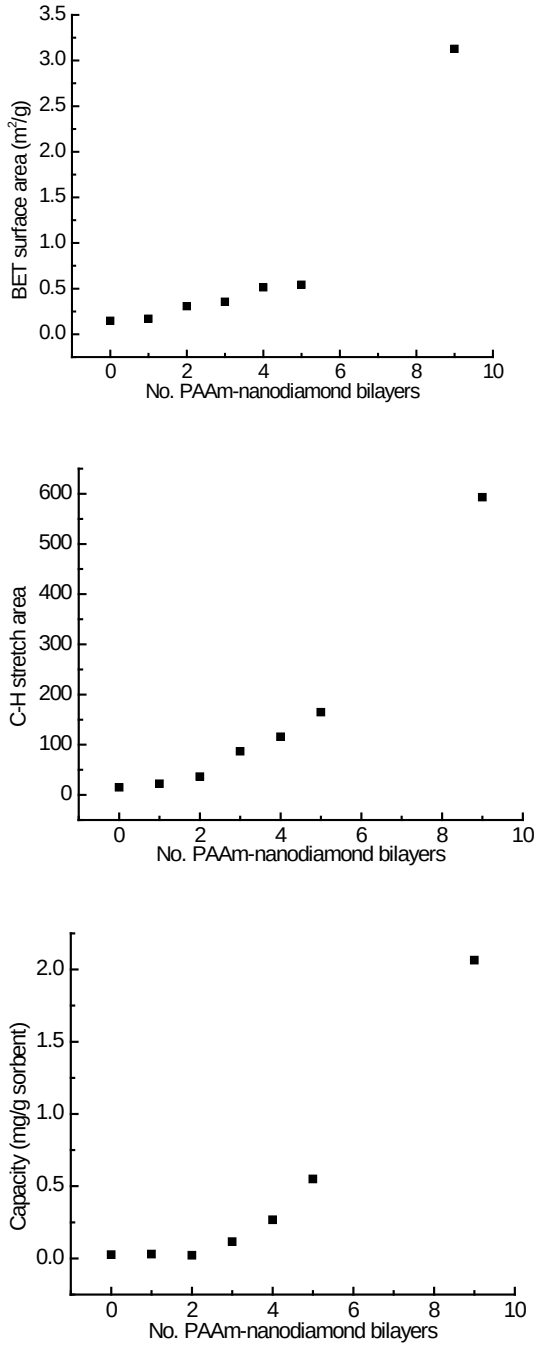

Figure 4.6. Plots of the area of the C-H stretching region, BET surface area, and analyte capacity vs number of PAAm-nanodiamond (100-250 nm) bilayers on 50-70 µm core diamond particles.

Table 4.1. Core-Shell Diamond Particles Produced with Bilayers of 10-50 nm Nanodiamond and PAAm.[a]

Core size (μm)	no. of bilayers	BET surface area (m^2/g)	average pore size (nm)
5	13	6.8	25.9
1.7	14	19.4	
1.7	28	30.3	20.4

[a] Note that diamond is ca. two times as dense as silica, so these surface area numbers should be multiplied by ca. 2 to put them on equal footing with silica.

and dinitrobenzene could be separated, where the dinitrobenzene showed significant tailing (see Figure 4.7 and Table 4.2). Nevertheless, this column showed good stability. Essentially no change in column performance was observed after the mobile phase (33:67 ethyl acetate:hexane with 0.2% TEA) was pumped through the column at 0.3 mL/min for 15.5 hr (see Figure 4.8). While of course amino and/or mixed mode phases are of importance in HPLC, most about twice as dense as silica, so surface areas per gram of diamond particles should be multiplied by two if they are to be compared directly to surface areas per gram of silica particles). As expected, when the size of the core particle shrinks, the surface area of the particles increases. For example, 1.7 μm cores particles with 14 and 28 PAAm-nanodiamond bilayers have 19 and 30 m^2/g of surface area, respectively (again these numbers should be multiplied by two if they are to be compared with silica).

As with the particles prepared for SPE above, the 28 bilayer particles were cross-linked with 1,2,5,6-diepoxycyclooctane to create a mixed mode stationary phase containing amino, hydroxyl, and cyclooctyl groups that would be expected to also have a strong normal phase character. These particles were packed in a 4.6 x 30 mm column and benzophenone separations are performed on C_{18} columns. Accordingly, 28 layer PAAm-nanodiamond particles were treated with 1,2-epoxyoctadecane to make a C_{18} phase, where as before, the carbon nitrogen bonds formed during oxirane ring opening are highly resistant to hydrolysis under either acidic or basic conditions. Separations showing good symmetry of peaks were performed on the resulting HPLC column (see Figure 4.7 and Table 4.2). That is, nearly baseline separation of a series of alkyl benzenes was obtained, and baseline separation of two pesticides was also demonstrated. The alkylbenzenes separated in Figure 4.7 show *ca*. 22,800, 27,700, 26,300, and

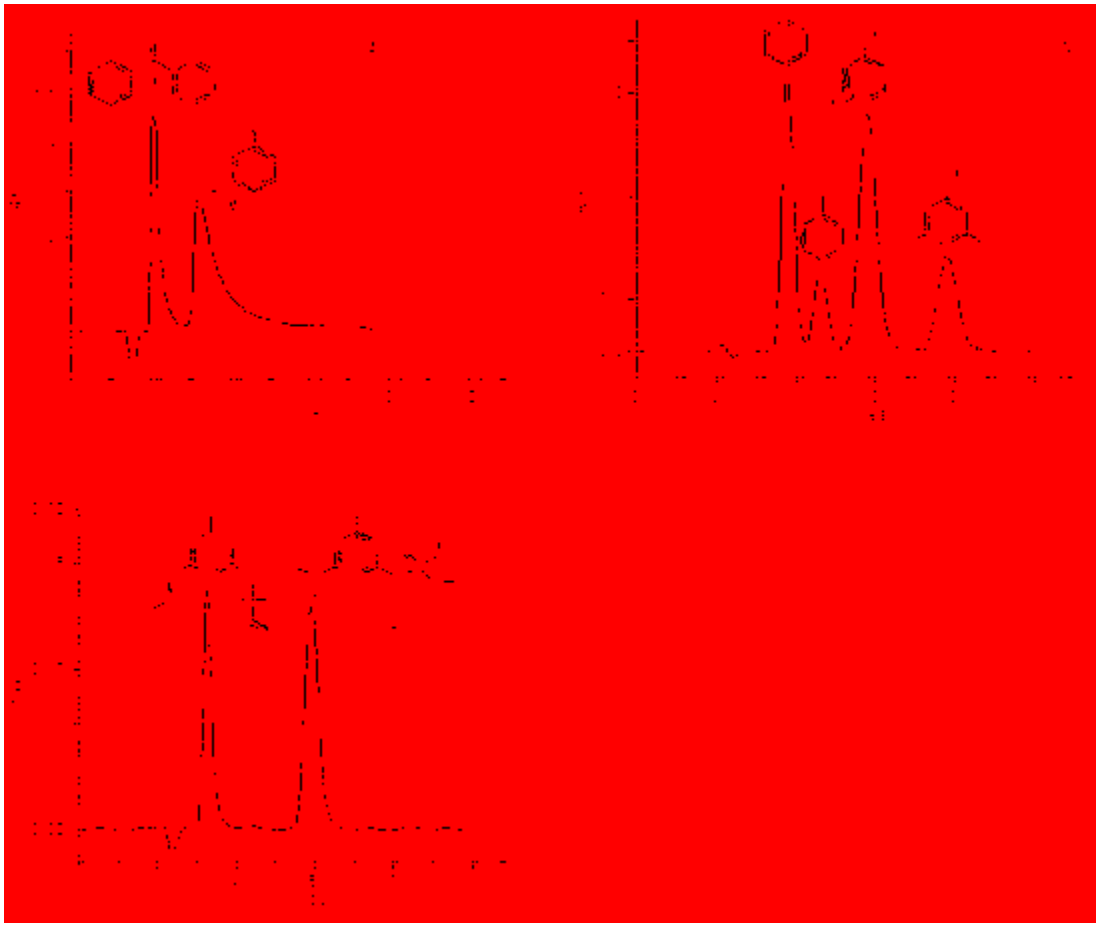

Figure 4.7. (a) Normal phase separation of benzophenone and nitrobenzene with a mobile phase composition of 70% hexane and 30% ethyl acetate (each containing 0.2% triethylamine). The flow rate was 0.3 mL/min. (b) Reversed-phase C18 separation of benzene, toluene, xylene, and mesitylene with a mobile phase composition of 50% acetonitrile and 50% water (each solvent contained 0.1% triethylamine). The flow rate was 0.2 mL/min. (c) Reversed-phase C18 separation of two pesticides (cyanazine and diazinon) with a mobile phase composition of 50% acetonitrile and 50% water (each solvent contained 0.1% triethylamine).

Table 4.2. Retention Factors (k), Plates per Meter (N/m), and Asymmetries for Compounds Separated by HPLC on Normal Phase and Reversed-Phase Diamond Core-Shell Particles.

Analytes	*K*	N/m	Asymmetry
Benzophenone[a]	0.521	22800	2.631
1,4-dinitrobenzene[a]	1.355	5720	5.184
Benzene[b]	0.760	22800	1.103
Toluene[b]	1.146	27700	n/a
Xylene[b]	1.691	26300	1.089
Mesitylene[b]	2.620	36300	1.074
Cyanazine[b]	0.511	40000	1.260
Diazinon[b]	1.760	54800	1.034

[a]Normal-phase, [b]Reversed-phase.

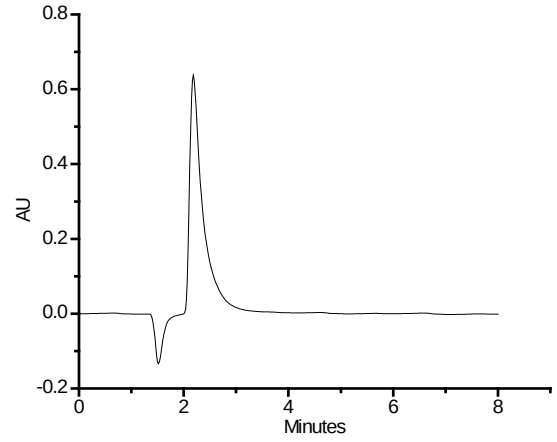

Before stability test (Retention time: 2.05 min.)

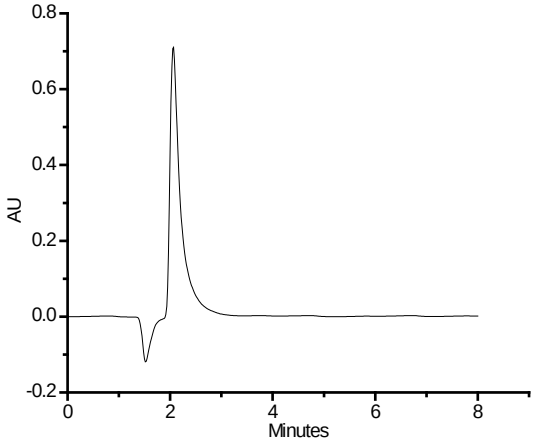

After stability test (Retention time: 2.16 min.)

Figure 4.8. Stability tests were performed on cross-linked core-shell diamond particles that show strong normal phase character. For the reference chromatogram, with benzophenone as the analyte, the mobile phase composition was ethyl acetate: hexane (33%:67%), where each solvent had 0.2% TEA in it, and the flow rate was 0.3 ml/min. For stability studies, the column was left in the above-mentioned mobile phase for 15.5 hours and a second chromatogram was produced. There was only a ca. 5% change in the retention time.

36,300 plates/m for benzene, toluene, xylene (more than one isomer in the sample mixture), and mesitylene, respectively. Even more impressive was a separation of two pesticides (cyanazine and diazinon), which showed 40,000 and 54,800 plates/m respectively. To the best of my knowledge, these results show the highest number of plates/m that have been reported for any diamond-based LC column.

Unfortunately, columns packed with these C_{18} particles were not as stable as those made by cross-linking with the diepoxide; degradation in the column was observed after mobile phase was pumped through it overnight. Taken together, these results of the mixed mode (crosslinked but not hydrophobic) and C_{18} materials (hydrophobic but not crosslinked) suggest that this general strategy for preparing core-shell particles can produce stable stationary phases (hydrophobic and crosslinked) for HPLC. Future work will focus on cross-linking the particles, after which they will be modified to form C_{18} phases.

4.5. Conclusions

I have reported the formation of porous core-shell diamond particles for SPE and HPLC. The effect of LbL deposition of nanodiamond particles on various parameters such as surface area, analyte capacity, IR absorption, *etc.*, was determined. Core-shell diamond particles have higher surface areas and capacities than solid diamond particles, where these properties increase with the number of PAAm-nanodiamond bilayers. HPLC separations with relatively high numbers of plates/m were demonstrated on C_{18} phases.

4.6. References

(1) Snyder, L. R.; Kirkland, J. J.; Glajch, J. L. *Practical HPLC Method Development*; 2 ed.; John Wiely: New York, 1997.

(2) Miller, J. M. *Chromatography: Concepts and Contrasts*; 2 ed.; John Wiley & Sons, Inc.: Hoboken, 2005.

(3) Nawrocki, J.; Dunlap, C.; Li, J.; Zhao, J.; McNeff, C. V.; McCormick, A.; Carr, P. W. *J. Chromatogr. A* **2004**, *1028*, 31-62.

(4) Majors, R. E. *LCGC North Am.* **2008**, *26*, 1074-1090.

(5) Kirkland, J. J.; Glajch, J. L.; Farlee, R. D. *Anal. Chem.* **1989**, *61*, 2-11.

(6) West, C.; Elfakir, C.; Lafosse, M. *J. Chromatogr. A, In Press, Corrected Proof*.

(7) Pereira, L. *J. Liq. Chromatogr. Relat. Technol.* **2008**, *31*, 1687 - 1731.

(8) Nawrocki, J.; Dunlap, C.; McCormick, A.; Carr, P. W. *J. Chromatogr. A* **2004**, *1028*, 1-30.

(9) Nawrocki, J.; Rigney, M.; McCormick, A.; Carr, P. W. *J. Chromatogr. A* **1993**, *657*, 229-282.

(10) Rigney, M. P.; Weber, T. P.; Carr, P. W. *J. Chromatogr. A* **1989**, *484*, 273-291.

(11) Cazes, J.; Ed. *Marcel Dekker: New York* **2004**, 147.

(12) Sun, L.; McCormick, A. V.; Carr, P. W. *J. Chromatogr. A* **1994**, *658*, 465-473.

(13) Sun, L.; Carr, P. W. *Anal. Chem.* **1995**, *67*, 3717-3721.

(14) Blackwell, J. *Chromatographia* **1993**, *35*, 133-138.

(15) Blackwell, J. A.; Carr, P. W. *J. Chromatogr. A* **1991**, *549*, 59-75.

(16) Blackwell, J. A.; Carr, P. W. *J. Liq. Chromatogr. Relat. Technol.* **1991**, *14*, 2875 - 2889.

(17) Nesterenko, P.; Haddad, P. *Anal. Bioanal. Chem.* **2010**, *396*, 205-211.

(18) Björkman, H.; Ericson, C.; Hjertén, S.; Hjort, K. *Sens. Actuators, B* **2001**, *79*, 71-77.

(19) Pierson, H. O. *Handbook of Carbon, Graphite, Diamond, and Fullerenes: Properties, Processing and Applications*; Noyes Publications: New Jersey, 1993.

(20) Nesterenko, P. N.; Fedyanina, O. N.; Volgin, Y. V. *Analyst* **2007**, 403-405.

(21) Purtov, K.; Puzyr', A.; Bondar', V. *Dokl. Biochem. Biophys.* **2008**, *419*, 72-74.

(22) Nesterenko, P. N.; Fedyanina, O. N.; Volgin, Y. V.; Jones, P. *J. Chromatogr. A* **2007**, *1155*, 2-7.

(23) Saini, G.; Gates, R.; Asplund, M. C.; Blair, S.; Attavar, S.; Linford, M. R. *Lab Chip* **2009**, *9*, 1789-1796.

(24) Saini, G.; Yang, L.; Lee, M. L.; Dadson, A.; Vail, M. A.; Linford, M. R. *Anal. Chem.* **2008**, *80*, 6253-6259.

(25) Saini, G.; Wiest, L. A.; Herbert, D.; Biggs, K. N.; Dadson, A.; Vail, M. A.; Linford, M. R. *J. Chromatogr. A* **2009**, *1216*, 3587-3593.

(26) Yang, L.; Lua, Y.-Y.; Tan, M.; Scherman, O. A.; Grubbs, R. H.; Harb, J. N.; Davis, R. C.; Linford, M. R. *Chem. Mater.* **2007**, *19*, 1671-1678.

(27) Yang, L., Brigham Young University, 2009.

(28) Kirkland, J. J.; Landlois, T. J.; DeStefano, J. J. *Am. Lab.* **2007**, *8*, 18-20.

(29) Lvov, Y. M.; Price, R. R. *Colloids Surf., B* **2002**, *23*, 251-256.

(30) Caruso, F.; Fiedler, H.; Haage, K. *Colloids Surf., A* **2000**, *169*, 287-293.

(31) Ge, J.; Li, Y. M.; Chen, L. R. J. Liq. Chromatogr. Related Technol. **2006**, *29*, 2329-2339.

(32) Kirkland, J. J.; Langlois, T. J. **2007**.

(33) Lange's Handbook of Chemistry, 15th ed.; McGraw-Hill Handbooks, 1999.

(34) Yang, L.; Vail, M. A.; Dadson, A.; Lee, M. L.; Asplund, M. C.; Linford, M. R. *Chem. Mater.* **2009**, *21*, 4359-4365.

Chapter 5. Directing Polyallylamine Adsorption onto Microlens Array Patterned Silicon for Microarray Fabrication*

5.1. Abstract

The selective adsorption of reagents is often essential for bioarray and lab-on-a-chip type devices. In this work, I demonstrate the application of microlens array patterning (MAP) in bioarray fabrication. As the starting point for a bioarray, alkyl monolayer-terminated silicon shards were photopatterned in a few nanoseconds with thousands of wells (spots) using an optical element, a microlens array. Polyallylamine (PAAm), a primary amine containing polymer, adsorbed with little selectivity to the spots, *i.e.*, silicon oxide, over the hydrophobic background. However, at appropriate concentrations, addition of a cationic surfactant, cetyltrimethylammonium chloride, to the PAAm deposition solution prevented the nonspecific adsorption of PAAm onto the hydrophobic monolayer, while directing it effectively to the active spots on the device. A nonionic surfactant was less effective in preventing the nonspecific adsorption of PAAm onto the hydrophobic monolayer. The localized reactions/interactions of adsorbed PAAm with four species that are useful for bioconjugate chemistry: glutaric anhydride, phenylenediisothiocyanate, biotin NHS ester, and an oligonucleotide (DNA) were shown in the spots of an array. The reactivity of PAAm was further demonstrated with an isocyanate. Time-of-flight secondary ion mass spectrometry (ToF-SIMS) played an important role in confirming

*This chapter is reproduced with permission from (Gaurav Saini, Richard Gates, Matthew C. Asplund, Steve Blair, Sachin Attavar, and Matthew R. Linford) *Lab Chip*, 2009, 9, 1789-1796.

selective surface reactivity and adsorption. X-ray photoelectron spectroscopy (XPS), spectroscopic ellipsometry, and wetting confirmed PAAm reactivity on planar substrates.

5.2. Introduction

Bioarrays are indispensable tools for genome and proteome analysis because of their high throughput nature. A common approach for fabricating bioarrays involves activating surfaces with a compound or polymer, and then dispensing drops of a probe solution onto the activated surface with a microarrayer.[1] Although widely employed, this approach has some limitations. First, the background of the bioarray often contains chemically reactive functional groups and is not chemically inert: side reactions or redeposition of adsorbed species during bioarray preparation or analysis may occur. Thus, for many bioarray preparations, background regions must be passivated or blocked,[2-5] adding additional steps to array fabrication. "Such passivation can potentially damage … spotted DNA, lower the quality of the microarray, or both."[6]

Commercially available microlens arrays, including home-built arrays of microbeads used for materials micromachining,[7,8] are powerful tools for chemically patterning surfaces.[9] Microlens arrays with different spacings and packings of lenses are commercially available. With microlens arrays, thousands of functionalized spots (wells) can be patterned onto surfaces in nanoseconds. For subsequent modification of such arrays, it is critical that reagents be developed that selectively deposit to either the wells or to the backgrounds. Accordingly, I desired to selectively deposit a polymer that is rich in primary amines (polyallylamine, or PAAm) into wells made with a microlens array. The selective deposition of amines in the wells of a microlens array patterned substrate would provide the foundation for virtually any additional functionalization of the chip to make a bioarray.[10]

As the background layer to these wells a hydrophobic alkyl monolayer on silicon was chosen. Hydrophobic backgrounds are useful parts of planar devices because they can limit the movement of, focus during evaporation, and/or localize droplets of aqueous solutions on surfaces.[11,12] Ablation or thermal removal of the alkyl monolayer on silicon by the microlens array should leave a pattern of silicon oxide-containing spots.[13 9] The silanol groups on SiO_2 are acidic, and the primary amines in PAAm are basic, which drives PAAm adsorption onto SiO_2. Spontaneous adsorption of other amine-containing polymers such as polylysine[2] and polyethylenimine[14,15] onto SiO_2 is well known.

I demonstrate the expected adsorption of PAAm to exposed wells on microlens array patterned alkyl monolayer terminated substrates. Unfortunately, this adsorption is accompanied by a significant and undesirable adsorption of PAAm to the hydrophobic background of the chip. I show that the appropriate addition of a cationic surfactant to the PAAm creates a solution that directs PAAm adsorption to the spots on the array, while prohibiting it in the background. The addition of a nonionic surfactant only partially prevents the non-specific adsorption of PAAm onto the hydrophobic background. Subsequent reactivity of selectively adsorbed PAAm is then demonstrated with four reagents that are useful for bioconjugate chemistry. Selective adsorption and reactivity are important topics in many areas of science, including separation science, the rational design of nano- and microscale materials, and surface modification. Surface reactivity was confirmed by imaging time-of-flight secondary ion mass spectrometry (ToF-SIMS)[16], and on planar surfaces by X-ray photoelectron spectroscopy (XPS), spectroscopic ellipsometry, and water contact angle measurements.

Surface adsorption of poly(allylamine hydrochloride) (not the neutral polymer) is well known, especially in the context of the layer-by-layer adsorption of polyelectrolyte

multilayers.[17-22] The chemical reactivity of adsorbed poly(allylamine hydrochloride) with an active form of biotin has been reported.[23] There has been less work on the adsorption of neutral polyallylamine (PAAm) and/or its subsequent reactivity.[24,25]

5.3. Experimental

5.3.1. Materials

Polyallylamine (20 wt. % in water), phenylene 1,4-diisothiocyanate (PDITC, 98%), glutaric anhydride (GA, 95%), biotin NHS ester (BNE, 98%), 1-hexadecene ($\geq$ 99%), cetyltrimethylammoniumchloride (CTAC, $CH_3(CH_2)_{15}N(CH_3)_3Cl$, 25 wt. % in water) and Brij 98 ($C_{18}H_{35}(OCH_2CH_2)_nOH$, n ~ 20) were purchased from Aldrich and used as received. A 30mer (otherwise unfunctionalized) oligonucleotide was purchased from New England Biolabs Inc, Massachusetes. Silicon wafers (test grade, n-type, <1-0-0> orientation, 2–6 Ω-cm) were purchased from UniSil Corporation, California and cleaved into *ca*. 1.5 × 1.5 cm pieces.

5.3.2. Formation of the hexadecyl monolayer

The hexadecyl (self-assembled[26]) monolayer was prepared on hydrogen terminated silicon (100) surface by adopting a reported approach.[27,28] The silicon surface was first plasma cleaned for 1 minute to remove organic contamination (Harrick plasma cleaner, model PDC-32G, 18 W). It was then immersed in a 5% HF solution for 3 minutes to remove the native oxide layer and form Si–H moieties. The hydrogen terminated surface was next immersed in neat 1-hexadecene at 210°C for 2 hours under N_2.

5.3.3. Microlens array patterning

Microlens array patterning of hexadecyl monolayer coated Si/SiO_2 surfaces was done by placing the substrate beneath a microlens array and firing a 4 ns pulse of 532 nm laser light through the array. The microlenses in this optical element focused the laser into thousands of individual spots on the surface, which resulted in the thermal removal of the hexadecyl monolayer, and hence exposure of the underlying reactive SiO_2 surface. In microlens array patterning, some laser light may pass between the microlenses, and thus remove or damage the hexadecyl monolayer at positions other than at the foci of the optical lenses. This may lead to some undesired adsorption of PAAm onto the background in addition to the spots.

5.3.4. Surface adsorption of polyallylamine (PAAm) onto silicon oxide in the presence of CTAC or Brij 98

All PAAm depositions, with or without CTAC or Brij 98, were with 0.1 wt. % solutions of PAAm, and all immersion times were 35 minutes. In practice it has been found that 35 minutes is more than enough time to saturate clean, oxide-terminated silicon with PAAm (*vide infra*). After this immersion, the surfaces were removed, and washed thoroughly with water. Solutions of 0.1 wt. % PAAm and either 5, 10, 15, or 20 wt. % CTAC were used to determine the appropriate concentration of CTAC that would prevent PAAm adsorption on a hydrophobic surface, while permitting it on a hydrophilic one. For the reactions with GA, PDITC, and BNE, 10 wt. % CTAC was present in the PAAm deposition solution. For the deposition of PAAm onto silicon oxide or the hexadecyl monolayer in the presence of the nonionic surfactant, 2.5%, 5.0% and 10 wt. % solutions of Brij 98 were used. *Note: 10 wt. % is at the edge of water solubility for this surfactant.*

5.3.5. Reaction of adsorbed PAAm with GA

A nearly saturated solution of GA was made by dissolving 10 g of GA in 10 ml of dry DMF. The preparation of this solution, along with those of PDITC and BNE described below, and the immersion of PAAm coated surfaces into these solutions, was performed under nitrogen. Patterned and planar surfaces with adsorbed PAAm were immersed in this solution overnight. The surface was then rinsed thoroughly with DMF and CH_2Cl_2.

5.3.6. Reaction of adsorbed PAAm with PDITC

PDITC was dissolved in a 9:1 solution of dry DMF:pyridine to make a 0.4 or 1.6 wt. % solution. PAAm functionalized surfaces were then immersed in this solution for 3 hours. After the 3 hr reaction with 1.6 wt. % solution of PDITC, the washed surface was characterized by spectroscopic ellipsometry and wetting, and then reimmersed in the 1.6 wt. % solution overnight. After these reactions, the surfaces were rinsed thoroughly with DMF and CH_2Cl_2.

5.3.7. Reaction of adsorbed PAAm with BNE

The Biotin-NHS ester solution was made by dissolving 25 mg of BNE in 5 ml of dry DMSO. PAAm functionalized surfaces were immersed in this solution for 4 hours, and then rinsed thoroughly with DMF and CH_2Cl_2.

5.3.8. Reaction of adsorbed PAAm with 1H,1H,2H,2H-Perfluorodecyl isocyanate

A 2.6 wt./v % solution of 1H,1H,2H,2H-Perfluorodecyl isocyanate was made by dissolving 0.834 g of this reagent in 29 ml of dry THF. PAAm treated surfaces were immersed in 15 ml of this solution. The reaction was performed in a sealed, thick walled glass tube at 75° C

for 4 hours. After the reaction, the surfaces were washed thoroughly with THF followed by dichloromethane.

5.3.9. Adsorption of an oligonucleotide onto PAAm

An 85.7 μM solution of an oligonucleotide (an unfunctionalized 30-mer) was made by diluting 30 μL of a 200 μM stock solution (made in 3 × SSC buffer containing 1 μM EDTA and 0.1% SDS) with 40 μL of printing buffer (150 mM PBS, pH 8.5). After dilution, the microvial containing diluted oligonucleotide solution was shaken on a vortex mixer to homogenize the solution. An aliquot (20 μL) of this solution was dispensed on a microlens array patterned surface (containing PAAm selectively adsorbed in spots), and another microlens array patterned surface (also containing PAAm selectively adsorbed onto spots) was placed on this surface with the patterned surfaces facing each other. The reaction (adsorption) was done in a humid atmosphere in a beaker for 14 hours at room temperature. After treatment with the oligonucleotide solution, the surfaces were washed extensively with copious amounts of sterilized water.

5.3.10. Reaction yields

The fraction of the amine groups in PAAm that had reacted with PDITC or BNE, *i.e.*, the ields of the reactions, was determined from the nitrogen to sulfur ratio, as measured by XPS, using the formulas given below, where these formulas ignore attenuation of photoelectrons from the thin films and therefore (conveniently) provide upper limits for the reported yields.

$$Yield_{PDITC\,\mathrm{Re}\,action} = \frac{0.5}{\frac{N_{TOT}}{S_{PDITC}} - 1} x100\%$$

$$Yield_{BNE\,\mathrm{Re}\,action} = \frac{1}{\frac{N_{TOT}}{S_{biotin}} - 2}\ x100\%$$

5.3.11. Surface characterization

Patterned and planar surfaces were characterized by time-of-flight secondary ion mass spectrometry (ToF-SIMS) (ION-TOF TOF-SIMS IV instrument with a two-lens $^{69}Ga^{+}$ gun), contact angle goniometry (Rame-Hart model 100-00 contact angle goniometer), spectroscopic ellipsometry (J.A. Woollam M-2000), and/or X-ray photoelectron spectroscopy (XPS) (Surface Science SSX-100 instrument with a monochromatized Al Kα source and a hemispherical analyzer). All ToF-SIMS images shown herein have the same dimensions. During the ToF-SIMS acquisition of the PO_3^- image, a large number of scans (750) were taken to increase the signal-to-noise ratio, which corresponds to 3.0×10^{12} primary ions/cm^2. For the other images in this work, *ca.* 100 scans were taken, placing them well within the static limit.

5.4. Results and discussion

To form a hydrophobic base layer on the silicon surface, monolayers of 1-hexadecene were deposited thermally on hydrogen-terminated silicon from the neat liquid[27,28]. The ellipsometric thickness of these monolayers was 18.8 ± 0.2 Å and their advancing water contact angle was 101 ± 1°. X-ray photoelectron spectroscopy (XPS) showed the expected C1s signal after monolayer formation (see Figure 5.1a). These results confirm formation of a hydrophobic monolayer of alkyl chains on the silicon surface. A hydrophobic background layer was chosen

because it would be expected to localize (and perhaps focus by evaporation) droplets of aqueous solutions above hydrophilic spots.[11,12]

The kinetics of PAAm adsorption onto SiO_2 were studied. Plasma cleaned SiO_2 terminated silicon surfaces (two each) were immersed in 0.1 wt. % PAAm solutions for seven different time periods: 5, 10, 20, 35, 50, 70 and 160 min. Even the 5 minute immersion was sufficient for PAAm to saturate this surface. The average ellipsometric film thickness for all of these surfaces was 7.3 Å, with a standard deviation of 1.8 Å. The advancing water contact angle of these surfaces was 30 ± 2°. ToF-SIMS of this surface shows peaks characteristic of the polymer including CH_2N^+, CH_4N^+, $C_2H_4N^+$, $C_2H_5N^+$, $C_2H_6N^+$, and $C_3H_6N^+$. XPS shows the expected N 1s signal after PAAm adsorption (see Figure 5.1b).

To investigate the effect of PAAm concentration on its adsorption on silicon oxide, 0.1 wt. %, 0.25 wt. %, 0.50 wt. % and 0.75 wt. % solutions of PAAm were prepared, and silicon oxide surfaces were immersed in these solutions for 35 minutes. The ellipsometric thicknesses of the resulting PAAm layers were 8.7 ± 1.8 Å, 8.9 ± 0.6 Å, 9.6 ± 0.5 Å, and 10.2 ± 1.5 Å, respectively, which are consistent with the hypothesis that PAAm undergoes self-limiting adsorption on silicon oxide that is not strongly affected by PAAm concentration. On the basis of this observation, a 0.1% PAAm solution was deemed adequate for further studies.

PAAm, with its high density of primary amines, has ideal chemistry for subsequent bioconjugate chemistry[10] and it adsorbs effectively to silicon oxide (*vide supra*). Unfortunately, it adsorbs to hydrophobic monolayers, which severely limits its utility in lab-on-a-chip type devices. Immersion of a 1-hexadecene monolayer on silicon into a dilute solution of PAAm leads to an increase in film thickness of 19 ± 2 Å, and a decrease in the advancing water contact angle from 101 ± 1° to 64 ± 1°. This water contact angle may be closer to the "true" value for PAAm.

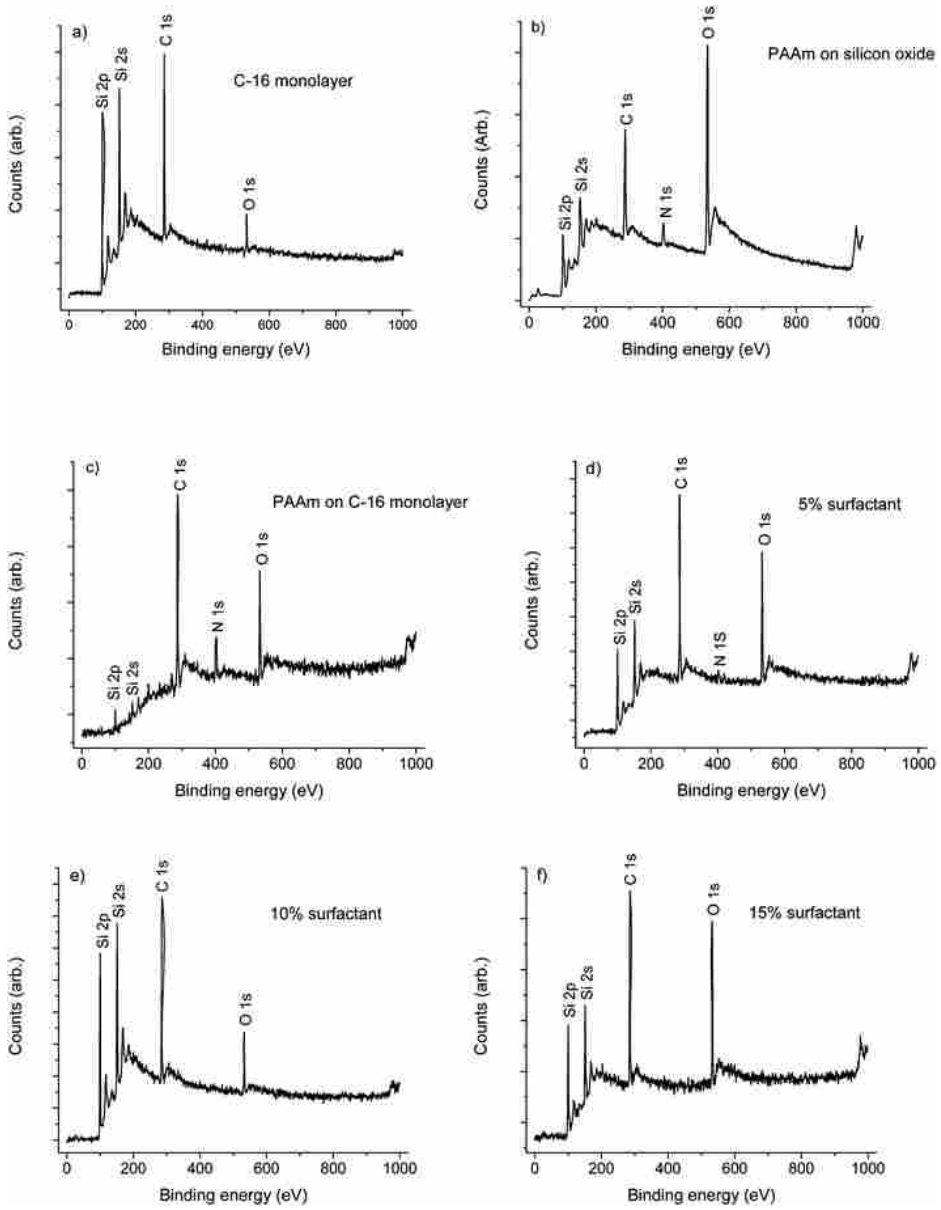

Figure 5.1. XPS survey scans of a) a monolayer of 1-hexadecene on hydrogen-terminated silicon, b) PAAm adsorbed on a native oxide coated silicon substrate, c) PAAm adsorbed on a monolayer of 1-hexadecene on hydrogen-terminated silicon, d) PAAm adsorbed on a monolayer of 1-hexadecene on hydrogen-terminated silicon in the presence of 5% CTAC, e) PAAm adsorbed on a monolayer of 1-hexadecene on hydrogen-terminated silicon in the presence of 10% CTAC, and f) PAAm adsorbed on a monolayer of 1-hexadecene on hydrogen-terminated silicon in the presence of 15% CTAC.

The lower water contact angle for the very thin (< 1 nm) film of PAAm (*vide supra*) probably reflects the effects of the extremely hydrophilic SiO_2 substrate it is on. XPS shows a strong N 1s signal from these surfaces, where no such nitrogen signal could be detected from the 1-hexadecene monolayer prior to PAAm adsorption (see Figs. 5.1a and 5.1c). The adsorption of PAAm onto the hydrophobic monolayer is probably a result of favorable hydrophobic-hydrophobic interactions between PAAm's backbone and the alkyl monolayer. That is, it can be seen as behaving like a protein with a hydrophilic exterior and a hydrophobic interior in its affinity towards this hydrophobic surface.

A hexadecyl monolayer can be patterned on silicon using a microlens array to make an array of spots and the resulting chemical contrast can be viewed by time-of-flight secondary ion mass spectrometry (ToF-SIMS).[9,13] In spite of the less than ideal properties of the hydrophobic background with regards to PAAm adsorption, a microlens array patterned 1-hexadecene monolayer on silicon was immersed in a dilute solution of PAAm. Some limited chemical contrast between spots and background could be seen on the resulting surfaces by imaging ToF-SIMS (see Figure 5.2a). However, it was apparent that the high level of nonspecific PAAm adsoption on the hydrophobic monolayer would lead to unacceptable background levels in microarrays made with this method.

To address the issue of nonspecific adsorption of PAAm, an additive was sought for that would limit or eliminate the nonspecific adsorption of PAAm on 1-hexadecene monolayers, while still allowing adsorption to take place on silicon oxide. To this end a cationic surfactant, cetyltrimethylammonium chloride ($CH_3(CH_2)_{15}N^+(CH_3)_3Cl^-$ or CTAC), was added to the PAAm adsorption solution. Polymer-surfactant interactions, especially, but not exclusively, those between polyelectrolytes and surfactants with opposite charges, have been studied. These reports

include studies of a mixture of polyallylamine hydrochloride and cetyltrimethylammonium bromide[29] or a mixture of poly(styrenesulfonate sodium salt) and cetyltrimethylammonium bromide in the synthesis of mesoporous silica,[30] and a report of ordered structures of poly(allylamine hydrochloride) and sodium dodecylbenzenesulfonate.[31]

Theoretically CTAC's hydrophobic tail would cause it to adsorb at the hydrophobic monolayer, sterically limiting access of PAAm to the monolayer. Furthermore, the permanent positive charge on CTAC should repel any protonated amines in PAAm chains. Figure 5.3 shows the effect of this surfactant on the changes in wetting and ellipsometric thickness of 1-hexadecyl monolayers on silicon. As noted, when no surfactant is present, there is a significant decrease in the water contact angle, and a significant increase in the ellipsometric thickness of 1-hexadecene monolayer coated substrates. However, when a monolayer on silicon is immersed in a PAAm solution containing 5 wt. % CTAC, the increase in thickness from the PAAm is only 7.6 Å and the water contact angle of this surface only decreases to 80°. At 10%, 15%, or 20% CTAC, the water contact angle and ellipsometric thickness of the 1-hexadecyl monolayer on silicon remains essentially constant after immersion in a PAAm solution. Indeed, hexadecyl monolayers on silicon that were immersed in PAAm solutions that contained 10 wt.% or more CTAC showed no nitrogen by XPS. Figure 5.2 shows the greatly improved contrast in ToF-SIMS of PAAm deposited with 10 wt. % CTAC on a microlens array patterned 1-hexadecene monolayer. Hence, the nonspecific adsorption of PAAm on 1-hexadecene monolayers on silicon is prevented at CTAC concentrations of 10 wt. % or higher. It is also significant that solutions of PAAm containing 10 wt. % CTAC allow PAAm to adsorb effectively onto oxide-terminated silicon. However, at 15 or 20 wt. % CTAC, the adsorption of PAAm onto oxide appears to be somewhat limited. The N/Si ratio for PAAm adsorption onto clean silicon oxide surfaces decreases a little.

Figure 5.2. ToF-SIMS images of a) PAAm deposited on a microlens array patterned 1-hexadecene monolayer on silicon, and b) PAAm deposited on a microlens array patterned 1-hexadecene monolayer on silicon in the presence of the surfactant CTAC.

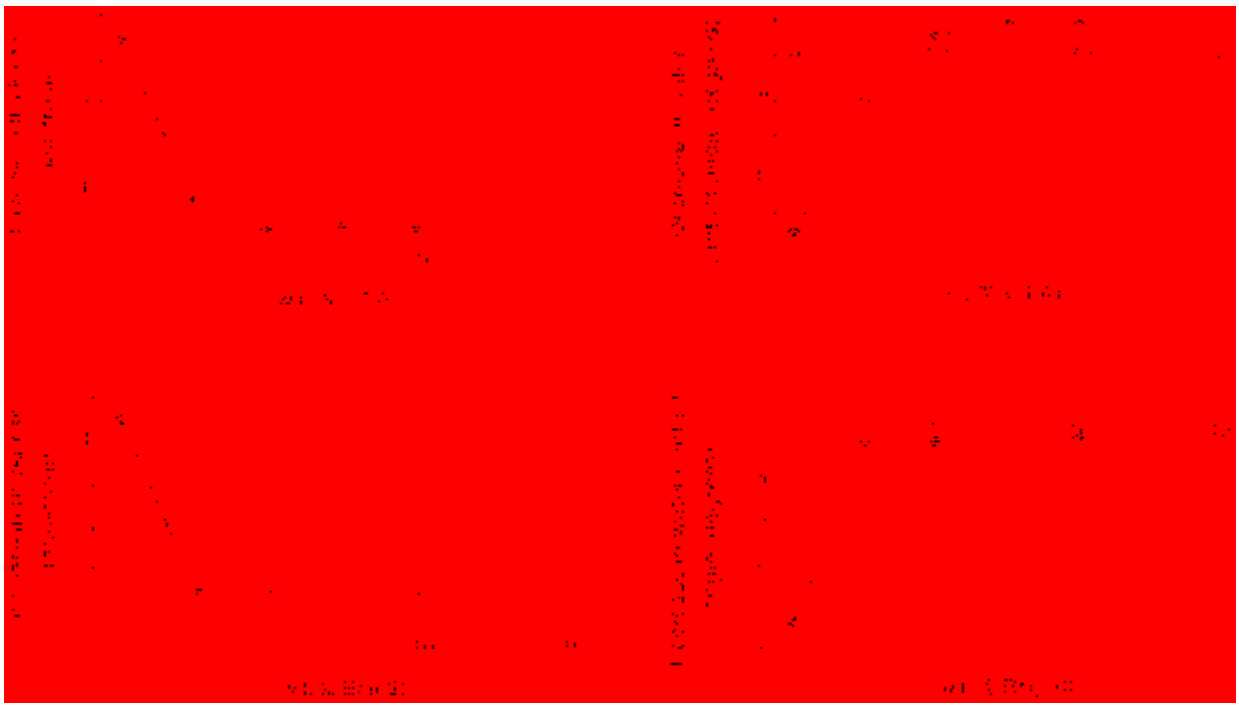

Figure 5.3. Increase in thickness and decrease in advancing water contact angle of 1-hexadecene monolayers on silicon after their immersion in dilute solutions of PAAm with no surfactant and in the presence of increasing amounts of two surfactants. All immersion times were 35 minutes.

Figure 5.4. The CN^- ion from negative ion ToF-SIMS images of MAP 1-hexadecene monolayers on silicon after immersion in PAAm solutions containing a) 10% CTAC, b) 15% CTAC, and c) 20% CTAC.

To determine whether the effects observed for CTAC were due to its cationic nature, or it just being a surfactant, a nonionic surfactant: Brij 98 (see Figure 5.5) was tried. Unlike CTAC, Brij 98 does not contain a cationic head group, so any surfactant adsorbed at the monolayer-water interface would be expected to sterically, but not electrostatically, limit PAAm adsorption. Figure 5.3 shows the effect of Brij 98 on the wetting and ellipsometric thickness of 1-hexadecyl monolayers that were treated with PAAm solution. As is evident, the surfactant *does* reduce the non-specific adsorption of PAAm onto 1-hexadecyl monolayers, but unlike CTAC, it is unable to completely prevent this undesirable adsorption at any wt. %. The average increase in thickness of 1-hexadecyl monolayers on silicon after treatment with PAAm solution in the presence of 2.5 wt. %, 5 wt. % and 10 wt. % surfactant was 5.9 Å with a tight standard deviation of 0.5 Å, and the contact angle decreased from 104° for 1-hexadecyl monolyers to a value of 94 ± 1° after immersion in PAAm solution. The N/Si ratio measured from XPS narrow scans for the 1-hexadecyl monolayers that were treated with PAAm solution in the presence of 2.5 wt. %, 5 wt. % and 10 wt. % surfactant was 0.05, 0.06 ± 0.02 and 0.06 ± 0.02, respectively, where this surfactant almost equally limits the adsorption of PAAm onto silicon oxide for the three different concentrations studied. The N/Si ratios by XPS for the silicon dioxide surfaces which were treated with 0.1 wt. % PAAm in the presence of 2.5, 5.0 and 10 wt. % of the Brij surfactant, were 0.21, 0.20 and 0.22, respectively.

Given that PAAm would adsorb selectivity into hydrophilic spots on microlens array patterned hydrophobic surfaces in the presence of CTAC, it was desirable to demonstrate that PAAm would retain its activity after adsorption and undergo reactions typical of primary amines. For this purpose, I chose four classic reactions/interactions of amines: their reaction with an

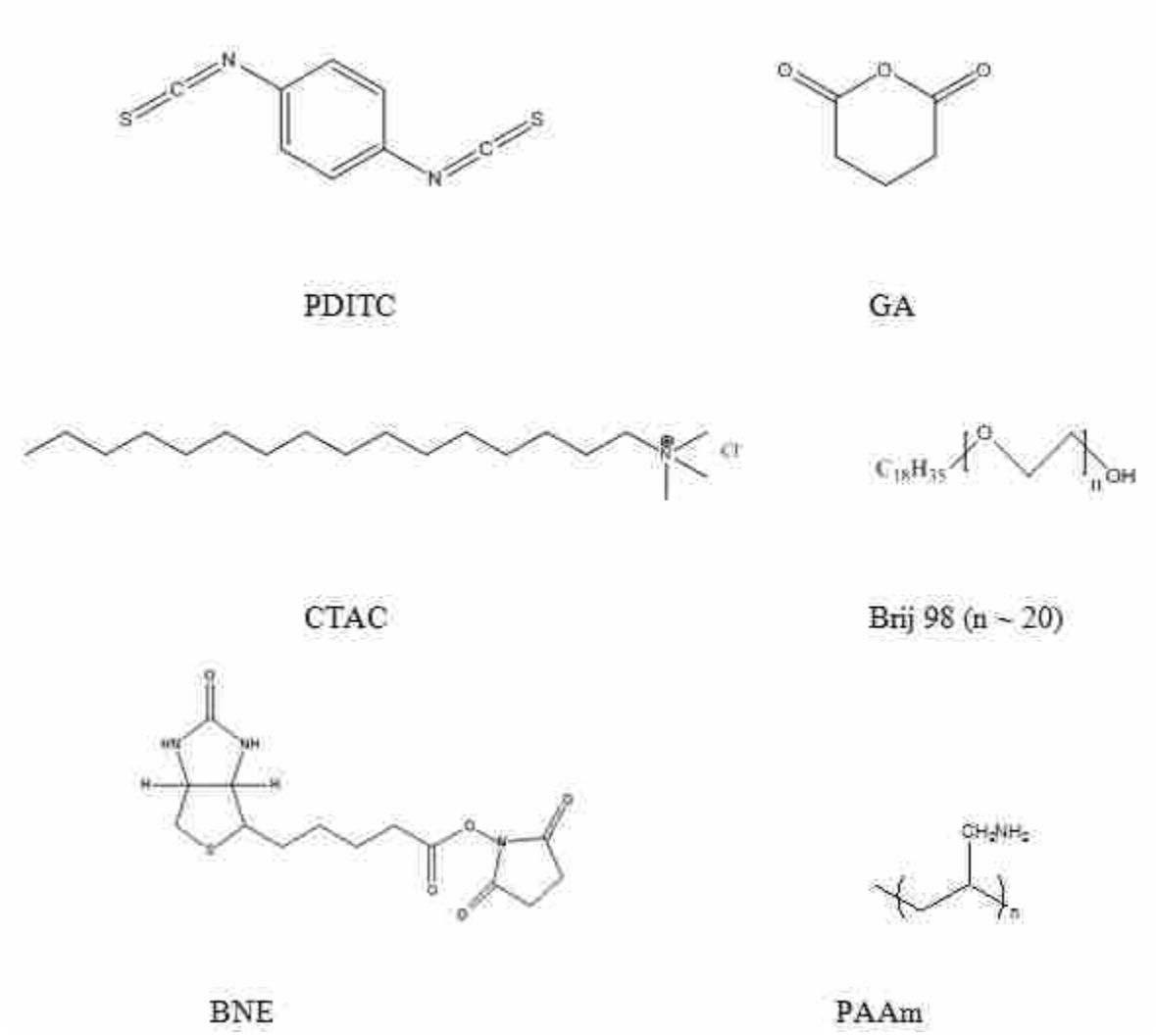

Figure 5.5. Chemical structures of various molecules employed in the study.

anhydride[32] (glutaric anhydride (GA)), an isothiocyanate[33] (phenylene diisothiocyanate (PDITC)), an activated ester[10] (biotin NHS ester (BNE)) (see Figure 5.5), and an oligonucleotide. Reactions with GA, PDITC, and BNE were first demonstrated on planar silica surfaces to which PAAm had adsorbed. Table 5.1 gives a summary of the changes in ellipsometric thicknesses, advancing water contact angles, and XPS results for these reactions. Using the nitrogen to sulfur ratios found by XPS (see Table 5.1) it was possible to calculate yields for the reactions of PDITC and BNE with adsorbed PAAm. For the PDITC reaction, the yield was determined to be 8% when the PDITC concentration was 0.4%, and 15% when the PDITC concentration was 1.6%, *i.e.*, 8% and 15% of the primary amine groups in the PAAm reacted. The yield of the BNE reaction was 35%. The lower yield of the PDITC reaction may reflect its activity as a crosslinker, which would limit access of PDITC molecules to lower parts of the PAAm films after some crosslinking had occurred.

ToF-SIMS images reveal that the desired reactions occur with PAAm adsorbed in arrays when CTAC is present, but that the subsequent reactions appear to take place on both the spots and the backgrounds when CTAC is not present in the adsorption solution. Figures 5.6a, c, and e show ToF-SIMS images of characteristic ions from a microlens array patterned surface after immersion in a solution of PAAm that did not contain surfactant, followed by reaction with PDITC, biotin NHS-ester, and glutaric anhydride. Minimal contrast between spots and backgrounds is occasionally discernable in the images , but overall the contrast in these images is is very poor. On the other hand, the ToF-SIMS images in Figures 5.6b, d, and f show that the presence of the CTAC surfactant during PAAm adsorption strongly improves localization of the desired reactions.

Table 5.1. Physical properties of PAAm coated silicon oxide surfaces after their reaction with PDITC, GA, and Biotin-NHS ester.

Reaction	Thickness change	Contact angle	XPS
PAAm-PDITC (0.4%, 3 hr)	7.7 ± 1.5 Å	62 ± 2°	N:S ratio 87.9:12.1
PAAm-PDITC (1.6%, 3 hr)	7.6 Å	72°	
PAAm-PDITC (1.6%, overnight)[a]	11.6 Å	79°	N:S ratio 81.5:18.5
PAAm-GA	10.5 ± 0.4 Å	32 ± 0°	C: 54 ± 3; N: 5.0 ± 0.1; O: 40 ± 3
PAAm-Biotin NHS ester	12.0 ± 2.6 Å	45 ± 5°	N:S ratio: 83 ± 1: 17 ± 1

[a]These results come from the "PAAm-PDITC (1.6%, 3 hr)" surface that was then immersed in the 1.6% PDITC solution overnight.

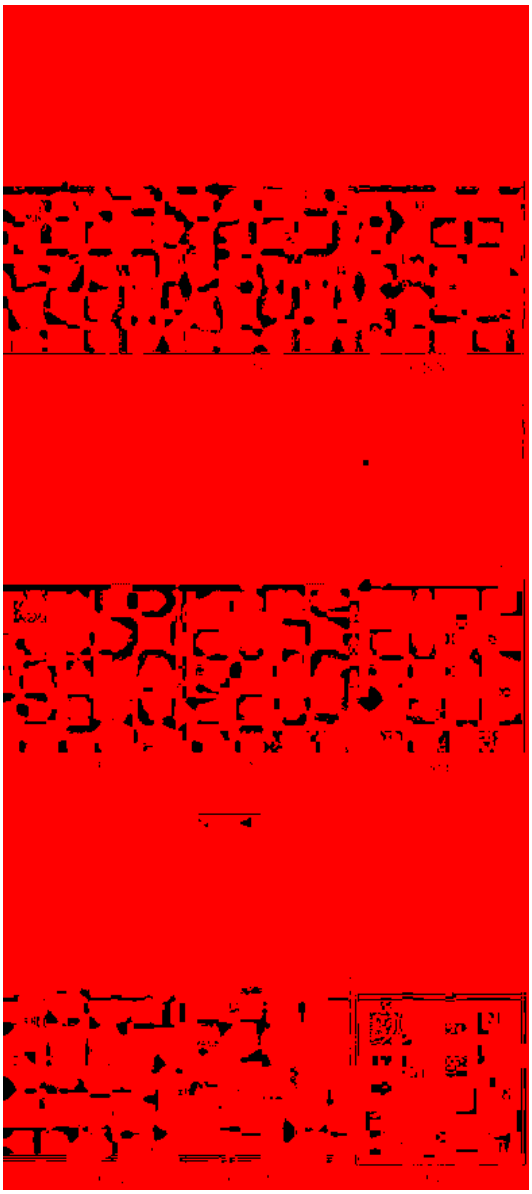

Figure 5.6. ToF-SIMS negative ion images of microlens array patterned 1-hexadecene monolayers on silicon after immersion of these surfaces in solutions of PAAm (a, c, and e) and after their immersion in solutions of PAAm and 10% CTAC (b, d, and f), followed by reaction with PDITC (a and b), BNE (c and d), GA (e and f), and oligonucleotide (g).

The adsorption of an unfunctionalized oligonucleotide onto PAAm in wells in arrays was characterized using ToF-SIMS. Figure 5.6g shows the negative ion ToF-SIMS image of the PO_3^- ion, which is characteristic of DNA.[34] from a microlens array patterned surface that was immersed in PAAm/CTAC solution, followed by a second immersion in a solution of an oligonucleotide. The desired effect of selective adsorption of the oligonucleotide onto the spots can be easily observed, which further justifies the application of our method in lab-on-a-chip type devices.

Because there is relatively little in the literature on the reactivity of adsorbed PAAm, I also report the reaction of adsorbed PAAm with an isocyanate (1H,1H,2H,2H-Perfluorodecyl isocyanate). The film thickness after this reaction increased by 16.2 ± 0.5 Å. The water contact angle for the isocyanate functionalized surface was 128 ± 3°, which is clearly consistent with a highly hydrophobic material.

5.5. Conclusions

Polyallylamine, PAAm, is an important synthetic polymer because of its high density of primary amine groups. I have demonstrated the selective adsorption of PAAm in patterned arrays by using a cationic surfactant. Less selectivity is obtained when a nonionic surfactant is employed. Furthermore, I have shown that PAAm remains active after its adsorption and will react with a series of molecules that are important in bioconjugate chemistry.

5.6. References

(1) Mukhopadhyay, R. *Anal. Chem.* **2006**, *78*, 5969-5972.

(2) Schena, M.; Shalon, D.; Davis, R. W.; Brown, P. O. *Science* **1995**, *270*, 467-470.

(3) Diehl, F.; Grahlmann, S.; Beier, M.; Hoheisel, J. *Nucleic Acids Res.* **2001**, *29*, e38.

(4) Valiokas, R.; Vaitekonis, S.; Klenkar, G.; Trinkunas, G.; Liedberg, B. *Langmuir* **2006**, *22*, 3456-3460.

(5) Vail, T. L.; Cushing, K. W.; Ingram, J. C.; St. Omer, I. *Biotechnol. Appl. Biochem.* **2006**, *43*, 85-91.

(6) De Paul, S. M.; Falconnet, D.; Pasche, S.; Textor, M.; Abel, A. P.; Kauffmann, E.; Liedtke, R.; Ehrat, M. *Anal. Chem.* **2005**, *77*, 5831-5838.

(7) Wu, M.-H.; Whitesides, G. M. *Appl. Phys. Lett.* **2001**, *78*, 2273-2275.

(8) Piglmayer, K.; Denk, R.; Bäuerle, D. *Appl. Phys. Lett.* **2002**, *80*, 4693-4695.

(9) Zhang, F.; Gates, R. J.; Smentkowski, V. S.; Natarajan, S.; Gale, B. K.; Watt, R. K.; Asplund, M. C.; Linford, M. R. *J. Am. Chem. Soc.* **2007**, *129*, 9252-+.

(10) Hermanson, G. T. *Bioconjugate Techniques*; Academic Press: SanDiego, 1996.

(11) Schuerenberg, M.; Luebbert, C.; Eickhoff, H.; Kalkum, M.; Lehrach, H.; Nordhoff, E. *Anal. Chem.* **2000**, *72*, 3436-3442.

(12) Xu, Y. D.; Watson, J. T.; Bruening, M. L. *Anal. Chem.* **2003**, *75*, 185-190.

(13) Gates, R.; Saini, G.; Zhang, F.; Bennion, E.; Linford, M. R.; Asplund, M. C. *Submitted to Langmuir* **2007**.

(14) Golander, C. G.; Eriksson, J. C. *J. Colloid Interface Sci.* **1987**, *119*, 38-48.

(15) Eriksson, J. C.; Golander, C. G.; Baszkin, A.; Terminassiansaraga, L. *J. Colloid Interface Sci.* **1984**, *100*, 381-392.

(16) ToF-SIMS . Surface Analysis by Mass Spectrometry; IM Publications: Huddersfield, U., 2001.

(17) Decher, G.; Schmitt, J. *Prog. Colloid Surf. Sci.* **1992**, *89*, 160-164.

(18) Lvov, Y.; Decher, G.; Möhwald, H. *Langmuir* **1993**, *9*, 481-486.

(19) Ferreira, M.; Rubner, M. F. *Macromolecules* **1995**, *28*, 7107-7114.

(20) Linford, M. R.; Auch, M.; Möhwald, H. *J. Am. Chem. Soc.* **1998**, *120*, 178-182.

(21) Decher, G. *Science* **1997**, *277*, 1232-1237.

(22) Ariga, K.; Hill, J. P.; Ji, Q. M. *Phys. Chem. Chem. Phys.* **2007**, *9*, 2319-2340.

(23) Erol, M.; Du, H.; Sukhishvili, S. *Langmuir* **2006**, *22*, 11329-11336.

(24) Dyer, M. A.; Ainslie, K. M.; Pishko, M. V. *Langmuir* **2007**, *23*, 7018-7023.

(25) Saini, G. W., L.A.; Herbert, D.; Biggs, K.N.; Dadson, A.; Vail, M.A.; Linford, M.R. *J. Chromatogr. A* **2008**.

(26) Ariga, K.; Hill, J. P.; Lee, M. V.; Vinu, A.; Charvet, R.; Acharya, S. *Science and Technology of Advanced Materials* **2008**, *9*.

(27) Linford, M. R.; Fenter, P.; Eisenberger, P. M.; Chidsey, C. E. D. *J. Am. Chem. Soc.* **1995**, *117*, 3145-3155.

(28) Sieval, A. B.; Demirel, A. L.; Nissink, J. W. M.; Linford, M. R.; van der Maas, J. H.; de Jeu, W. H.; Zuilhof, H.; Sudhölter, E. J. R. *Langmuir* **1998**, *14*, 1759-1768.

(29) Pang, J.; Na, H.; Lu, Y. *Microporous Mesoporous Mater.* **2005**, *86*, 89-95.

(30) Tao, C.; Li, J. *Langmuir* **2003**, *19*, 10353-10356.

(31) Rama Rao, G. V.; Konishi, T.; Ise, N. *Polymer* **2001**, *42*, 6817-6821.

(32) Benters, R.; Niemeyer, C. M.; Drutschmann, D.; Blohm, D.; Wöhrle, D. *Nucleic Acids Res.* **2002**, *30*, e10.

(33) Thiel, A. J.; Frutos, A. G.; Jordan, C. E.; Corn, R. M.; Smith, L. M. *Anal. Chem.* **1997**, *69*, 4948-4956.

(34) Arlinghaus, H. F.; Ostrop, M.; Friedrichs, O.; Feldner, J.; Gunst, U.; Lipinsky, D. *Surf. Interface Anal.* **2002**, *34*, 35-39.

PART III. USE OF CHEMICAL VAPOR DEPOSITION FOR THE SURFACE FUNCTIONALIZATION OF SILICON AND NYLON SUBSTRATES

Chapter 6. Two-Silane Chemical Vapor Deposition Treatment of Polymer (Nylon) and Oxide Surfaces that Yields Hydrophobic (and Superhydrophobic), Abrasion-Resistant Thin Films*

6.1. Abstract

I describe a two-silane, chemical vapor deposition (CVD) approach to creating hydrophobic (or even superhydrophobic), abrasion-resistant coatings on silicon oxide and polymer (nylon) substrates. This multistep approach employs only reagents delivered in the gas phase, as follows: (i) plasma cleaning/oxidation of the substrate, (ii) CVD of 3-isocyanatopropyltriethoxysilane, which is used as an adhesion promoter for the substrate, (iii) hydrolysis with water vapor, and (iv) CVD of (tridecafluoro-1,1,2,2-tetrahydrooctyl) trichlorosilane (the "R_f-Cl silane"). Surfaces are characterized by wetting, spectroscopic ellipsometry, X-ray photoelectron spectroscopy (XPS), and time-of-flight secondary ion mass spectrometry (ToF-SIMS). This work has the following unique features. First, I explore an all gas phase deposition of a new silane coating that is scientifically interesting and technologically useful. Second, I show that the presence of an adhesion promoter in the process leads to thinner films that are more robust in abrasion testing. Third, results obtained

*This chapter is reproduced with permission from (Gaurav Saini, Ken Sautter, Frank E. Hild, Jerry Pauley and Matthew R. Linford), *J. Vac. Sci. Technol. A* 26(5), 1224-1234, 2008.

using plasma/deposition equipment that is relatively inexpensive and/or available in most laboratories are compared to those obtained with a much more sophisticated, commercially available plasma/CVD system (the YES-1224P). The entire deposition process can be completed in only ~1 h using the industrial equipment (the 1224P). It is of significance that the polymer surfaces modified using the 1224P are superhydrophobic. Fourth, the thickness of the R_f-Cl silane layer deposited by CVD correlates well with the thickness of the underlying spin coated nylon surface, suggesting that the nylon film acts as a reservoir of water for the hydrolysis and condensation of the R_f-Cl silane.

6.2. Introduction

Silane coatings are inherently hybrid materials as they contain both oraganic carbon and inoraganic silicon as their constituents. They offer the flexibility and reactivity of a broad range of organic functional groups, while they also offer the strength and potential cross-linking of the inorganic Si–O–Si linkage between monomer units. Polymer surface modification is important because many polymers/plastics have extremely desirable bulk properties such as low density, low cost, good strength, and ease of processing that have allowed them to become integral components of countless consumer goods and devices. However, many plastics that have ideal bulk properties for certain applications are lacking in their surface properties, such as abrasion resistance or wetting. As a result, it is often necessary to coat a polymer/plastic to modify its surface so that its favorable bulk properties can be exploited. CVD of silanes is an effective, solvent-free method for the covalent attachment of these reagents to surfaces. In general, this method can be made more reproducible and robust than silane deposition from solution because it is often difficult to control the degree of hydrolysis and oligomer formation of

silanes in solution.[1] In contrast, in the CVD of silanes it is unlikely that hydrolyzed or oligomerized species will reach the substrate because their volatility typically decreases significantly when they hydrolyze or condense with each other. In general, gas phase deposition of silanes is also much cleaner than the liquid phase approach because the surface is not exposed to impurities that may be in the solvent, and no surface rinsing or cleaning is required after adsorption. In addition, if no solvent is required during silane adsorption or in subsequent substrate cleaning, the gas phase approach will generally be more environmentally friendly and industrially viable. Silanes with a variety of terminal functionalities, including amino, vinyl, alkyl, perfluoro, glycidyl, isocyanato, Si–H, and polyethylene glycol, and with different numbers of reactive groups on Si, *e.g.*, –Cl, –OMe, and –OEt, are commercially available, and have been deposited by CVD.[1-8] One of these reports showed alternating deposition of gaseous aminopropyltrimethoxysilane and water vapor on porous silica surfaces via atomic layer deposition.[4] Another study showed the liquid phase deposition of 3-(mercaptopropyl)trimethoxysilane onto silver surfaces, followed by hydrolysis in aqueous 0.1*M* HCl, with subsequent treatment by gas phase deposition of octadecyltrichlorosilane or dimethylchlorooctadecylsilane.[6] The sequential deposition of 3-aminopropyltriethoxysilane and (tridecafluoro-1,1,2,2-tetrahydrooctyl)dimethylchlorosilane onto polymer substrates has also been reported.[9] However, the polymer substrates in this study were not plasma treated, as they are in this work, and all depositions were out of solution. Reagent delivery and/or surface modification in this study takes place entirely in the gas phase and consists of (i) cleaning and/or oxidizing a polymer (nylon) or silicon surface with an air or oxygen plasma, (ii) vapor depositing 3-isocyanatopropyltriethoxysilane (denoted the "isocyanato silane" herein) onto these primed substrates, (iii) a hydrolysis step in which water vapor reacts with this surface, and (iv) vapor

deposition of (tridecafluoro-1,1,2,2-tetrahydrooctyl)trichlorosilane[10-12] (denoted the "R_f-Cl silane" herein). Plasma cleaning of inorganic surfaces to remove organic contamination is a well known cleaning procedure.[13,14] Plasma treatment of polymer surfaces is also a known and effective approach for oxidizing their surfaces.[15,16] Plasma treatment of polymer surfaces should allow the silanes employed in this study to polymerize more readily on them (Figure 6.1 shows their structures). To repeat, no reagents are delivered from solution, and no rinsing of the surface is necessary between, or after, the steps in the process. I have demonstrated this process with native oxide coated silicon, spin-coated nylon 6,6 on silicon, and bulk, glass-reinforced nylon 6,6 substrates. It should be possible to coat virtually any polymer or organic material using this method, provided it has a surface that can be oxidized and/or provide reactive –OH groups. Almost all polymers meet these qualifications. Surface reactions are confirmed and followed by water and hexadecane contact angles, spectroscopic ellipsometry, X-ray photoelectron spectroscopy (XPS), time-of-flight secondary ion mass spectrometry (ToF-SIMS),[17] and abrasion testing.

6.3. Experimental

6.3.1. Reagents

(Tridecafluoro-1,1,2,2-tetrahydrooctyl)trichlorosilane ($\geq$ 97%, Aldrich), 3-isocyanatopropyltriethoxysilane (95%, Gelest, Morrisville, PA), *m*-cresol (97%, Aldrich), and nylon 6/6 pellets (Aldrich, Cat. No.181129) were used as received. The "aqueous salt/acid" solution employed herein is a formulation for artificial sweat, which was 0.34*M* NaCl, 0.08*M* urea, 0.33*M* NH_4Cl, 0.04*M* CH_3COOH and 0.12*M* lactic acid. The solution was adjusted to pH 4.7 with 2*M* NaOH.

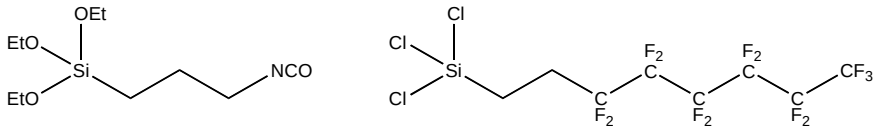

the "isocyanato silane" the "R_f-Cl silane"

Figure 6.1. Structures of 3-isocyanatopropyltriethoxysilane (the “isocyanato silane”) and (tridecafluoro-1,1,2,2-tetrahydrooctyl)trichlorosilane (the “R_f-Cl silane”).

6.3.2. Substrates

Silicon wafers (test grade, *n*-type, <1-0-0> orientation, 2–6 Ω cm) were purchased from UniSil Corporation, California and cleaved into ~1.5×1.5 cm^2 pieces. Reinforced nylon 6/6 surfaces were FDA grade and contained 35% chopped glass fiber by weight (1/8–3/16 in. long). This material contains FDA-compliant additives, *i.e.*, colorants, and no UV or high flow additives.

6.3.3. Surface cleaning

Prior to any surface chemistry, reinforced nylon surfaces were sonicated in an aqueous 2% sodium dodecyl sulfate (SDS) solution for 5 min. They were then sonicated in deionized water for 10 min. This water was changed three times during sonication. Bare Si wafers were also cleaned with SDS solution and water but without sonication. Spin-coated nylon surfaces were heated to remove residual *m*-cresol (see below) and then plasma cleaned without any other cleaning.

6.3.4. Spin coating

Spin coating was performed with an instrument from Laurell Technologies Corporation model WS-400B-6NPP/LITE. Spin-coated nylon surfaces were prepared by spin coating a solution of nylon 6/6 pellets in *m*-cresol onto native oxide coated silicon wafers using the following program: 1000 rpm (10 s) followed by 5000 rpm (90 s). The initial concentration of the nylon 6/6 solution was <3% (*w*/*w*), but this solution was diluted in *m*-cresol until these spin coating conditions gave a film thickness of approximately 170 Å.

6.3.5. Plasma cleaning/treatment (for depositions in the dessicator and vacuum oven)

Plasma cleaning was performed with a plasma cleaner model PDC-32G from Harrick Plasma (Ithaca, NY) at medium power (10.5 W applied to the RF coil) for 30 s.

6.3.6. Isocyanato silane deposition (for depositions in the vacuum oven)

After plasma cleaning, all of the surfaces were dehydrated at 100°C at reduced pressure. The vacuum for this oven was provided by a rotary vane pump. The apparatus contained a dry ice/acetone-cooled glass trap that prevented both backstreaming of oil from the pump and solvents and/or reagents from entering the pump. The reinforced and spin-coated nylon surfaces appear to be stable for extended periods of time at 100°C. Aldrich gives the melting point of the nylon 6/6 they provided as 263°C, and its glass transition temperature as 45°C. After introducing the surfaces into the oven, the pump was turned on for ~3 min to attain a pressure of 15 Torr (−25 in.), and the valve to the pump was then closed. The surfaces were allowed to dehydrate under these conditions for 30 min. The pump was then turned on again for 3 min to pump off water vapors, and the valve to the pump was again closed. An aliquot of 250 μL of (3-isocyanatopropyl triethoxysilane) was injected into the vacuum oven through a septum, and it evaporated quickly. The surfaces were then allowed to react with the vapors of the -NCO silane under these static conditions for 30 min. The valve to the vacuum pump was then opened to pump off any unreacted -NCO silane. A Petri dish containing 5 ml of water was then introduced into the oven. The door to the oven was closed and the surfaces were allowed to hydrolyze at atmospheric pressure and at 100°C for 30 min.

6.3.7. Testing the abrasion resistance of the films

An apparatus was built to test abrasion resistance (see Figure 6.2). It consisted of an electric drill (Craftsman, model No. 315.101160) that was clamped vertically. A commercially-available polishing disk (Craftsman), which is designed to be used with an electric drill, was attached to the chuck of the drill, and a piece of abrasive felt (15×14.7 cm^2) was pasted onto it. Thus, when the drill was turned on, it caused the felt disk to rotate parallel to the bench top. A sample holder was made from two rectangular strips of plywood joined end to end with a steel hinge. The end of one of these pieces was clamped to a stand. The reinforced nylon sample was attached to the end of the other piece with double-sticky tape. The sample was then placed on the felt wheel 4.5 cm from its center, and allowed to ride on the wheel as it rotated. A brass cylinder weighing 164 g was placed directly above the sample on the wood strip. The rotational speed of the drill was controlled with a powerstat and the felt was also marked on its edge so as to count the number of cycles during the abrasion tests.

6.3.8. R_f-Cl silane deposition in a dessicator

The R_f-Cl silane was deposited onto hydrolyzed -NCO silane coated surfaces by placing these surfaces in a dessicator along with an open vial of the R_f-Cl silane for at least 16 h.[8] After this reaction, the surfaces were removed from the dessicator and cured in an oven at 80°C for 1 h at atmospheric pressure.

6.3.9. Surface analytical instrumentation

ToF-SIMS was performed with an ION-TOF (TOF-SIMS IV) instrument with a two-lens, monoisotopic $^{69}Ga^+$ gun as a primary ion source. XPS was performed with an SSX-100

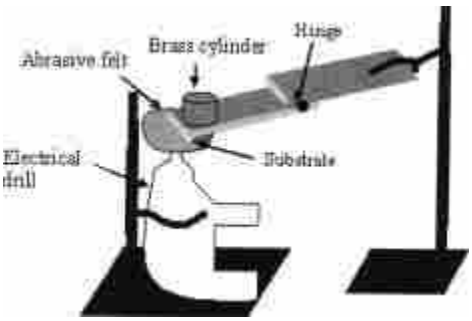

Figure 6.2. Abrasion apparatus consisting of an automatic electric drill configured to rotate a piece of abrasive felt under a coated substrate. The weight of the brass cylinder was 164 g.

instrument from Surface Sciences using an Al *Kα* source and a hemispherical analyzer. An electron flood gun was employed for charge compensation of the reinforced nylon samples, and this charge compensation was further enhanced by placing a fine Ni mesh ~0.5–1.0 mm above the surface of the glass reinforced polymer. No charge compensation was necessary for the silicon or spin-coated nylon-on- silicon samples. Water contact angles were measured with a Ramé-Hart (model 100-00) contact angle goniometer. Spectroscopic ellipsometry was performed with an M-2000 instrument from the J.A. Woollam Co., Inc. The wavelength range was 190.5–989.4 nm, and the angle of incidence was fixed at 75°. Silicon oxide, hydrocarbon deposited silane films, and spin coated nylon were modeled using the optical constants of silicon oxide that were found in the instrument software. This is a good approximation for such ultrathin films, and good fits to the data were obtained for all of the results reported in this work.

6.3.10. Commercially available CVD system

The results obtained using conventional and/or inexpensive equipment available in the laboratory were compared to those found using a commercially available, fully automated CVD system: the YES-1224P from Yield Engineering Systems (Livermore, CA). The YES-1224P Chemical Vapor Deposition System incorporates a plasma cleaning method into a heated vacuum deposition chamber. Reactant chemicals are vaporized in temperature controlled vessels and introduced via heated lines to the main chamber. The system allows precise control of chemical volume, reaction temperature, and exposure time. The plasma cleaning process prepares substrates for surface reactions.

6.4. Results

I describe a two-silane functionalization of spin coated nylon, reinforced nylon, and native oxide coated silicon. The resulting thin films exhibit good hydrophobicity, abrasion resistance, and are invisible to the eye. In the first section, I describe work that was performed with three pieces of equipment that are inexpensive and/or available to most researchers. In the second section I show that it is possible to significantly shorten the deposition procedure and also eliminate the use of one of the pieces of equipment. In the third section, I demonstrate the use of a single piece of highly automated equipment: a commercially-available plasma/CVD system.

6.4.1. Silane deposition with conventional/inexpensive equipment

In this section, surfaces were first oxidized/cleaned in a small Harrick Plasma device. The isocyanato silane was then deposited in a vacuum oven, and the R_f-Cl silane was deposited at atmospheric pressure in a dessicator.

6.4.1.1. Plasma cleaning/treatment

All of the surfaces were cleaned with an air plasma. The air plasma should generate numerous oxygen atoms from O_2, which should effectively oxidize and etch the organic species at the surfaces. The small plasma system employed in this work was specifically designed not to have enough power to etch inorganic materials. As expected, Table 6.I shows that the advancing water contact angles [$\theta_a(H_2O)$] for the three different surfaces decrease noticeably after plasma cleaning. The moderately high water contact angle for the Si/SiO_2 surface prior to plasma cleaning appears to be a reflection of adventitious hydrocarbon contamination on this surface, which is removed by plasma cleaning.

Table 6.1. Advancing water contact angles [$\theta_a(H_2O)$] of substrates before and after plasma cleaning, and after treatment with the isocyanato silane. (Notes: A reported advancing water contact angle less than 15° implies that the surface is wet by water. The number in parentheses indicates the number of experiments that were performed to get the average and standard deviation reported in this table, where each experiment employed two to three surfaces, each of which was characterized).

Substrates	Before plasma cleaning	After plasma cleaning	After –NCO silane treatment
Bare Si/SiO2	40°	< 15°	[a]82±6°
Spin-coated nylon	60±3° (5)	34±3° (6)	[b]82±7°
Reinforced nylon	69±2° (3)	32±2° (5)	87±3° (5)

[a]This value is the average and standard deviation of measurements made on seven different surface prepared in three separate experiments.
[b]This value is the average and standard deviation of measurements made on six different surfaces prepared in three seperate experiments.

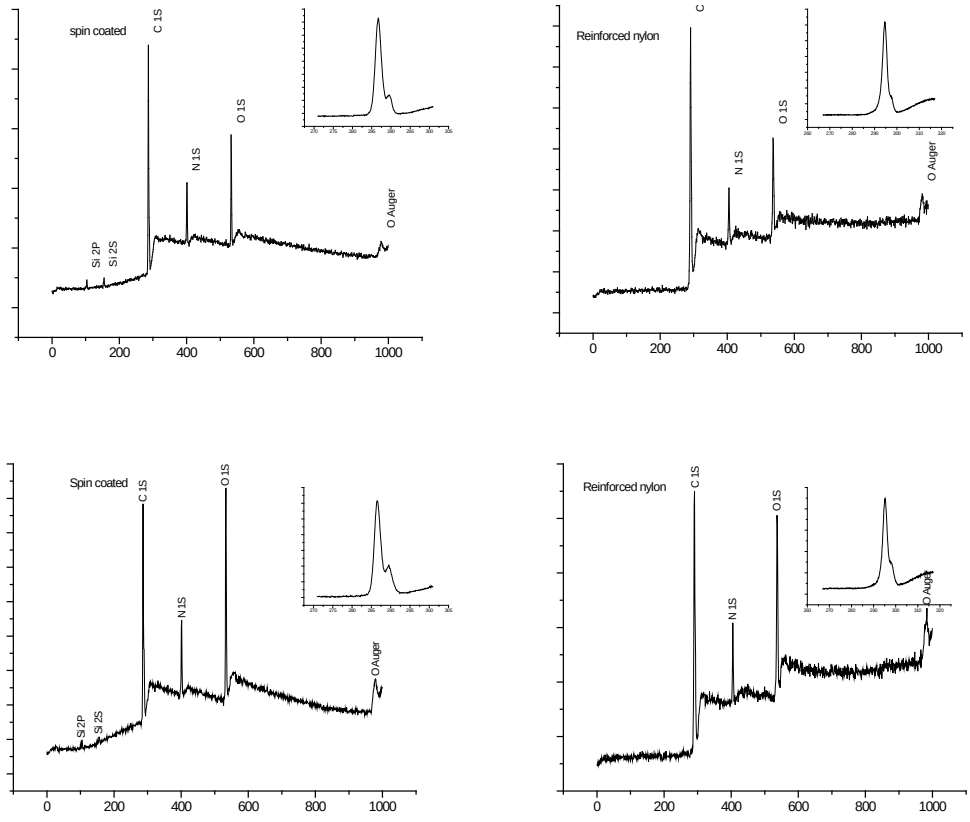

Figure 6.3. XPS survey and C 1s narrow scans of spin-coated nylon (left) and bulk reinforced nylon (right) before plasma treatment (top) and after plasma treatment (below).

The expected surface oxidation of nylon by plasma cleaning is further confirmed by XPS. Figure 6.3 shows the XPS of spin-coated and fiberglass reinforced nylon before and after plasma cleaning. Prior to plasma cleaning the XP spectra are dominated by signals from oxygen (O 1s), nitrogen (N 1s), and carbon (C 1s) (see Figure 6.3). The same three peaks dominate the XP spectra after plasma cleaning (see again Figure 6.3), and the nitrogen to carbon ratio is nearly the same in both spectra. However, the O 1s signal, as measured by the O 1s/C1s peak ratio, increases significantly after plasma cleaning, going from, for example, 0.16 to 0.28 for a glass-reinforced nylon sample and from 0.18 to 0.35 for a spin-coated nylon surface. As expected, the C 1s narrow scans show a notable increase in oxidized (chemically shifted) carbon (see Figure 6.3). The negative ion ToF-SIMS spectra of the glass-reinforced and spin-coated nylon surfaces also suggest an increase in the oxygen content of these surfaces after plasma cleaning. For example, the area ratios of the O^- to the C^- peaks on three different glass-reinforced nylons and three different spin-coated nylon surfaces in the negative ion spectra are 3.6±0.2 and 4.7±0.2 before plasma treatment and 9.2±0.5 and 11.4±1.3, respectively, after plasma treatment, *i.e.*, these results, like the XPS results, indicate that the amount of oxygen in the near surface region of the sample increases significantly.

Not only is surface oxidation after plasma cleaning observed, but the expected etching of organic material from the surfaces is also confirmed. Thus, the ellipsometric thicknesses of the "silicon oxide" layer on the as received silicon oxide terminated silicon wafers decreased after plasma cleaning. A typical example is a silicon/silicon oxide surface where the thickness of the layer on the silicon substrate decreases from 23.2 to 17.6 Å after plasma cleaning, demonstrating the removal of organic material. The spin-coated nylon surfaces show an even larger decrease in thickness of the nylon layer after plasma treatment. For example, for a set of representative

surfaces, the thicknesses of spin-coated nylon films decreased from 135.2, 222.9, 133.6, 132.5, and 223.2 Å to 88.2, 139.5, 78.2, 74.2, and 165.6 Å after 30 s of plasma treatment, respectively, which corresponds to an average loss of 60±14 Å of material. The variability in this removal may be due to somewhat different positions of the substrates in the plasma cleaner, and the difficulty associated with exact control of the plasma power and duration in the device. Because a fairly large amount of polymer (tens of angstroms) was removed from the polymer surfaces during plasma cleaning, it did not seem necessary to optimize this step in the procedure. That is, etching a little more or a little less of the polymer would not be expected to change the surface chemistry after plasma etching/oxidation. This decision was further confirmed by the optimization of the time for plasma etching reported in Sec. 6.4.3 (*vide infra*).

6.4.1.2. Isocyanato silane treatment

After treatment of the plasma-cleaned surfaces with the isocyanato silane, the water contact angles of all of the surfaces increase substantially, as shown in Table 6.1.[18] XPS was also used to characterize these surfaces. For the bare silicon surface, no N 1*s* signal could be observed before -NCO silane treatment, but a small N 1s signal was present in the survey spectrum after this exposure. The thickness of this isocyanato layer was 9.5 Å by spectroscopic ellipsometry.

For the spin-coated nylon surface, there is a small silicon peak in the survey spectrum (presumably from the substrate) prior to isocyanato silane deposition that increases after isocyanato silane deposition. For example, on one such surface, the Si/C ratio was 0.045 and 0.098 before and after NCO silane treatment, respectively. It was difficult to observe an increase in thickness for spin coated nylon after isocyanato silane deposition, presumably because solvent

loss during isocyanato silane deposition changed the thickness of the nylon layer.[19] In one experiment, spin coated nylon surfaces were baked in a vacuum oven at 100°C for 2 h at reduced pressure to drive off *m*-cresol. The film thickness increase after isocyanato silane deposition was observed to be 4.8±0.6 Å.

6.4.1.3. Hydrolysis of the isocyanato silane treated surfaces

The isocyanato silane treated surfaces were hydrolyzed with water vapor for 30 min at 100°C, and at atmospheric pressure. The ellipsometric thicknesses of the covalently attached isocyanatosilane layer on Si/SiO_2 and spin-coated nylon substrates remained essentially constant after hydrolysis. As a representative example, for one Si/SiO_2 surface and one spin coated nylon surface, the total thicknesses (on top of the silicon substrate) before and after hydrolysis of the isocyanato layer were found to be 27.9 and 142.3 Å, and then 28.3 and 141.3 Å, respectively.

6.4.1.4. Reaction of the hydrolyzed surfaces with the R_f-Cl silane

After hydrolysis, the isocyanato silane-treated surfaces were placed in a dessicator overnight (12–16 h) where they were exposed to the vapors from an open vessel of (tridecafluoro-1,1,2,2-tetrahydrooctyl) trichlorosilane, which is referred herein as the R_f-Cl silane. Table 6.2 gives the ellipsometric thicknesses of the isocyanato silane-treated bare silicon surface and spin-coated nylon surfaces after hydrolysis and then after exposure to the R_f-Cl silane (the fiber-reinforced nylon surfaces are not sufficiently flat for ellipsometry to be performed). It is clear that significant deposition of the R_f-Cl silane occurs, especially in the case of the spin-coated nylon surface.

These results suggest cross-linking of R_f-Cl silane molecules into a polymeric thin film

Table 6.2. Spectroscopic ellipsometric thicknesses of coatings on bare silicon and spin-coated nylon surfaces at different stages of the deposition.

Substrates	After -NCO silane treatment and hydrolysis	After Rf-Cl silane treatment
Bare Si	29.1±0.6 Å	78±7 Å
Spin-coated nylon	125.9, 138.8, 124.3, 136.4 Å	272.3, 192.1, 196.2, 202.7 Å

[a]The thicknesses of the films reported here include the thickness of the native oxide, which was 18.0±0.5 Å.

Table 6.3. Advancing contact angles for different probe liquids (water, an artificial sweat formulation, and hexadecane) for different substrates that were plasma treated, treated with the isocyanato silane, hydrolyzed, and then treated with the Rf-Cl silane. Each of the experiments reported in these columns was performed once.

Substrates	θ_a (H_2O)	θ_a (artificial sweat)	θ_a (hexadecane)
Bare Si	126°	118°	75°
Spin-coated nylon	127°	120°	72°
Reinforced nylon	132°	130°	71°
Average	128°±3°	123°±6°	73°±2°

on the substrates. In my belief, these reactions are facilitated by water that diffuses out from underlying polymer layers. As expected, the advancing water contact angles, advancing contact angles for an artificial sweat formulation, and advancing hexadecane contact angles for these R_f-Cl silane treated surfaces are quite high, and consistent for a material with an extremely low surface free energy, such as a fluorocarbon (see Table 6.3).[20] XPS and ToF-SIMS also confirm the presence of large amounts of fluorine after CVD of the R_f-Cl silane on the hydrolyzed isocyanato silane surface (*vide infra*).

6.4.1.5. Effect of the adhesion promoter on the thickness of the R_f-Cl silane coating

To determine the effect of the adhesion promoter, the isocyanato silane, on the thickness of the R_f-Cl silane coating, plasma-treated (bare) Si/SiO_2 and nylon spin-coated surfaces having no adhesion promoter coating were exposed to the R_f-Cl silane. These surfaces without the adhesion promoter, and the surfaces treated with the adhesion promoter were placed together in the oven during the hydrolysis step. After the hydrolysis, all the surfaces were allowed to react with the R_f-Cl silane as described previously. Table 6.4 shows a comparison of the thickness of the R_f-Cl silane coating for bare Si/SiO_2 and nylon spin-coated surfaces made with and without the adhesion promoter coating. Interestingly, the surfaces coated with the adhesion promoter (the isocyanato silane film) are considerably thinner than the surfaces that were not treated with the isocyanato silane. This may be because the thin film of the isocyanato silane acts as a diffusion barrier to water at or near the surface of the substrate. In spite of the thinness of these films, these thinner layers appear to have superior abrasion resistance over R_f-Cl silane deposited on surfaces that were not treated with the adhesion promoter (*vide infra*).

Table 6.4. Increase in ellipsometric thicknesses after treatment with the Rf-Cl silane.[a,b]

Substrates	With adhesion promoter (Å)	Without adhesion promoter (Å)
Bare Si	48±8	117±13
Spin-coated nylon	67±11	233±37[b]

[a]These results are the averages from three silicon surfaces and three spin-coated nylon surfaces, where each underwent the same exposure to the R_f-Cl silane.
[b]The thickness of the native silicon oxide layer on silicon was subtracted from the total ellipsometric thicknesses to give the results in this table.

6.4.1.6. XPS analysis of surfaces treated with the R_f-Cl silane

XPS confirms the addition of the R_f-Cl silane to the isocyanato silane treated surfaces. For example, Figure 6.4 shows XPS of the reinforced nylon surface after the coating process: plasma treatment, reaction with the isocyanato silane, hydrolysis, and exposure to the R_f-Cl silane. The dominant feature of this spectrum is the F 1*s* signal, with its accompanying F Auger peaks. The split carbon signal that is observed is due to (i) carbon bonded to carbon and/or hydrogen and/or mildly oxidized carbon at lower binding energy, and (ii) carbon in CF_2 groups at higher binding energy, where each F atom bonded to a C atom shifts the C 1s signal by *ca.* 2.9 eV. It is significant that no N 1s signal from the substrate or the isocyanato silane layer can be observed. This indicates that the R_f-Cl silane film is free from pinhole defects, and/or that it is relatively thick in all places. A small oxygen signal is also present, which would be expected from Si-O linkages in the film.

6.4.1.7. ToF-SIMS analysis

ToF-SIMS in both the negative and positive ion modes was performed on silicon oxide, spin-coated nylon, and reinforced nylon samples after treatment with the isocyanato silane and again after treatment with the R_f-Cl silane. ToF-SIMS, which has an information depth of only about 2 nm, is more surface sensitive than XPS,[17] which probes at least 10 nm into a material. Positive ion ToF-SIMS spectra of the silicon oxide, spin-coated nylon, and glass reinforced nylon surfaces after the complete process, which culminated in the deposition of the R_f-Cl silane, shows a series of peaks that are characteristic of a perfluorinated hydrocarbon. The two largest peaks in these spectra are identified as the CF^+ and CF_3^+ peaks. The negative ion spectra from

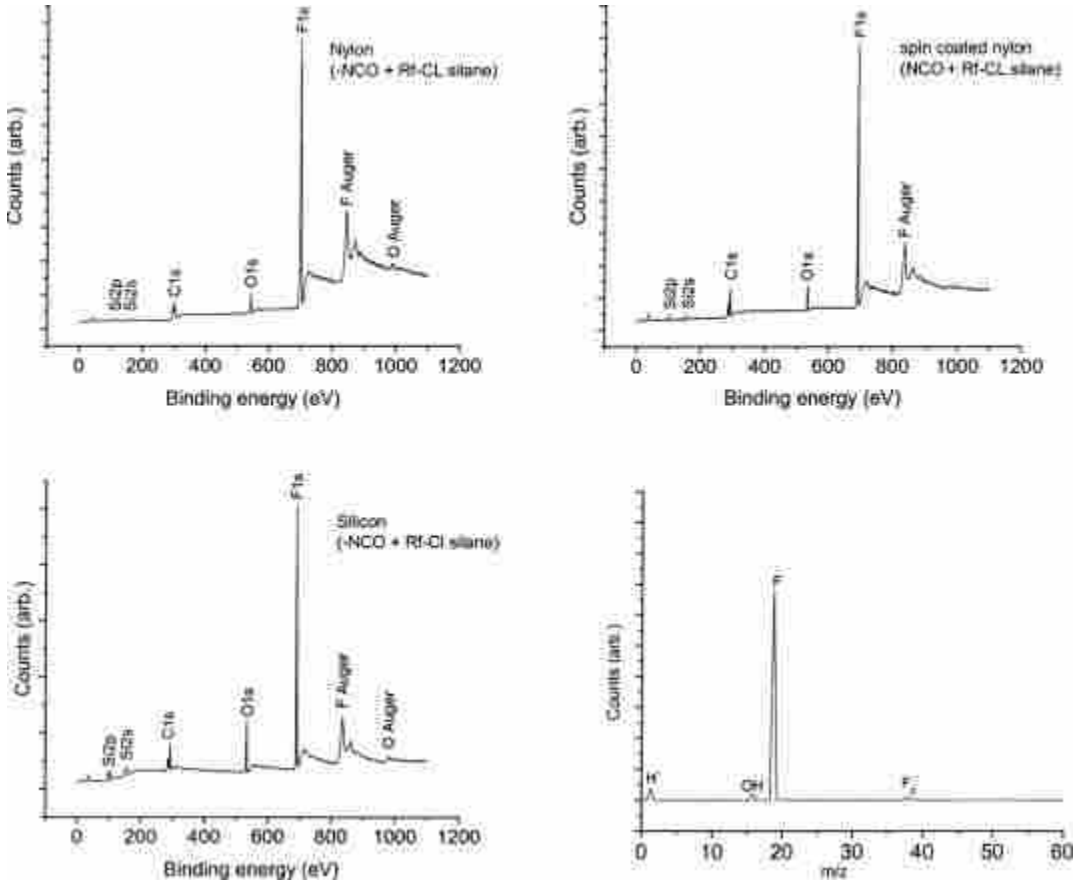

Figure 6.4. XPS after deposition of the R_f-Cl silane on reinforced nylon ("nylon"), spin coated nylon, and bare Si/SiO_2. Lower right: negative ion ToF-SIMS after applying the silane multilayer film to the reinforced nylon substrate.

these same surfaces are dominated by a single peak: F^-. The F_2^- ion, which is generally less than 5% intense as the F^- signal, (see Figure 6.4) is also observed.

6.4.1.8. Abrasion tests

A goal of this research was to create a surface that would have a high degree of hydrophobicity, along with excellent resistance to abrasion. It was believed that the combination of the perfluorinated tails of the silane compound with the strong inorganic Si–O–Si linkages between the condensed R_f-Cl silane molecules would produce a thin film with these properties. To better understand the abrasion resistance of these thin films, identical pairs of fiberglass-reinforced nylon coupons that had been plasma cleaned and then (i) exposed to the isocyanato silane, hydrolyzed, and finally exposed to the R_f-Cl silane, or (ii) only hydrolyzed and then exposed to the R_f-Cl silane, were tested. Figure 6.5 shows the effect of the isocyanato silane on the robustness of R_f-Cl silane coating. That is, after 920, 160, and 430 cycles on three different pairs of coupons of different colors in a homebuilt abrasion testing apparatus, the water contact angle of the surfaces with the isocyanato silane adhesion promoting layer is ~10° higher than the surfaces prepared without the isocyanato compound. To confirm these results, XPS was taken of two surfaces coated with the R_f-Cl silane after abrasion testing, one with the adhesion promoter and one without. The C1s/F1s ratio after the abrasion test for the surface with the adhesion promoter was 43:57, while for the surface having no adhesion promoter coating, it was found to be 49:51. The higher level of fluorine is consistent with the higher water contact angles found for the surfaces made with the adhesion promoter.

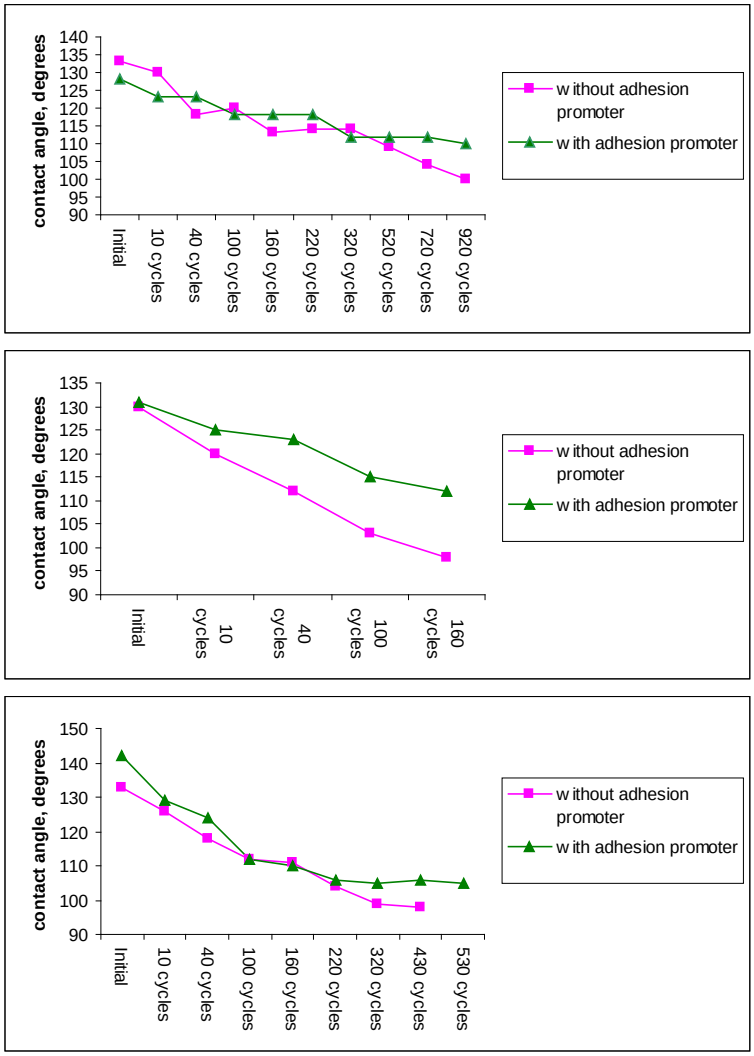

Figure 6.5. Results from abrasion tests (advancing water contact angles vs number of cycles in the abrasion tester) of surfaces silanized with the Rf-Cl silane, with and without the adhesion promoter (isocyanato silane).

6.4.2. Comparison of results obtained with conventional laboratory equipment to results obtained with a commercially-available Plasma/CVD system

While the data I have shown clearly demonstrate that this procedure for coating polymers and inorganic substrates with durable hydrophobic films is viable, and that the adhesion promoter improves the durability of the final film, this procedure, as implemented in the laboratory, has some sources of error in it. Multiple pieces of equipment must be used (the plasma cleaner, a vacuum oven, and a dessicator), and the samples must be transported between these pieces of equipment during the procedure. Each piece of equipment introduces some uncertainty into the procedure. For example, in practice, it is somewhat challenging to control the nature of the plasma and its exact duration in the Harrick plasma cleaner. The vacuum oven is difficult to clean, and in spite of the best efforts, a small amount of carryover between runs or small amounts of contamination originating from other uses of the instrument seems unavoidable. The dessicator was opened to the air each time it was used. The relative humidity in the laboratory would vary from day to day and therefore have some influence on the results. However these possible sources of error did not seem to prevent me from reproducibly verifying the validity of the procedure, and the results in Sec. 6.4.1 are important because they were obtained with inexpensive equipment and/or equipment that is available in most laboratories. However, I wondered if it would not be possible to improve the implementation of this procedure. As a first effort in this direction, I shortened the procedure and eliminated one of the pieces of equipment necessary for the process (the dessicator) by performing both silanes' depositions in the vacuum oven. I also studied various deposition conditions to optimize the CVD process. For example, I raised the temperature of the R_f-Cl silane deposition, where all of the experiments in Secs. 6.4.2.1 and 6.4.2.2 were performed at ~100°C.

6.4.2.1. Deposition of the adhesion promoter

The experiments described in this section were performed under the same conditions as those described in Sec. 6.4.1.2. Plasma-cleaned silicon wafers were first placed in the vacuum oven. They were then dehydrated as described in Sec. 6.3.6 and finally exposed to the isocyanato silane. Three different experiments were performed to optimize this process. In the first, two injections of the isocyanato silane (250μl and then 200 μl) were made ~30 min apart into the vacuum oven. The material from the first injection was not pumped off before injecting the second aliquot of the compound. This ~1 h exposure of the surface to the isocyanato compound led to an increase in film thickness of 10.3±0.7 Å (the average of four measurements from four surfaces in two separate experiments). This experiment was then repeated, except the total exposure time was ~30 min (the two injections of the silane (250 μl and then 200 μl) were about 15 min. apart). The increase in film thickness after this experiment was 10.3±1.4 Å (the average of three measurements from three surfaces in three separate experiments). In a final experiment, the surfaces were exposed to the vapors from a single injection of 250 μl of the isocyanato silane for 30 min. The resulting film thicknesses were 9.5±0.4 Å (the average of five measurements from five surfaces in four different experiments). To within experimental error, there was no significant difference between the results of these three experiments. This suggests that any of these reaction conditions is adequate to saturate the silicon surface with approximately a monolayer of the isocyanato silane.

These same three experiments, which were performed on silicon, were also performed on spin-coated nylon and glass reinforced nylon, which had been plasma treated (oxidized) and dehydrated. Although glass reinforced nylon (because of its non-reflective nature) could not be analyzed by ellipsometry, spin-coated nylon surfaces were amenable to such analysis. Unlike the

reproducible results obtained on silicon/silicon oxide, the experiments on spin-coated nylon were ambiguous. That is, the resulting thickness changes were often a few angstroms positive or even a few angstroms negative. The low thicknesses (usually 1–3 Å), as well as negative thicknesses (usually 0 to −4 Å, but in two cases −16 and −27 Å), were attributed to solvent (*m*-cresol, with the additional possibility of water) diffusing out of the polymer. Such solvent is difficult to remove. In spite of these ambiguous results, the increase in water contact angle that was observed when the isocyanato silane was deposited on spin-coated nylon (*vide supra*) provides solid evidence for the deposition of this compound. As an additional characterization tool, XPS was also used to monitor the reaction. Figure 6.6 shows the XP spectra of oxidized and isocyanato silane treated silicon, spin-coated nylon and glass reinforced nylon surfaces.

6.4.2.2. Deposition of the R_f-Cl silane

For deposition of the R_f-Cl silane onto isocyanato silane-coated silicon, increases in film thickness were relatively modest, and appeared to depend on the reaction time and hydrolysis conditions. For example, for three isocyanato silane coated silicon surfaces in two separate experiments that were hydrolyzed with water vapor for 60–62 min at 100–107 °C, and then exposed to the vapors of the R_f-Cl silane for 60–65 min at 100–106°C, the increase in film thickness was 31±3 Å. In contrast, for six isocyanato silane surfaces on silicon/silicon oxide in five separate experiments, which were hydrolyzed with water vapors for 30–31 min at 100–106°C, and then exposed to the vapors of the R_f-Cl silane for 45–46 min at 104–107°C, the increase in film thickness was 14±5 Å. These results are to be compared to the thicker films (48 Å, *vide supra*) found in Sec. 6.4.1 in which R_f-Cl silane deposition onto adhesion promoter-

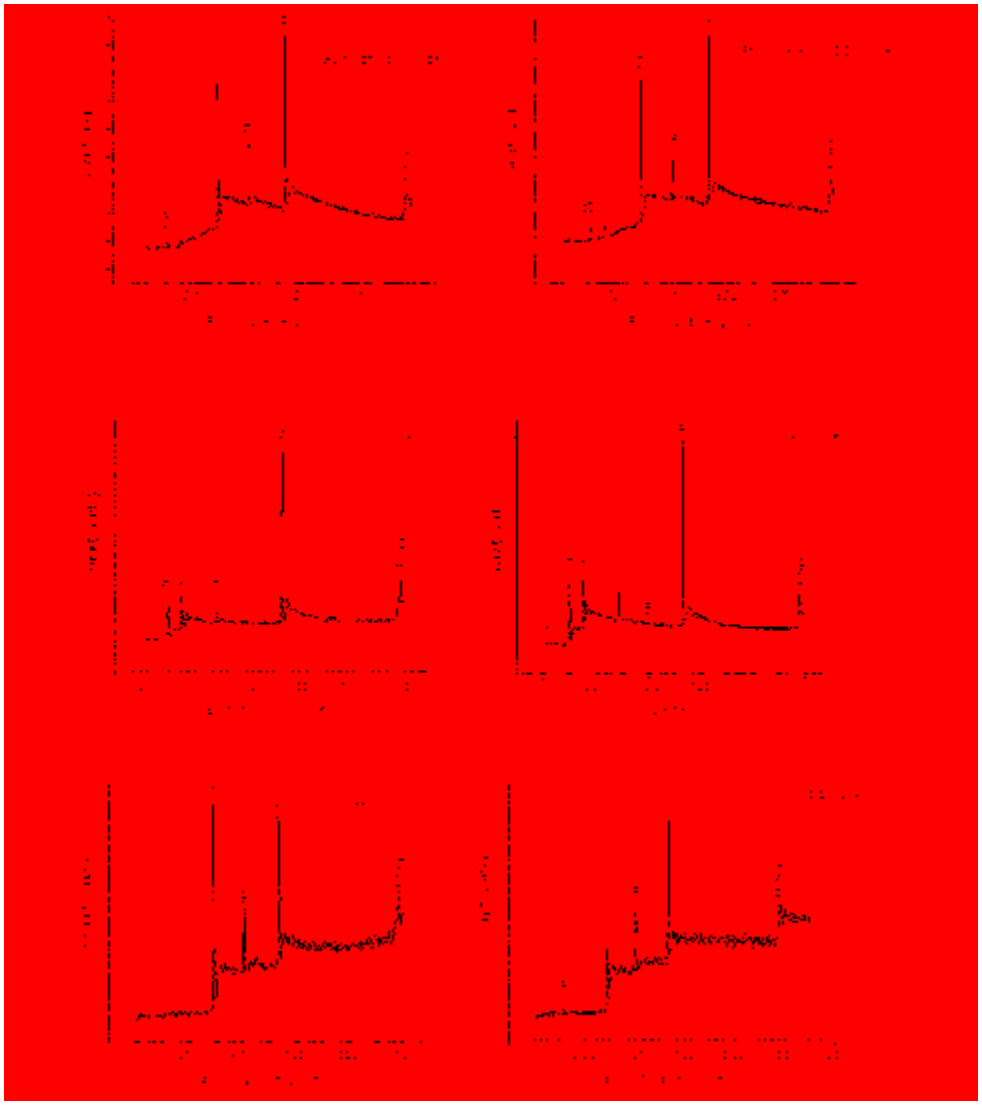

Figure 6.6. XPS of the spin coated nylon surface (top), native oxide coated silicon surface (middle), and glass reinforced nylon surface (bottom) after oxidation (left panels), and after deposition of the isocyanato silane (right panels).

dessicator (67 Å, *vide supra*). For deposition of the R_f-Cl silane in the vacuum oven, I observed a strong correlation between the thickness of the spin coated nylon after plasma treatment and the thickness of the subsequent R_f-Cl silane coating (Figure 6.7). This correlation can be attributed to the polymer film acting as an increasingly thick (large) reservoir of water, which can cause hydrolysis and condensation of the R_f-Cl silane at the surface.

6.4.3. Deposition using a commercially available CVD system

After performing these processes in two different pieces of equipments, the procedure was undertaken in a commercially-available CVD system that was specifically designed for silane deposition, and that also contained built in plasma cleaning capabilities. This equipment is more precise and reproducible because this single tool replaces two or three other pieces of equipment. In addition, the plasma capabilities of the YES-1224P allow the deposition chamber to be more rigorously cleaned on a regular basis than the smaller vacuum oven employed in the process. It was found that this method of depositing multilayer films is superior to previous approaches. Indeed, using the YES-1224P, deposition time for the complete process was shortened to ~1 h, which makes the procedure industrially viable. In addition, the nylon surfaces treated with this equipment were superhydrophobic.

6.4.3.1. Plasma cleaning/treatment

Because of the change in the equipment, it was necessary to reoptimize some of the deposition parameters of the process. Accordingly glass-reinforced nylon surfaces were treated with an oxygen plasma in the YES-1224P for 1, 2.5, 5, and 7.5 min. As shown in

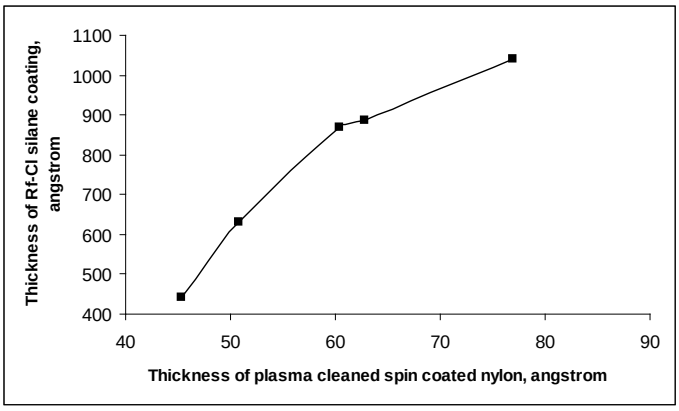

Figure 6.7. Thickness of the R_f-Cl silane coating as a function of the thickness of the underlying plasma treated nylon surface. In general, thicker spin-coated nylon surfaces than those reported in this figure yielded R_f-Cl silane coatings that could not be analyzed using the same ellipsometric model that was employed for the thinner coatings, i.e., they appear to be too thick. (Hydrolysis time: 30 min, hydrolysis temperature: 100–106 °C, temperature for the R_f-Cl silane reaction: 105–106 °C, time for the reaction: 45 min.).

Table 6.5. Advancing water contact angles for glass fiber-reinforced nylon after oxygen plasma treatment. The number in parenthesis indicates the number of surfaces used for the contact angle measurements.

Plasma treatment time (minutes)	$\theta_a(H_2O)$
1	47±0 (3)
2.5	45±0 (3)
5	37±0 (3)
7.5	34±0 (3)

table 6.5, the advancing water contact angle decreases steadily as the oxidation time increases. Based on these numbers (compare to Table 6.1), 6 min of oxygen plasma cleaning was felt to be adequate to oxidize the surface, and hence promote the deposition of the adhesion promoter silane . Unfortunately, this plasma clean completely removes the spin coated nylon film so it was not possible to obtain ellipsometric thicknesses from these substrates.

6.4.3.2. Isocyanato silane treatment

After 6 min of plasma cleaning, 5 mL of isocyanato silane was introduced into the oven, and the surfaces were exposed to the vapors of this silane for 10 min. The temperature of the oven was maintained at 100°C. It was much easier to accurately maintain the temperature of the YES 1224P than the small vacuum oven we previously employed. Spetroscopic ellipsometry was done on the silicon oxide surface after this reaction, and the thickness of the adhesion promoter coating was observed to be 11.8±1.8 Å. Figure 6.8 shows the XPS survey spectrum of a native oxide coated silicon surface after isocyanato silane treatment, which shows the expected N 1s signal.

6.4.3.3. Hydrolysis of the isocyanato silane treated surface

After the isocyanato silane treatment, 3 ml of water was introduced into the chamber, and the surfaces were exposed to these water vapors for 30 min at 100°C.

6.4.4.4. Reaction of the hydrolyzed surfaces with the R_f-Cl silane

Finally, 5 ml of R_f-Cl silane was introduced into the oven, and the surfaces were exposed to vapors of this compound for 15 min. The temperature of the oven was again maintained at

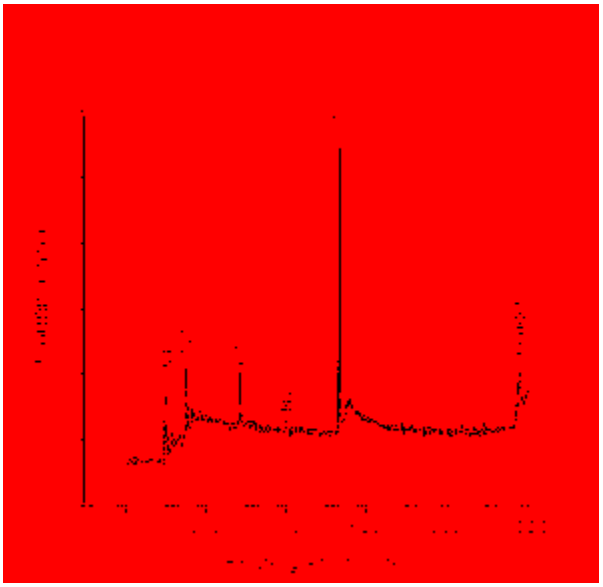

Figure 6.8. XPS survey spectrum of isocyanato silane treated silicon dioxide.

100°C. Advancing water contact angles for silicon oxide and reinforced nylon surfaces after R_f-Cl silane treatment were 125° and 155±3°, respectively. The final thickness of the coating on the bare Si surface after R_f-Cl silane treatment was 173±7Å, which includes the thickness of the native oxide and isocyanato silane layers. Figure 6.9 shows the XPS survey spectrum after this R_f-Cl silane treatment.

6.4.4.5. Scanning electron microscopy characterization of coated surfaces

In Sec. 6.4.1, advancing water contact angles of 128°±3° were reported after R_f-Cl silane deposition on reinforced nylon (overnight deposition in a dessicator at room temperature). These water contact angles rose substantially to 155±3° after the two-silane deposition was performed at higher temperature in the YES-1224P. These much higher water contact angles indicate that a superhydrophobic surface was created, and superhydrophobicity is often a result of surface roughness.[21] To investigate the possibility of surface roughening, reinforced nylon coupons were examined by scanning electron microscopy (SEM) before and after treatment with the two-silane process in the YES-1224P, as outlined in this section. Figure 6.10 shows SEM micrographs of reinforced nylon surfaces before and after silane deposition. It is clear from these micrographs that the surfaces have become rougher after the two-silane treatment, developing a cauliflower-like structure. This increase in surface roughness is attributed to HCl produced during R_f-Cl silane condensation leading to etching of the surface. Indeed, I observed that reinforced nylon parts dissolve slowly in concentrated, aqueous hydrochloric acid.

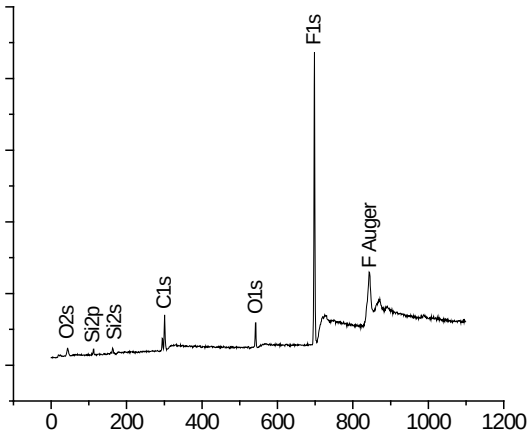

Figure 6.9. XPS survey spectrum of a silicon/silicon dioxide surface that was plasma cleaned, exposed to the isocyanato silane, hydrolyzed, and treated with the R_f-Cl silane, all in the YES-1224P tool.

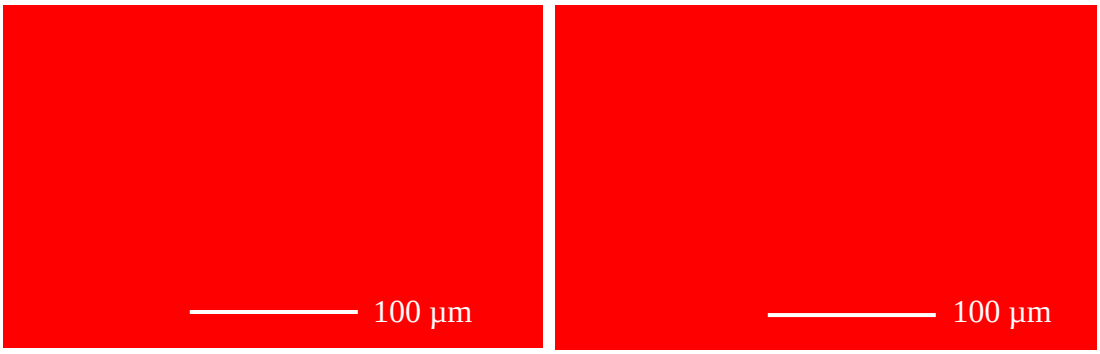

Figure 6.10. Representative SEM micrographs of a reinforced nylon coupon (left) before silane deposition and (right) after the two-silane deposition in the YES-1224P.

6.5. Discussion

Based on the results, and standard organic and surface chemistry, the following can be proposed. For the silane deposition in this study, the isocyanato silane reacts with the cleaned silicon oxide surface by condensation to form Si–O–Si linkages, which tethers the molecule to the surface. It is likely that some cross-linking/polymerization of these molecules also occurs. The isocyanato silane should react, at least in part, with C–OH groups on the plasma treated nylon surfaces to form urethane linkages and this film should act as an adhesion promoter for deposition of the next silane (see Figure 6.11). Abrasion tests of the complete films indicate that this silane does perform this function. Some reaction of the surface C–OH groups with the isocyanato silane to form C–O–Si bonds may also occur. Water vapor will hydrolyze silanes and lead to condensation between monomer units to form robust Si–O–Si bonds, or create Si–OH sites that allow future reactions to take place. Water vapor should also facilitate hydrolysis of unreacted isocyanate groups to form amines as follows:

$$R\text{–}NCO + H_2O \rightarrow R\text{–}NH_2 + CO_2. \qquad (1)$$

The resulting amines are Brønsted-Lowry bases that should accept protons and form ionic bonds with carboxyl groups at the surface of the polymer (created by plasma cleaning of the surface), and surface[22] and bulk silanol groups in subsequent silane layers, which are also acidic. Upon heating, the amino groups that are ionically bonded to carboxyl groups (as $–NH_3^+ {}^-OOC–$) may form strong amide linkages (–NH–C(O)–) with evolution of water.[23] These interactions should help stabilize films of these materials. In the final step, the R_f-Cl silane should chemisorb onto the isocyanato silane coated surface to form a network of strong Si–O–Si linkages, which will be

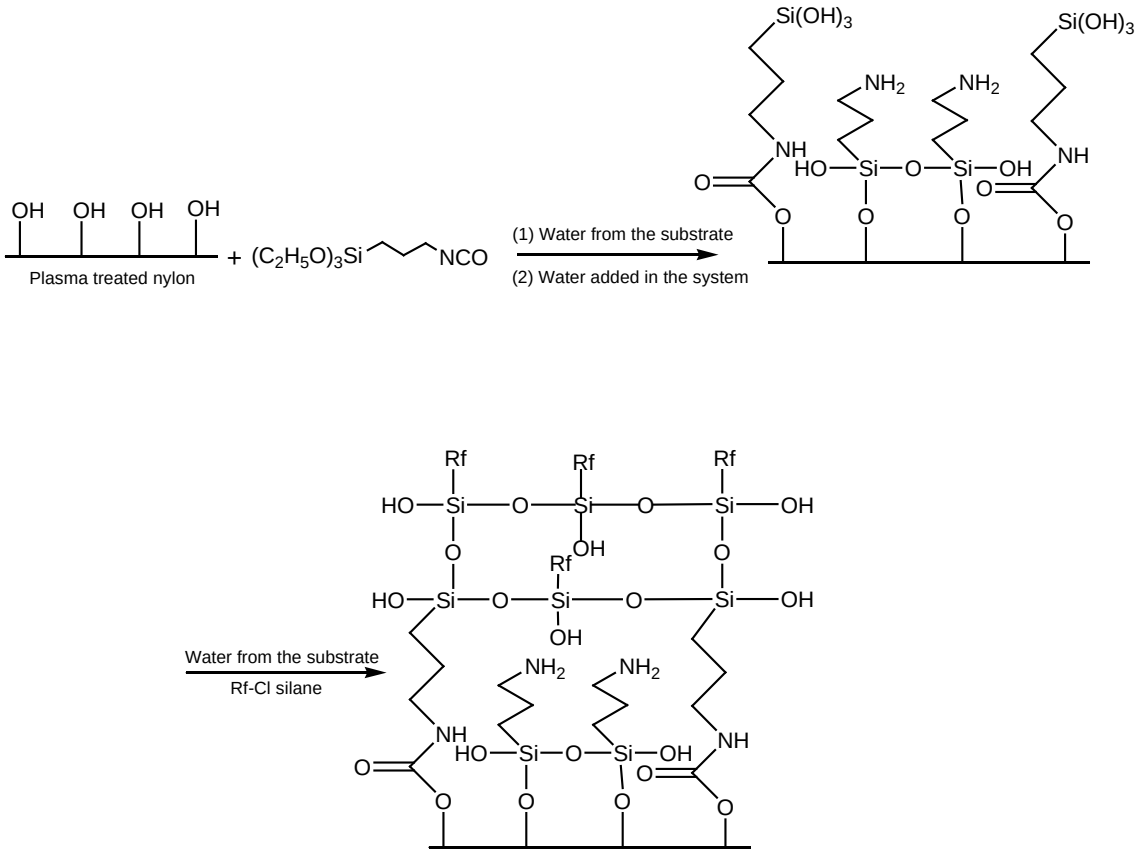

Figure 6.11. Reaction of plasma treated nylon with the isocyanato and Rf-Cl silanes.

covalently bonded to the silicon or polymer substrate through the isocyanato silane linking layer. The isocyanto silane layer and the substrate appear to act as a water reservoir to facilitate this condensation (see Figure 6.7).

6.6. Conclusions

I have shown a two-silane, CVD approach to creating hydrophobic, abrasion-resistant coatings on silicon oxide and polymer (nylon) substrates. This coating is applied using three different arrangements of scientific equipment. Surfaces at each stage in the process are characterized by XPS, ToF-SIMS, wetting, and spectroscopic ellipsometry. This work has a number of unique features. First, it represents an all gas phase deposition of a new silane coating that is scientifically interesting and technologically useful. Second, the presence of an adhesion promoter in the process leads to thinner films that are more robust in abrasion testing. Third, results obtained using plasma/deposition equipment that is relatively inexpensive and/or available in most laboratories are compared to those obtained with a much more sophisticated, commercially available plasma/CVD system (the YES-1224P). The entire deposition process can be completed in only ~1 h using industrial equipment (the YES-1224P), and the polymer surfaces modified using the 1224P are superhydrophobic. Fourth, the thickness of the R_f-Cl silane layer deposited by CVD correlates well with the thickness of the underlying spin-coated nylon surface, suggesting that the nylon film acts as a reservoir of water for the hydrolysis and condensation of the R_f-Cl silane.

6.7. References

(1) Kanan, S. M.; Tze, W. T. Y.; Tripp, C. P. *Langmuir* **2002**, *18*, 6623-6627.

(2) Hoffmann, P. W.; Stelzle, M.; Rabolt, J. F. *Langmuir* **1997**, *13*, 1877-1880.

(3) Pallandre, A.; Glinel, K.; Jonas, A. M.; Nysten, B. *Nano Lett.* **2004**, *4*, 365-371.

(4) Ek, S.; Iiskola, E. I.; Niinisto, L.; Vaittinen, J.; Pakkanen, T. T.; Keranen, J.; Auroux, A. *Langmuir* **2003**, *19*, 10601-10609.

(5) Cecchet, F.; De Meersman, B.; Demoustier-Champagne, S.; Nysten, B.; Jonas, A. M. *Langmuir* **2006**, *22*, 1173-1181.

(6) Cai, M.; Ho, M.; Pemberton, J. E. *Langmuir* **2000**, *16*, 3446-3453.

(7) Montanari, T.; Herrera Delgado, M. C.; Bevilacqua, M.; Busca, G.; Larrubia Vargas, M. A.; Alemany, L. J. *J. Phys. Chem. B* **2005**, *109*, 879-883.

(8) Hansma, H. G.; Revenko, I.; Kim, K.; Laney, D. E. *Nucl. Acids Res.* **1996**, *24*, 713.

(9) Howarter, J. A.; Youngblood, J. P. *Macromolecules* **2007**, *40*, 1128 - 1132.

(10) Kasai, T.; Bhushan, B.; Kulik, G.; Barbieri, L.; Hoffmann, P. *J. Vac. Sci. Technol. B* **2005**, *23*, 995-1003.

(11) Pellerite, M. J.; Wood, E. J.; Jones, V. W. *J. Phys. Chem. B.* **2002**, *106*, 4746-4754.

(12) Pompe, T.; Fery, A.; Herminghaus, S.; Kriele, A.; Lorenz, H.; Kotthaus, J. P. *Langmuir* **1999**, *15*, 2398-2401.

(13) Krass, H.; Papastavrou, G.; Kurth, D. G. *Chem. Mater.* **2003**, *15*, 196-203.

(14) Huang, N.-P.; Voros, J.; DePaul, S. M.; Textor, M.; Spencer, N. D. *Langmuir* **2002**, *18*, 220-230.

(15) James, C. D.; Davis, R. C.; Kam, L.; Craighead, H. G.; Isaacson, M.; Turner, J. N.; Shain, W. *Langmuir* **1998**, *14*, 741-744.

(16) Duffy, D. C.; McDonald, J. C.; Schueller, O. J. A.; Whitesides, G. M. *Anal. Chem.* **1988**, *70*, 4974-4984.

(17) ToF-SIMS . Surface Analysis by Mass Spectrometry; IM Publications: Huddersfield, U., 2001.

(18) The water contact angle for the reinforced nylon is higher than the contact angles for the other materials. The plaques of reinforced nylon that were used in this study appear to be somewhat rougher than the spin coated surfaces, which would raise the observed water contact angles. In addition, throughout our study we observe that our results vary somewhat between the reinforced nylon samples that have different colors. This underscores the importance of the use of spin coated nylon surfaces, which are not pigmented and appear to be much more representative of the true polymer. The reinforced nylon surfaces are important because they show that our process is applicable to an industrially viable material.

(19) While a change in water contact angle could always be observed after deposition of the isocyanato silane, we did not always observe a change in thickness by optical ellipsometry. We attribute the difficulty in seeing this change in thickness to diffusion of the solvent used in spin coating out of the nylon film, which would make the film thinner, during deposition of the isocyanato silane.

(20) Ulman, A. *An Introduction to Ultrathin Organic Films: from Langmuir-Blodgett to Self-Assembly*; Academic Press: Boston, 1991.

(21) Yeh, K. Y.; Chen, L. J.; Chang, J. Y. *Langmuir* **2008**, *24*, 245-251.

(22) White, L. D.; Tripp, C. P. *J. Colloid Interface Sci.* **2000**, *232*, 400.

(23) Harris, J. J.; DeRose, P. M.; Bruening, M. L. *J. Am. Chem. Soc.* **1999**, *121*, 1978-1979.

PART IV. CONCLUSIONS

Chapter 7. Conclusions and Recommendations for Future Work

7.1. Conclusions

I have described the synthesis of normal and reversed phases on diamond, and demonstrated the applicability of diamond as a potential sorbent in SPE and HPLC. The amino phase on solid diamond particles was used in the SPE separation of a mixture of three different lipids. The stability of the amine functionalized diamond particles was improved by thermal curing and chemical cross-linking. These particles were much more stable under extreme pH conditions than a commercially available silica amino sorbent. Reversed phases on solid diamond particles were synthesized by the reaction of amine functionalized diamond particles with long chain alkyl and perfluorinated isocyanates. Like amino modified diamond particles, these particles were also chemically much more stable than their silica counterparts. They were used for the extraction of two common pesticides - cyanazine and diazinon from water. However these particles could not be used as packing material for HPLC due to their non-porous nature and, hence, very low surface area. This issue was addressed by synthesizing highly porous core-shell diamond particles by adopting the layer-by-layer deposition approach. These particles had much higher surface area and analyte loading capacity than non-porous solid diamond particles. The normal and reversed phased core-shell particles were then used to separate a mixture of different analytes. A plate number of 54,800 plates/meter was achieved using these C_{18} core-shell particles, which is the highest number of plates ever achieved using a diamond based column.

PAAm was used in most of the work reported in this dissertation, which is a unifying characteristic. In addition, Microlens array patterning (MAP) was used for the synthesis of microarrays on silicon substrates. A microlens array was used to pattern an alkyl monolayer terminated silicon substrate. PAAm, was then selectively deposited on the spots in the presence of a cationic surfactant, and its reactions with glutaric anhydride, phenylendiisothiocyante, biotin NHS ester and an oligonucleotide were demonstrated.

A highly durable superhydrophobic coating was synthesized on nylon and silicon substrates. The coating was synthesized by performing sequential chemical vapor deposition of 3-isocyantopropyltrimethoxysilane and 1,1,2,2-tetrahydrooctyltrichlorosilane. The coating was much more durable when 3-isocyanatopropyltriethoxysilane was used as an adhesion promoter.

7.2. Recommendations for Future work

The primary objective of my graduate research was to synthesize pH stable normal and reversed phases on diamond, and demonstrate their application in SPE and HPLC. Such phases were successfully made for SPE. Normal phase core-shell diamond particles for HPLC were also made. Although reversed phase core-shell diamond particles could be used in HPLC, but unlike normal phase particles they were not stable under extremely basic conditions. Future work will focus on improving the pH stability of these particles. As far as the shape of the core-shell particles, ESEM showed that these particles were not spherical. The irregular shape of the particles led to high back pressures during the analyses and limited the analysis to low flow rates. As noted, irregular solid diamond particles were used as core. In the future, spherical core (metallic, graphitic or polymeric) particles will be used for the synthesis of spherical core-shell diamond particles. This will also help improve the efficiency of the column by decreasing eddy

diffusion (A term in the Van deemter equation) of the analytes. As noticed in the ESEM images, the shell of the core-shell particles is not fully uniform - nanodiamond particles sometimes deposit as agglomerates and not as individual particles on the solid core. Although Van Deemter curves could not be obtained for these particles due to flow rate constraints, I anticipate mass transfer properties of these particles to be less than ideal. Future work will also focus on the synthesis of uniform shell core-shell diamond particles by preventing the formation of nanodiamond agglomerates. Since diamond is thermally very conductive, and it may prevent the formation of thermal gradients in UHPLC, the potential of core-shell diamond particles as a packing material in UHPLC will also be studied. These particles were used for the analysis of some common analytes, *i.e*. substituted benzenes. In the future the potential of these particles in the analysis of more complex molecules such as drugs and peptides will be determined. The processes for the synthesis of normal and reversed phase stationary phases on diamond employ different chemical species than those employed for silica. Hence theoretically there would be a difference in the chemical interactions of various analytes with diamond and silica based stationary phases. Future work will also focus on comparing the selectivities of diamond and silica stationary phases for different analytes.

APPENDIX. ANALYTICAL METHODS

Contact angle goniometry

This technique is used to determine surface free energies and/or wetting properties of the surface. The instrument consists of a few main parts: an optical microscope, a back light, a stage, and a vertically clamped syringe that stores the liquid used for probing the surface energy. The liquid is usually water or an alkane, such as hexadecane. Water is used to determine hydrophobicity or hydrophilicty of the surface, and alkanes are used to measure the oleophobicity or oleophilicity of the surface. The substrate is placed under the needle of the syringe and the liquid is dispensed in the form of a droplet onto the substrate. While the droplet is watched through the microscope, a tangent is drawn to the edge of the drop and the angle is measured between the tangent and the substrate. The higher the contact angle, the lower the free energy of the surface, and vice versa.

Spectroscopic ellipsometry

This technique is used to measure the thickness of thin films on a substrate. It can measure thickness from a fraction of an angstrom to several μm. It measures the relative phase and amplitude change of linearly polarized light after it is reflected off the surface. As the reflection properties of a surface change with a change in its nature (film thickness or composition), the thickness change or a change in optical constants is determined.

X-ray photoelectron spectroscopy (XPS)

X-ray photoelectron spectroscopy is a quantitative technique that measures the elemental composition and chemical (oxidation) state of the elements on a surface. This technique typically

uses monochromatic Al *Kα* X-rays (1486.7 eV) as the probing beam. Its information depth is *ca*. 0-10 nm into the surface. As X-rays irradiate the surface, photoelectrons are emitted from various atoms near the surface. Photoelectrons from different atoms have different kinetic energies that depend on their binding state in the atom. The kinetic energy of the emitted photoelectrons is determined by an analyzer. The binding energy of a photoelectron is a characteristic of the atom it came from. Since the energy of the X-rays is known, the binding energy of the photoelectron is determined (to a first approximation) by calculating the difference between the photon energy and the binding and kinetic energies, which reveals the identity of the atoms present of the surface. The amount of signal from each atom is used for measuring the atomic composition of the surface.

Time of flight secondary ion mass spectrometry (ToF-SIMS)

This is a semiquantitive technique that is used for determining the identity of molecules on a surface. In the BYU instrument, a beam of high energy $^{69}Ga^{+}$ is focused onto the surface. This results in the generation of various types of chemical species, *i.e*. positive ions, negative ions and neutral species in the near surface region. The generated positive and negative ions are analysed using a time of flight detector. The signal due to these ions can produce a fragmentation pattern of the molecules present on the surface.

Diffuse reflectance infrared Fourier transform spectroscopy (DRIFT)

This technique is used for the qualitative and quantitative analysis of the different functional groups/moieties present in a surface material. The sample is irradiated with an IR beam. As the radiation transmits through the sample, energy at different wavenumbers is

absorbed to different extents, which depends on the relative number density of the functional groups. Thus, DRIFT often reveals the identity and the relative amounts of different functional groups.

Scanning electron microscopy (SEM)

Scanning electron microscopy gives information about the topography of a substrate's surface. It uses a beam of high energy electrons that is rastered across a surface to image it. When electrons strike the surface they interact with the atoms on the surface, which produces secondary electrons. The emitted secondary electrons are detected to yield a magnified picture of the surface of the sample.

Environmental scanning electron microscopy (ESEM)

ESEM is used for imaging the surface of insulators. It is a form of SEM; it uses a focused beam of electrons that is rastered across a surface, but the analysis is done in low vacuum usually in the presence of water vapor. Water vapor aids in neutralization of the charge developed on the insulator's surface during the analysis.

Rutherford backscattering spectroscopy (RBS)

This technique is used to determine the structure and composition of materials by measuring the scattering of high energy helium ions by various atoms at or near the surface. Different nuclei scatter helium ions to different degrees and with different energies (heavier nuclei scatter He^+ more efficiently than lighter ones), which gives qualitative and quantitative information about the composition of a surface, and the region around it.

Nuclear reaction analysis (NRA)

Nuclear reaction analysis is used to obtain absolute concentrations of various elements, *e.g*., C, O, and F, at surfaces. A beam of high energy nuclei (*e.g*. deuterons: D^+) is used for the analysis. As these nuclei come in contact with a target atom, they fuse with the target atom, which results in the formation of emitted species (protons). The energy of the emitted protons is characteristic of the atom that emitted them.

LIST OF ABBREVIATIONS AND SYMBOLS

SPE	Solid-phase extraction
PAAm	Polyallylamine
HPLC	High-performance liquid chromatography
ESI-MS	Electrospray-mass spectrometry
POPC	Palmitoyloleoylphosphaitidylcholine
LbL	Layer-by-layer
MeV	Mega electronvolt
MSDNs	Microdispersed sintered detonation nanodiamonds
IPA	Isopropyl alcohol
PDITC	Phenylene 1,4-diisothiocyanate
GA	Glutaric anhydride
BNE	Biotin NHS ester
CTAC	Cetyltrimethylammoniumchloride
MAP	Microlens array patterning
CVD	Chemical vapor deposition
XPS	X-ray photoelectron spectroscopy
ToF-SIMS	Time of flight secondary ion mass spectrometry
SEM	Scanning electron microscopy
ESEM	Environmental scanning electron microscopy

NRA	Nuclear reaction analysis
RBS	Rutherford backscattering spectroscopy
DRIFT	Diffuse reflectance infrared Fourier transform
BET	Brunauer-Emmett-Teller
Ω	Ohm
W	Watt
C	Centigrade
μ	Micron
Å	Angstrom
F	Flow
P	Pressure
R^2	Coefficient of variation
m	Mass of an ion or slope
z	Charge on an ion
b	Intercept
k	Retention factor
N	Number of plates
M	Molar
θ_a	Advancing contact angle